Properties of Dark Matter at Small Scales

Ottavia Balducci

MÜNCHEN 2022

Properties of Dark Matter at Small Scales

Dissertation
an der Fakultät für Physik
der Ludwig-Maximilians-Universität München

vorgelegt von Ottavia Balducci
aus Triest

München, den 28. Februar 2022

Erstgutachter: Prof. Dr. Stefan Hofmann
Zweitgutachter: Prof. Dr. Ivo Sachs
Tag der mündlichen Prüfung: 5. Mai 2022

Zusammmenfassung

Das Standardmodell der Teilchenphysik deckt nur etwa 5% der Energiedichte des Universums ab. Die restlichen Komponenten, Dunkle Materie (DM) und Dunkle Energie, sind noch weitgehend unbekannt. Das Λ-Cold-Dark-Matter kosmologische Modell, welches kollisionslose und vor dem Materie-Strahlung-Gleichgewicht nicht-relativistische DM postuliert, ist äußerst erfolgreich bei der Erklärung von astronomischen Beobachtungen auf großen Skalen, jedoch versagt seine Vorhersagekraft auf kleinen (Kiloparsec-) Skalen. In dieser Arbeit werden drei Modifikationen des Λ-Cold-Dark-Matter-Modells vorgestellt, welche die Diskrepanzen zwischen Beobachtungen und Vorhersagen auf kleinen Skalen lösen. Ihre gemeinsamen Merkmale sind eine späte kinetische Entkopplung zwischen den Teilchen der Dunklen Materie und einem relativistischen Streupartner, welche das Power-Spektrum der Dunklen Materie bei kleinen Skalen unterdrückt, und die Einführung von Selbstwechselwirkungen, welche den Entropietransfer zwischen verschiedenen Regionen der Dunklen Materie erhöhen. Das erste Modell untersucht die Möglichkeit eines vollständig abgeschotteten Dunklen Sektors mit einer dunklen U(1)-Eichsymmetrie, sowie mehreren Generationen von dunklen Fermionen. Das zweite Modell beinhaltet die Möglichkeit einer Kopplung zwischen Dunkler Materie und Neutrinos, welche als relativistische Streupartner dienen. Das dritte Modell bietet hingegen einen Annihilationskanal der Dunklen Materie in Elektronen und Positronen.

Die DM-Dichte spielt eine wichtige Rolle bei der Bestimmung der Streuungsraten (beziehungsweise Annihilations-/Zerfallsraten), welche zum Nachweis von DM führen könnten. Ihre großräumige Verteilung ist durch numerische Simulationen im ΛCDM-Modell gegeben, aber astrophysikalische Effekte können Auswirkungen auf lokaler Ebene haben. Der letzte Teil dieser Arbeit untersucht die Möglichkeit der Erzeugung von lokalisierten DM-Überdichten durch gravitative Wechselwirkungen zwischen DM und einem rotierenden Schwarzen Loch: Einfallende Teilchen können innerhalb der Ergosphäre des Schwarzen Lochs zerfallen und bevorzugt entlang der Rotationsachse ausgestoßen werden. Es wird gezeigt, dass dieser Effekt zu einem schwachen DM-Strahl führt.

Abstract

The Standard Model of particle physics covers only about 5% of the energy density of the Universe. The remaining components, Dark Matter (DM) and Dark Energy, are largely unknown. The Λ Cold Dark Matter (ΛCDM) cosmological model, postulating DM which is collisionless and non-relativistic before matter-radiation equality, is extremely successful at explaining astronomical observations at large scales; however, its predictive power fails at small (kiloparsecs) scales. In this work, three modifications of the ΛCDM model are presented which resolve the discrepancies between observations and predictions at small scales. Their common features are: a late kinetic decoupling between the DM particles and a relativistic scattering partner, suppressing the DM power spectrum at small scales, and the introduction of self-interactions, increasing the entropy transfer between DM regions. The first model consists of a completely secluded Dark Sector with a U(1) gauge symmetry and multiple generations of fermions. The second one includes the option of a coupling between DM and neutrinos, which serve as relativistic scattering partners. The third model features a DM annihilation channel into electrons and positrons.

The DM density plays an important role in determining the scattering (or annihilation/decay) rates which could lead to DM detection. Its large-scale distribution is given by ΛCDM numerical simulations, but astrophysical effects can have a relevant impact locally. The final part of this thesis studies the possibility of generating localized DM overdensities through gravitational interactions between DM and a rotating black hole: infalling particles can scatter or decay within the black-hole's ergosphere and be expelled preferentially along the rotation axis. It is shown that this effect creates a faint DM beam.

Contents

1 Introduction

1.1 The structure of Dark Matter at small scales

This thesis is devoted to the discussion of small-scale properties of Dark Matter. Since the discovery of Dark Matter via gravitational observations, a lot of effort has been made to understand its real nature. While a lot of constraints on the properties of Dark Matter have been set, the puzzle is still far from being solved. In particular, direct and indirect detection experiments have not been decidedly successful yet. Indeed, Dark Matter remains particularly elusive to non-gravitational observations. For this reason, a lot of new motivation for Dark Matter research currently comes from cosmological observations. In particular, new insights can be gained by looking at the Dark Matter properties at small scales, since in that range particle properties (e.g. self-interaction cross sections) can be probed without the explicit need for a connection to the Standard Model. Furthermore, at small scales, discrepancies between observations and predictions by the established Λ Cold Dark Matter (ΛCDM) cosmological model have been noticed and, thus, new physics seems to be unavoidable.

The ΛCDM model has been highly successful at explaining the Universe and its history. From the existence of the Cosmic Microwave Background to the accelerated expansion of the Universe, the list of the puzzles solved by the ΛCDM model is long. Some of the unsolved issues between this model and observations at small scales are the following. The Dark Matter density near the center of halos, below distances of a few kiloparsecs, is lower than expected. Furthermore, the number of observed satellites of the Milky Way is lower than predicted by simulations and the brightest dwarf spheroidal satellites have velocity profiles which are incompatible with the most massive Dark Matter subhalos. Finally, the rotation curves in the inner regions of galaxies can vary greatly even between galaxies which otherwise have very similar properties. These discrepancies with observations might open the way to modifications of the ΛCDM model. Three such specific modifications will be discussed in this thesis. The common ground between them is given by the fact that they all feature self-interacting Dark Matter and a late kinetic decoupling between the Dark Matter particles and some relativistic scattering partner. These two features are crucial to solving the above mentioned small-scale problems.

Self-interactions facilitate energy transport within the halo and thus eliminate cuspy density profiles. A lower central density also makes it possible for the most massive observed satellites of the Milky Way to be located in the most massive subhalos. Furthermore, self-interactions increase the velocity dispersion of Dark Matter particles which means that the Dark Matter density profile is more sensitive to the baryon density near the center of each halo. This can explain the differences between inner rotational curves of similar halos. Since the ΛCDM is in very good agreement with observations at large scales, self-interactions should change structures only at small ones. This is the case for velocity-dependent self-interaction cross sections: at large scales the rotational velocities are much larger and the Dark Matter particles can be regarded as being collisionless.

When Dark Matter particles stay in thermal equilibrium with a relativistic scattering partner until late times, the elastic momentum transfer between them washes out any structures that might form up until the time when the two kinds of particles are decoupled from each other. This can explain the lack of observations of dwarf spheroidal satellites of the Milky Way with masses below $10^8 - 10^{10}$ solar masses.

The first model described in this thesis and implementing such features is a simple Dark Matter model with a U(1) gauge symmetry. It postulates a completely secluded dark sector with no bridge to the Standard Model and thus no possibility of direct or indirect detection. However, predictions made by such a model could still be tested against observations of the structure of the Universe at small scales. Beyond the Dark Matter candidate, the proposed theory postulates a massive U(1) gauge boson, which mediates velocity-dependent self-interactions between the Dark Matter particles, and a very light dark fermion, which constitutes a relativistic scattering partner for Dark Matter up until temperatures of a few hundred eV.

The second model is a Dark Matter model which couples to the Standard Model through a sterile-neutrino bridge. This mediates an effective coupling to Standard Model neutrinos. Indeed, within this model, the relativistic scattering partners of Dark Matter are Standard Model neutrinos. This is of particular interest since neutrinos are the only particles in the Standard Model that can efficiently maintain elastic scatterings with Dark Matter until late times and can thus provide a solution to the small-scale problems.

The final Dark Matter model is one where the Dark Matter particles have an annihilation channel into electrons and positrons. This renders it particularly interesting from the perspective of indirect detection, for example through experiments searching for electron and positron excesses in cosmic rays. In this case, self-interactions cannot be mediated by the same boson which facilitates annihilations into leptons, since this would require Dark Matter to be electromagnetically charged.

All of these models are discussed with a special focus on the consequences they have for the small-scale structure of Dark Matter. In particular, they all solve the small-scale problems mentioned above: cusp vs core, too-big-to fail, missing satellites and diversity of rotation curves.

1.2 Local Dark Matter overdensities

The second part of the thesis is dedicated to the investigation of a specific scenario which might generate local Dark Matter overdensities. In order to explain some of the tentative signals of Dark Matter annihilation (or decay) which have been measured, a boost factor for the cross section is usually postulated a posteriori to enhance the annihilation rate of Dark Matter. While no clear reason for such a boost factor is known, possible causes include inhomogeneities in the Dark Matter densities and Sommerfeld enhanced cross sections. A third possibility is considered here: a Dark Matter overdensity might be generated by rotating supermassive black holes.

The formation of astrophysical jets from rotating black holes is mostly due to electromagnetic processes and thus does not involve Dark Matter particles. However, gravitational effects contribute to jet formation as well: particles from the accretion disk can fall into the ergosphere and be expelled preferentially along the rotation axis through the Penrose process. Thus, in principle, Dark Matter particles can be collimated by rotating supermassive black holes and yield a Dark Matter overdensity along the axis of rotation. The Carter constant is used to determine which of the Dark Matter particles in the accretion disk have the potential to end up in the beam. After numerically scanning the parameter space of the infalling particles, an upper bound for the Dark Matter density near the rotation axis is obtained. The consequence is that this effect is negligible at large distances from the black hole. However, the presence of a Dark Matter beam is confirmed by the analysis of the Dark Matter density at different distances from the rotation axis: at greater angles from it the Dark Matter density decreases rapidly. Furthermore, it is shown that supermassive black holes with masses of approximately a billion solar masses produce the largest beam densities and that the closer to the Schwarzschild radius the larger is the Dark Matter density.

2 The current status of Dark Matter and the open questions

This chapter contains a brief summary of the current status of Dark Matter research as well as an outlook on the many open questions which still remain. Particular focus is laid on the small-scale properties of Dark Matter, forming the basis for the research presented in the subsequent chapters.

2.1 The ΛCDM model

The ΛCDM model, also known as the concordance model, is the most widely accepted and successful model of cosmology. Its predictive power is huge (CMB, large-scale structure, abundance of primordial elements, accelerated expansion, etc.) and rests on just six free parameters which are fitted to cosmological observations. The evolution of the universe is governed by the Friedmann equations,

$$\left(\frac{\dot{a}\left(t\right)}{a\left(t\right)}\right)^2 = \frac{8\pi G}{3}\rho - \frac{k}{a^2\left(t\right)} \tag{2.1.1}$$

and

$$\frac{\ddot{a}\left(t\right)}{a\left(t\right)} = -\frac{4\pi G}{3}\left(\rho + 3p\right) \ , \tag{2.1.2}$$

where $a\left(t\right)$ is the scale factor, G is Newton's gravitational constant, ρ is the energy density present in the universe, p is the pressure and k is the curvature of spacetime. These equations follow from the Friedmann-Robertson-Walker metric, i.e. the most generic metric which embodies the empirical properties of homogeneity and isotropy,

$$ds^2 = -dt^2 + a^2\left(t\right)\left[\frac{dr^2}{1-kr^2} + r^2\left(d\theta^2 + \sin^2\left(\theta\right)d\phi^2\right)\right] \ . \tag{2.1.3}$$

The ΛCDM model assumes a flat universe ($k = 0$), which is in excellent agreement with experiments [1]. The energy density has three main components: dark energy, cold dark matter (CDM) and ordinary (almost exclusively baryonic) matter. Their dimensionless energy densities are [1] $\Omega_\Lambda \approx 0.69$, $\Omega_{\text{CDM}} \approx 0.26$ and $\Omega_\text{b} \approx 0.05$ respectively, where $\Omega_i = \rho_i/\rho_{\text{crit.}}$ and $\rho_{\text{crit.}}$ is the critical energy density of the universe.

2.1.1 Evidence of Dark Matter

There is large evidence for the Dark Matter component of the universe. Historically, the first main hint at the existence of Dark Matter came from the application of the virial theorem to the Coma cluster by F. Zwicky in 1933 [2], who concluded that the mass of the cluster is dominated by some new form of matter. Further early signals of Dark Matter came from observations of rotational curves of spiral galaxies which appear to be flat at large radii [3, 4]. This is incompatible with the assumption that galaxies only contain ordinary matter, since in that case the velocity profile would fall as $r^{-1/2}$ at large radii. The existence of Dark Matter can be inferred also from both strong and weak gravitational lensing observations [5, 6], which give important information on the total mass of observed objects. The measurement of the temperature of interstellar gas through X-ray detection provides another proof of the existence of Dark Matter: the observed temperature is higher than expected, indicating the presence of more than just the visible matter [7]. The angular power spectrum of the temperature fluctuations of the Cosmic Microwave Background provides yet more evidence for Dark Matter. The peak structure agrees perfectly with a flat universe (1st peak) with baryons and non-baryonic dark matter (2nd and 3rd peaks). The Cosmic Microwave Background radiation provides also another important information: the baryonic density fluctuations at the time of recombination were at most of the order of 10^{-4}, i.e. $\delta\rho/\rho \lesssim 10^{-4}$. This, however, is insufficient to create the non-linear inhomogeneities, $\delta\rho/\rho \gg 1$, observed today in the short period of time elapsed since recombination [8]. Finally, absorption spectra of Lyman-α lines are also in agreement with the ΛCDM model [9].

2.1.2 Particle properties of Cold Dark Matter

Although much is known about the density and distribution of Dark Matter, its particle properties remain quite unconstrained.

A lower bound on the mass of Dark Matter particle comes from the observation that

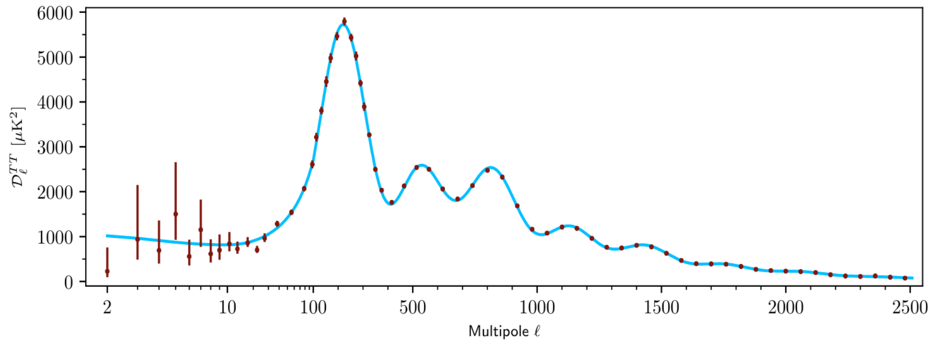

Figure 2.1: The angular power spectrum of the Cosmic Microwave Background Radiation confirms the existence of Dark Matter. Figure from Ref. [1].

Dark Matter should be coherent at the scales of dwarf galaxies, which is equivalent to a constraint on its de Broglie wavelength. On the other end of the spectrum, an upper bound of $m \lesssim 10^{70}$ eV can be found by arguments of stability of globular clusters which would otherwise be disrupted if Dark Matter particles were more massive than that. Thus, in principle, an incredibly wide range of masses is allowed.

Of course, Dark Matter should be stable on cosmological time scales. It should also be electrically neutral or at least interact very weakly with the Standard Model [10, 11, 12].

Within the ΛCDM model, Dark Matter is assumed to be collisionless. However, this does not necessarily have to be the case. Constraints on self-interactions of Dark Matter at the scales of clusters, $\sigma_{\chi\chi}/m_\chi < 1\,\mathrm{cm}^2\,\mathrm{g}^{-1}$, follow from observations of cluster mergers [13].

In the ΛCDM model, Dark Matter is also assumed to be cold, i.e. it should be non-relativistic long before the time of matter-radiation equality. Indeed, hot Dark Matter is highly disfavored because it leads to large damping scales and excessively suppresses the matter power spectrum of the Universe [14].

2.1.3 Direct and indirect Dark Matter detection

A large number of experiments are currently being carried out in order to detect Dark Matter particles. The search for Dark Matter particles is being pursued on three fronts: direct detection, indirect detection and Dark Matter production at colliders, as exemplified in Fig. 2.2.

Direct detection experiments look for scintillation resulting from nucleon-Dark Matter interactions, mostly deep underground to avoid the background coming from inter-

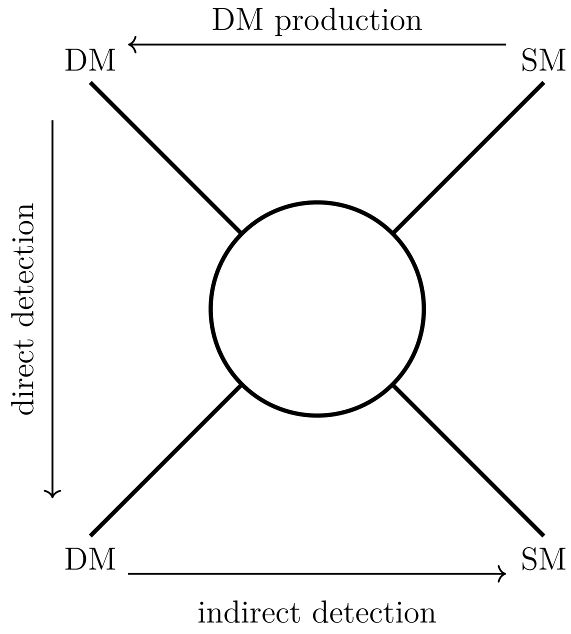

Figure 2.2: The current possible paths for Dark Matter search: direct detection, indirect detection and production.

actions with cosmic rays. The negative results so far have lead to stringent constraints on the cross-section for WIMP-nucleon scattering [15]. Recently, an excess in the low-energy electronic recoil data was measured at the XENON1T experiment which might be explained by bosonic Dark Matter with a mass of approximately 2 keV [16].

Indirect detection experiments search for annihilation or decay products of Dark Matter particles. While there is no definitive evidence, a number of anomalous events have been measured, which could be explained by the presence of Dark Matter: positron excesses were observed by the PAMELA detector [17] and the AMS-02 experiment [18], while rare highly energetic neutrino events have been detected by IceCube [19].

2.2 Dark Matter at small scales

Much is known about the properties of Dark Matter at large scales; however, at the scales of kiloparsecs, there are still observations which cannot be explained by the usual Cold-Dark-Matter model. These will be discussed in this section.

2.2.1 Cuspy Dark Matter halos

The density profile of a Dark Matter halo can be quite accurately predicted through N-body simulations of collisionless Dark Matter. The Navarro-Frenk-White (NFW) profile [20],

$$\rho_{\mathrm{NFW}}(r) = \frac{\rho_0}{\frac{r}{r_\mathrm{s}}\left(1+\frac{r}{r_\mathrm{s}}\right)^2} , \tag{2.2.1}$$

is the most famous result of such simulations. The parameters depend on the particular characteristics of each halo. In particular, the slope $\alpha = d\log\rho_{dm}/d\log r$ of the profile for small radii is $\alpha \approx -1$ in the case of a NFW profile. This corresponds to a rotation curve behaving as $v(r) \propto \sqrt{r}$ at small radii.

Measurements of galaxy rotation curves have been undertaken in order to compare them with these predictions. Dwarf galaxies are very well suited for such observations, because their dynamics is mostly governed by Dark Matter. Another testing ground are low surface brightness galaxies, due to their high mass-to-light ratio Υ_* and especially quiescent evolution, which helps to exclude supernova-driven outflows and other baryonic effects as possible factors affecting the observed rotation curves [21]. Both types of galaxies display rotation curves which are much flatter for small radii, $v(r) \propto r$ [22, 23, 24], meaning that they favor a Dark Matter density profile with a shallower inner slope, $\alpha \approx 0$.

The difference between the expected density profile and the one inferred from observations is known as the “cusp versus core” problem. It is important to note, that these differences appear only at small radii of approximately ~ 1 kpc, while measurements and simulations agree at larger scales.

2.2.2 Missing satellites

Another tension between the ΛCDM predictions and observations is given by the so-called missing satellites problem. Indeed, ΛCDM simulations predict that halos like the one of the Milky Way should have several hundreds of smaller subhalos [25, 26, 27]. This is in accordance with the hierarchical structure formation which assumes that larger structures in the Universe have formed from smaller ones. On the other hand, only about 50 satellite dwarf galaxies have been observed so far within the virial radius of the Milky Way [28, 29]. Historically, this number was much lower at the time when this discrepancy was first noted [30] and has since increased to the current value of approximately 50 thanks to observations of fainter objects which remained previously unnoticed. It is, however, highly unlikely that more such discoveries could fill the gap between the predictions and the observations.

It should be noted that missing satellites have been reported also within the Local Group but not for the Virgo cluster. Thus, like the cusp vs core problem, this is only related to small scales. A possible solution is given by the hypothesis that the missing satellites have not been observed due to their extremely low baryonic content. This depletion of baryons in dwarf halos could be due to heating of the gas after the reionization epoch which suppresses gas accretion in low-mass halos [31].

In this work, possible modifications of the ΛCDM model are considered which allow to solve the missing satellites problem without the need for baryonic effects [32, 33, 34]. In particular, all the models discussed feature a late (i.e. at $T < 1$ keV) kinetic decoupling of the Dark Matter particles from some relativistic scattering partner and can successfully address this problem by suppressing Dark Matter structure at mass scales below $M_{\mathrm{halo}} \lesssim 10^8 - 10^{10} M_\odot$ [35, 36, 37].

2.2.3 Diversity of rotation curves

Galaxy observations revealed another puzzle at small scales. When plotting the rotational velocity of each galaxy at a radius of 2 kpc versus the maximal rotational velocity, i.e. the velocity at very large radii, a large diversity in the inner velocities becomes apparent: even though two galaxies might have the same maximal velocity, their velocity at $r = 2$ kpc can vary by as much as 50 km/s [38]. Since rotational velocity and density profile are correlated, this means that similar halos can have very different inner density profiles.

2.2.4 Too big to fail

By abundance matching [8], i.e. establishing a monotonic one-to-one correspondence between the Milky Way subhalos predicted by ΛCDM simulations and the observed galaxy satellites, it is expected that the brightest (and thus most massive) satellites are located in the most massive subhalos. However, the observed low rotational velocities of these massive satellites are incompatible with the high central densities of the most massive subhalos [39]. It remains unclear why the most massive subhalos should fail to form galaxies, in particular since their gravitational potential is the deepest and any stripping gas mechanisms would be less effective than on the smaller halos.

Explicitly, ΛCDM simulations predict subhalos with inner circular velocities larger than 25 km/s. However, the most massive satellites observed, which should have the fastest circular velocities, reach at most $v_{\mathrm{circ}} \approx 20\,\mathrm{km/s}$.

This discrepancy is not peculiar to the satellites of the Milky Way: field galaxies and satellites of Andromeda show the same problem [40].

The too big to fail and the cusp vs core problems can be solved simultaneously by the same mechanism, since they both would benefit from smaller central densities in Dark Matter subhalos. On the one hand, a smaller central density yields a more cored profile, while on the other hand, a smaller density implies a smaller rotational velocity near the center and thus the most massive satellites could be hosted by the most massive subhalos after all.

3 Flavored U(1) dark sector at small scales

The first and simplest one of the models discussed in this thesis, addressing the small-scale problems of ΛCDM explained in Chapter 2, is presented in this chapter. A U(1) sector secluded from the rest of the Standard Model is postulated and the possibility of multiple Dark Matter generations is considered.

3.1 Introduction

The model presented in this Chapter is the simplest one, in the sense that it consists of a secluded Dark Sector and can thus evade a number of phenomenological constraints which would apply if Dark Matter were coupled in some way to the Standard Model. In fact, this model is not completely secluded since thermal production is assumed and thus a very early coupling between the Dark Sector and the Standard Model is present. However, this coupling ceases to be relevant at early times ($T \gg T_{\mathrm{BBN}}$) and from that moment forward there is no contact between the two sectors.

The main goal of this model is to obtain a simple theory which is able to explain simultaneously the observed Dark Matter relic density and the discrepancies between ΛCDM predictions and observations at small scales. The simplest way to achieve this is by introducing at least three new kinds of particles in the Dark Sector: two Dirac fermions and one U(1) gauge mediator. The heavier of the two Dirac fermions is the Dark Matter candidate, while the lighter one is its relativistic scattering partner which allows for a late kinetic decoupling. Furthermore, the U(1) gauge boson mediates self-interactions between the Dark Matter particles. These two features allow to solve the small scale problems of ΛCDM, as will be discussed in the rest of this Chapter.

Moreover, an expansion of this simple model is presented as well: the possibility of multiple generations, i.e. further pairs of heavy and light fermions in the Dark Sector, is analyzed. This allows for a larger choice of parameters yielding the desired phenomenology.

Even though the new particles are secluded from the Standard Model, a number of constraints must still be taken into consideration. In particular, quantum consistency of the new theory and the deviation of the effective number of neutrino degrees of freedom will be discussed in detail.

3.2 Assumptions

The main assumptions within this model are the following.

1. **Coupling to the Standard Model:** The Dark Sector is assumed to have been in thermal equilibrium with the Standard Model only at early times, long before Big Bang Nucleosynthesis. After that, the Dark Sector is assumed to decouple completely from the Standard Model. This assumption is motivated by the lack of definitive non-gravitational evidence for Dark Matter particles. Such a secluded Dark Sector is usually known as a *nightmare scenario*, because it does not allow any direct or indirect detection of Dark Matter processes. However, such a model could still be tested via cosmological observations, e.g. comparisons between observations and predictions of small-scale structures.

2. **Visible entropy:** It is assumed that the entropy of the Standard Model is not affected by the Dark Sector, i.e. the effective number of entropy degrees of freedom $g_{*,S}$ of SM particles is unchanged. This means in particular that even though the Dark Sector and the Standard Model were in thermal contact at early times, no entropy transfer has taken place (e.g. no annihilations of dark particles into Standard-Model particles).

3. **Dark Matter:** The mass of the Dark Matter candidates is assumed to lie in the TeV range. This is a valid assumption, since it is well known that masses in this range accompanied by an interaction below the weak scale are able to solve the small-scale problems [41, 42]. For this reason, a mediator with mass in the MeV range is also assumed.

4. **Quantum consistency:** The theory is assumed to be anomaly-free to ensure that unitarity is not violated. This poses constraints on the charges, which will be discussed in Sec. 3.3.2.

5. **Symmetry breaking:** It is postulated that the U(1) gauge symmetry present in the Dark Sector is spontaneously broken before the electroweak phase transition. It will be shown in Section 3.6.1 that this ensures that the Dark Matter particles have already attained their mass before freezing out and thus the correct relic density is recovered.

3.3 The Dark Sector

The dark sector is assumed to be populated by $2N$ fermions $\chi^{(j)}$ and $\chi'^{(j)}$ with $j \in \{1, \ldots, N\}$ which are singlets under the symmetries of the Standard Model. The total number of fermions must be even due to quantum consistency as will be shown below. Furthermore a vector mediator X_μ and a complex scalar field $\tilde{H}$ are also present. The postulated model has the following Lagrangian density:

$$\begin{aligned}\mathcal{L} \;=\;& \sum_{j=1}^{N} \overline{\chi_{\mathrm{L}}^{(j)}} \mathrm{i} \not{D} \chi_{\mathrm{L}}^{(j)} + \sum_{j=1}^{N} \overline{\chi_{\mathrm{R}}^{(j)}} \mathrm{i} \not{D} \chi_{\mathrm{R}}^{(j)} + \sum_{j=1}^{N} \overline{\chi_{\mathrm{L}}'^{(j)}} \mathrm{i} \not{D} \chi_{\mathrm{L}}'^{(j)} + \sum_{j=1}^{N} \overline{\chi_{\mathrm{R}}'^{(j)}} \mathrm{i} \not{D} \chi_{\mathrm{R}}'^{(j)} \\ & - \sum_{j=1}^{N} \overline{\chi_L^{(j)}} \frac{\tilde{H}}{v_{\mathrm{d}}} m_\chi^{(j)} \chi_R^{(j)} - \sum_{j=1}^{N} \overline{\chi_L'^{(j)}} \frac{\tilde{H}^*}{v_{\mathrm{d}}} m_{\chi'}^{(j)} \chi_R'^{(j)} - \mathrm{H.c.} \\ & - \frac{1}{4} X^{\mu\nu} X_{\mu\nu} - \frac{\epsilon}{2} B^{\mu\nu} X_{\mu\nu} + \left(D_\mu \tilde{H}\right)^* D^\mu \tilde{H} - \frac{\lambda}{2} \left(\tilde{H}^* \tilde{H} - v_{\mathrm{d}}^2\right)^2 + a^2 \tilde{H}^* \tilde{H} H^\dagger H \,.\end{aligned} \tag{3.3.1}$$

Here, $\chi_L^{(\prime)}$ and $\chi_R^{(\prime)}$ are the left- and right-chiral projections of the fermionic fields, respectively. The covariant derivative D_μ is defined as $D_\mu = \partial_\mu - \mathrm{i} X_\mu Q$, where Q is the charge operator corresponding to the $\mathrm{U}(1)_{\mathrm{DS}}$ symmetry in the Dark Sector. Note that the symmetry of the dark sector is denoted by $\mathrm{U}(1)_{\mathrm{DS}}$ in order to distinguish it from the $\mathrm{U}(1)_Y$ symmetry of the Standard Model. The dark fermions have chiral charges $Q_L^{(j)}$, $Q_R^{(j)}$, $Q_L'^{(j)}$, and $Q_R'^{(j)}$, and $\tilde{H}$ has charge $Q_{\tilde{H}}$. $B_{\mu\nu}$ is the field-strength tensor of the vector boson B_μ corresponding to the $U(1)_Y$ symmetry of the Standard Model, before the electroweak phase transition. $X_{\mu\nu}$ is the field-strength tensor associated with the new mediator X_μ and is defined as $X_{\mu\nu} = \partial_\mu X_\nu - \partial_\nu X_\mu$. Since it is allowed by the symmetry of the theory, a kinetic mixing term $B^{\mu\nu} X_{\mu\nu}$ is included for completeness. ϵ is a real parameter determining the strength of this mixing. Due to this coupling, the dark fermions obtain Standard-Model charges $Q_L \epsilon$ and $Q_R \epsilon$. This poses a strict constraint on the parameter ϵ which will be discussed in a later Section. v_{d} is the location of the minimum of the potential for the complex scalar field, while λ is the coupling strength of this potential. Furthermore, the parameter a describes the coupling between the dark complex scalar field and the Higgs doublet H in the Standard Model. This is the only relevant coupling between the Dark Sector and the Standard Model and will be discussed in more detail in the following.

3.3.1 Spontaneous symmetry breaking

The role of the complex scalar field $\tilde{H}$ is very similar to that of the Higgs field in the Standard Model. The complex scalar potential in Eq. (3.3.1) allows for a spontaneous symmetry breaking which results in the mediator X becoming massive at late times. The potential $-\lambda/2\left(\tilde{H}^*\tilde{H}-v_{\mathrm{d}}^2\right)^2$ is minimized by $\tilde{H}_0 = v_{\mathrm{d}}$. The field $\tilde{H}(x)$ can be expanded around this minimum as $\tilde{H}(x) = v_{\mathrm{d}} + \tilde{h}(x)/\sqrt{2}$ in unitary gauge, where $\tilde{h}(x)$ is a real scalar field. After the symmetry breaking, $\tilde{h}$ attains a mass $m_{\tilde{h}} = \sqrt{2\lambda}v_{\mathrm{d}}$. Furthermore, the kinetic term $\left(D_\mu\tilde{H}\right)^* D^\mu\tilde{H}$ yields a term $X_\mu X^{\mu *}Q_{\tilde{H}}^2 v_{\mathrm{d}}^2$ when expanded around the minimum of the complex scalar potential. This means that the previously massless mediator X now acquires a mass $m_X = Q_{\tilde{H}}v_{\mathrm{d}}$. It should be noted that in order for this to happen, it is crucial that $\tilde{H}$ is charged under the $\mathrm{U}(1)_{\mathrm{DS}}$ symmetry. Finally, the symmetry breaking is also responsible for the Dirac masses of the fermions of the theory, $m_\chi^{(j)}$ and $m_{\chi'}^{(j)}$, thanks to the Yukawa couplings in Eq. (3.3.1).

3.3.2 Quantum consistency

The newly postulated $\mathrm{U}(1)_{\mathrm{DS}}$ symmetry in the Dark Sector is non-anomalous if the condition $\partial_\mu\left\langle J^\mu_{\mathrm{U}(1)_{\mathrm{DS}}} J^\alpha_{\mathrm{U}(1)_{\mathrm{DS}}} J^\beta_{\mathrm{U}(1)_{\mathrm{DS}}}\right\rangle = 0$ is satisfied. Here, $J^\mu_{\mathrm{U}(1)_{\mathrm{DS}}}$ is the current

$$\begin{aligned} J^\mu_{\mathrm{U}(1)_{\mathrm{DS}}} &= \sum_{j=1}^{N}\left(Q_L^{(j)}\overline{\chi^{(j)}}\gamma^\mu\chi_L^{(j)} + Q_R^{(j)}\overline{\chi^{(j)}}\gamma^\mu\chi_R^{(j)}\right) \\ &\quad + \sum_{j=1}^{N}\left(Q_L'^{(j)}\overline{\chi'^{(j)}}\gamma^\mu\chi_L'^{(j)} + Q_R^{(j)}\overline{\chi'^{(j)}}\gamma^\mu\chi_R'^{(j)}\right) \end{aligned} \tag{3.3.2}$$

and $\langle\dots\rangle$ denotes the expectation value of the operator it surrounds. This condition is the same as for the Standard Model $\mathrm{U}(1)_Y$ symmetry and yields the following constraint on the charges,

$$\sum_{j=1}^{N}(Q_L^{(j)\,3} - Q_R^{(j)\,3}) = \sum_{j=1}^{N}(Q_R'^{(j)\,3} - Q_L'^{(j)\,3})\,. \tag{3.3.3}$$

Also analogously to the Standard Model, the $\mathrm{grav}^2 \times \mathrm{U}(1)_{\mathrm{DS}}$ anomaly vanishes if the condition

$$\sum_{j=1}^{N}(Q_L^{(j)} - Q_R^{(j)}) = \sum_{j=1}^{N}(Q_R'^{(j)} - Q_L'^{(j)}) \tag{3.3.4}$$

is satisified.

These charges are furthermore related to the charge of the dark scalar field $\tilde{H}$ through the Yukawa coupling in Eq. (3.3.1), from which it follows that

$$Q_{\tilde{H}} = Q_L^{(j)} - Q_R^{(j)} \quad , \tag{3.3.5}$$

$$Q_{\tilde{H}} = Q_R'^{(j)} - Q_L'^{(j)} \; . \tag{3.3.6}$$

From Eq. (3.3.4) it is clear that the number of χ fermions must be equal to the number of χ' fermions. Indeed, considering N_χ flavors for the χ particles and $N_{\chi'}$ for the χ' ones, the condition in Eq. (3.3.4) can be rewritten as

$$(N_\chi - N_{\chi'})\, Q_{\tilde{h}} = 0 \; . \tag{3.3.7}$$

This means that $N_\chi \stackrel{!}{=} N_{\chi'}$.

A relation for the charges satisfying both Eq. (3.3.4) and Eq. (3.3.3) is then given by

$$Q_L^{(j)} = -Q_L'^{(j)} \; , \; Q_R^{(i)} = -Q_R'^{(j)} \; . \tag{3.3.8}$$

Other solutions are present as well, but this one can be chosen without loss of generality.

3.3.3 Further remark on the dark charges

As discussed in Section 3.3.1, the mass of the dark mediator is $m_X = Q_{\tilde{H}} v_\mathrm{d}$. Since by assumption (3.) m_X is supposed to lie in the MeV range and by assumption (5.) $v_\mathrm{d} = \mathcal{O}(1)$ TeV, the conclusion $Q_{\tilde{H}} \lesssim 10^{-6}$ can be drawn. In particular, this means that $Q_R^{(j)} \approx Q_L^{(j)}$ and $Q_R'^{(j)} \approx Q_L'^{(j)}$ is true for all $j \in \{1, \ldots, N\}$. Thus, the approximation $g_j \approx Q_L^{(j)} \approx Q_R^{(j)}$ is valid. Analogously, the approximation $g_j \approx Q_L'^{(j)} \approx Q_r'^{(j)}$ can be made as well. The kinetic terms of the dark fermions are thus of the form $\overline{\chi^{(j)}}\mathrm{i}\left(\partial\!\!\!/ - \mathrm{i}X\!\!\!/ g_j\right)\chi^{(j)}$ and $\overline{\chi'^{(j)}}\mathrm{i}\left(\partial\!\!\!/ - \mathrm{i}X\!\!\!/ g_j'\right)\chi'^{(j)}$.

3.4 Relevant cross sections and decay rates

The cross sections which are relevant for the cosmological phenomenology of this model are calculated in this section. The annihilation cross section will determine the Dark Matter relic density. The temperature of kinetic decoupling will follow from the elastic scattering cross section and the self-interaction cross section will be responsible for decreasing the Dark Matter density near the center of halos.

3.4.1 Dark Matter annihilation

The Dark Matter particles can annihilate both into lighter dark fermions and into the dark mediator X. The diagrams for these two processes are given in Fig. 3.1 and Fig. 3.2.

The amplitude for the first process $\mathcal{M}_{\chi^{(i)}\chi^{(i)}\to\chi^{(\prime)\,(j)}\chi^{(\prime)\,(j)}}$ is given by

$$\begin{aligned} -\mathrm{i}\mathcal{M}_{\chi^{(i)}\chi^{(i)}\to\chi^{\prime\,(j)}\chi^{\prime\,(j)}} &= g_i g_j^{\prime}\frac{1}{(p_1+p_2)^2-m_X^2}\left[g_{\mu\nu}-\frac{(p_1+p_2)_\mu (p_1+p_2)_\nu}{m_X^2}\right] \\ &\quad \times\left[\overline{u}\,(p_3)\,\gamma^\nu v\,(p_4)\right]\left[\overline{v}\,(p_2)\,\gamma^\mu u\,(p_1)\right]\ . \end{aligned} \tag{3.4.1}$$

Since the mass of the annihilation products, $m_{\chi^{(\prime)}}^{(j)}$, is assumed to be negligible, the amplitude can be simplified as

$$-\mathrm{i}\mathcal{M}_{\chi^{(i)}\chi^{(i)}\to\chi^{(\prime)\,(j)}\chi^{(\prime)\,(j)}} = g_i g_j^{(\prime)}\frac{g_{\mu\nu}}{(p_1+p_2)^2-m_X^2}\left[\overline{u}\,(p_3)\,\gamma^\nu v\,(p_4)\right]\left[\overline{v}\,(p_2)\,\gamma^\mu u\,(p_1)\right]\ , \tag{3.4.2}$$

where the massless Dirac equations, $\overline{u}\,(p_3)\,\not{p}_3 = 0$ and $\not{p}_4 v\,(p_4) = 0$, have been used. The average of the square of this amplitude is then

$$\begin{aligned} \left\langle\left|\mathcal{M}^2_{\chi^{(i)}\chi^{(i)}\to\chi^{(\prime)\,(j)}\chi^{(\prime)\,(j)}}\right|\right\rangle &= \frac{\left(g_i g_j^{(\prime)}\right)^2}{4}\frac{32}{\left((p_1+p_2)^2-m_X^2\right)^2}\left(m^2_{\chi^{(i)}}\,(p_3\cdot p_4)\right. \\ &\quad \left. +\,(p_1\cdot p_4)\,(p_2\cdot p_3)+(p_1\cdot p_3)\,(p_2\cdot p_4)\right)\ . \end{aligned} \tag{3.4.3}$$

The prefactor 1/4 is due to the average over all ingoing spins. In the center-of-mass frame and in the non-relativistic limit, i.e. $\vec{p}_1, \vec{p}_2 \approx 0$, the averaged amplitude can be further simplified to

$$\left\langle\left|\mathcal{M}^2_{\chi^{(i)}\chi^{(i)}\to\chi^{(\prime)\,(j)}\chi^{(\prime)\,(j)}}\right|\right\rangle = 2\left(g_i g_j^{(\prime)}\right)^2\ . \tag{3.4.4}$$

where also the relation $m_{\chi^{(i)}} \gg m_X$ has been used. The thermally averaged cross section can then immediately be obtained from the amplitude and reads

$$\langle \sigma v_{\rm rel} \rangle_{\chi^{(i)}\chi^{(i)} \to \chi^{(\prime)\,(j)}\chi^{(\prime)\,(j)}} = \frac{1}{16\pi} \frac{\left(g_i g_j'\right)^2}{m^2_{\chi^{(i)}}} \,. \tag{3.4.5}$$

The two diagrams in Fig. 3.2 represent Dark Matter annihilations into the dark mediator X and have amplitudes

$$-\mathrm{i}\mathcal{M}_1 = -\mathrm{i}g_i^2 \overline{v}\,(p_2)\,\gamma^\mu \frac{\not{p}_1 - \not{p}_3 + m_{\chi^{(i)}}}{\left(p_1 - p_3\right)^2 - m^2_{\chi^{(i)}}} \gamma^\nu u\,(p_1)\,\epsilon_\nu\,(p_3)\,\epsilon_\mu\,(p_4) \tag{3.4.6}$$

and

$$-\mathrm{i}\mathcal{M}_2 = -\mathrm{i}g_i^2 \overline{v}\,(p_2)\,\gamma^\mu \frac{\not{p}_1 - \not{p}_4 + m_{\chi^{(i)}}}{\left(p_1 - p_4\right)^2 - m^2_{\chi^{(i)}}} \gamma^\nu u\,(p_1)\,\epsilon_\nu\,(p_4)\,\epsilon_\mu\,(p_3) \,. \tag{3.4.7}$$

These amplitudes must be added to obtain the total amplitude $\mathcal{M}_{\chi^{(i)}\chi^{(i)} \to XX} = \mathcal{M}_1 + \mathcal{M}_2$. In the center-of-mass frame and in the non-relativistic limit, the average of the squared amplitude is

$$\left\langle \left|\mathcal{M}_{\chi^{(i)}\chi^{(i)} \to XX}\right|^2 \right\rangle = 4g_i^4 \frac{1}{\left(2m^2_{\chi^{(i)}} - m_X^2\right)^2} \left(2m^4_{\chi^{(i)}} + 4m^2_{\chi^{(i)}} m_X^2\right) \,. \tag{3.4.8}$$

This can be further simplified using $m_{\chi^{(i)}} \gg m_X$,

$$\left\langle \left|\mathcal{M}_{\chi^{(i)}\chi^{(i)} \to XX}\right|^2 \right\rangle = 2g_i^4 \,. \tag{3.4.9}$$

The thermally averaged cross section is finally given by

$$\langle \sigma v_{\rm rel} \rangle_{\chi^{(i)}\chi^{(i)} \to XX} = \frac{1}{16\pi} \frac{g_i^4}{m^2_{\chi(j)}} \,. \tag{3.4.10}$$

Eqs. (3.4.5) and (3.4.10) can be combined to obtain the total cross section for the annihilation of Dark Matter particles $\chi^{(i)}$,

$$\left\langle \sigma_{\mathrm{ann},\,\chi^{(i)}} v_{\rm rel} \right\rangle = \frac{\pi}{m^2_{\chi^{(i)}}} \left(\sum_{j=1}^{N} \alpha'^2_{ij} + \sum_{j=1}^{N} \Theta\left(m_{\chi^{(i)}} - m_{\chi^{(j)}}\right) \alpha^2_{ij} + \Theta\left(m_{\chi^{(i)}} - m_X\right) \alpha^2_{ii} \right) \,, \tag{3.4.11}$$

where the notation $\alpha_{ij} \equiv g_i g_j / 4\pi$ and $\alpha'_{ij} \equiv g_i g'_j / 4\pi$ has been introduced. The Heavi-

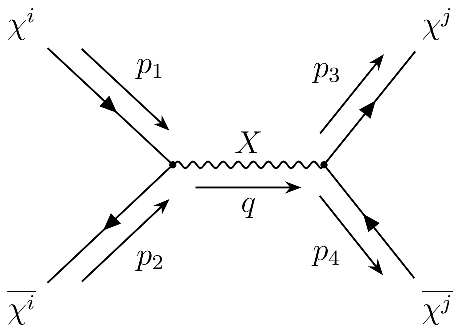

Figure 3.1: The Dark Matter annihilation channel into lighter fermions χ^j.

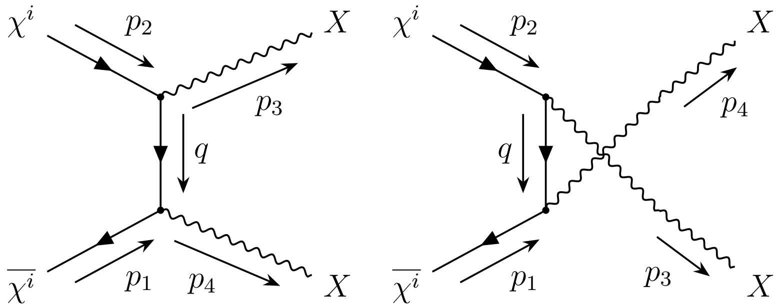

Figure 3.2: The Dark Matter annihilation channel into the mediator X.

side step functions ensure that only annihilations into lighter products are considered.

3.4.2 Elastic scattering

The cross section for the process of elastic scattering in Fig. 3.3 determines the kinetic decoupling of the Dark Matter particles from the radiation plasma of the Dark Sector.

The amplitude of this process is

$$-i\mathcal{M} = \frac{i g_i g_j'}{(p_4 - p_2)^2 - m_X^2} \left(g_{\mu\nu} - \frac{(p_4 - p_2)_\mu (p_4 - p_2)_\nu}{m_X^2} \right) \tag{3.4.12}$$

$$\times \left[\overline{u_{\chi^{(i)}}} (p_3) \gamma^\mu u_{\chi^{(i)}} (p_1) \right] \left[\overline{u_{\chi'^{(j)}}} (p_4) \gamma^\nu u_{\chi'^{(j)}} (p_2) \right] . \tag{3.4.13}$$

The longitudinal part of the propagator can be neglected here as well, since $\overline{u_{\chi'^{(j)}}} (p_4) \not{p}_4 \approx 0$ and $\not{p}_2 u_{\chi'^{(j)}} (p_2) \approx 0$. The average of the squared amplitude can thus be approximated by

$$\left\langle |\mathcal{M}|^2 \right\rangle \approx \frac{8 g_i^2 g_j'^2}{\left((p_4 - p_2)^2 - m_X^2\right)^2} \left[- \left(m_\chi^{(i)} \right)^2 p_2 \cdot p_4 + p_1 \cdot p_4 p_2 \cdot p_3 + p_1 \cdot p_2 p_3 \cdot p_4 \right] . \tag{3.4.14}$$

In the center-of-mass frame and assuming that the heavy dark fermions have negligible spatial momentum, the averaged squared amplitude is

$$\left\langle |\mathcal{M}|^2 \right\rangle = \frac{16 g_i^2 g_j'^2}{\left(2E^2 \left(1 - \cos\left(\theta\right)\right) + m_X^2\right)^2} E^2 \left(m_\chi^{(i)} \right)^2 \left(1 - \sin^2 \left(\frac{\theta}{2} \right) \right) , \tag{3.4.15}$$

where θ is the angle between the ingoing and outgoing $\chi'^{(j)}$'s and E is their energy.

The momentum-transfer cross section

$$\sigma_T = \int_0^{2\pi} \mathrm{d}\varphi \int_{-1}^{1} \mathrm{d}\cos\left(\theta\right) \left(1 - \cos\left(\theta\right)\right) \left(\frac{\mathrm{d}\sigma}{\mathrm{d}\Omega} \right)_{\mathrm{CM}} \tag{3.4.16}$$

can then be computed and yields

$$\sigma_T v_{\mathrm{rel}} = \frac{2}{3\pi} \frac{g_i^2 g_j'^2}{m_X^4} E^2 , \tag{3.4.17}$$

where v_{rel} is the relative velocity between the ingoing particles $\chi^{(i)}$ and $\chi'^{(j)}$.

Averaging over a Fermi-Dirac distribution in the highly relativistic approximation, since $\vec{p} \gg m_{\chi'^{(j)}}$, finally yields

$$\begin{aligned} \left\langle \sigma_T v_{\mathrm{rel}} \right\rangle &= \frac{2}{3\pi} g_i^2 g_j'^2 \frac{1}{4 m_X^4} \frac{\int_0^\infty \mathrm{d}p\, p^4 \frac{1}{\exp\left(\frac{p}{T}\right)+1}}{\int \mathrm{d}p\, p^2 \frac{1}{\exp\left(\frac{p}{T}\right)+1}} & (3.4.18) \\ &= \frac{1}{\pi} G_{ij'}^2 \frac{80 \zeta\left(5\right)}{\zeta\left(3\right)} T^2 , & (3.4.19) \end{aligned}$$

where $G'_{ij} = \sqrt{2} g_i g'_j / 4 m_X^2$ has been introduced.

3.5 Constraints on the parameter set

3.5.1 Masses in the Dark Sector

The dark matter particles $\chi^{(i)}$ are assumed to be stable and produced in local thermal equilibrium. Then, by requiring partial-wave unitarity of the scattering matrix, a

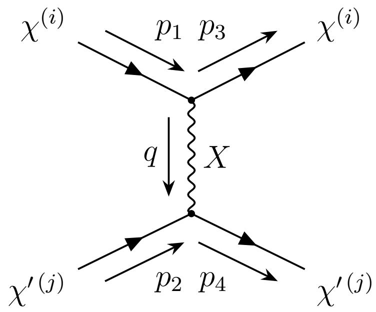

Figure 3.3: The diagram for the elastic scattering between the Dark Matter candidates and lighter particles in the Dark Sector.

maximal value for the annihilation cross section in the primordial Universe as a function of $m_\chi^{(i)}$ can be found. Since the relic density depends directly on this cross section, this bound can be transformed into a universal bound on the mass of the Dark Matter particle, $m_\chi^{(i)} < \mathcal{O}(300)$ TeV, by imposing $\Omega_{\chi^{(i)}} h^2 < 1$ [43].

The lightest dark fermion is the last scattering partner of Dark Matter and should be relativistic at the time of kinetic decoupling, T_{kd}. Without loss of generality this lightest fermion can always be renamed as $\chi'^{(1)}$ and then $m_{\chi'}^{(1)} \ll T_{\mathrm{kd}}$ must hold. A much more stringent constraint comes from requiring that the relic density of this lightest scattering partner is negligible. The relic density for this hot relic is $\Omega_{\chi'^{(1)}} h^2 = 7.83 \times 10^{-2}\,(g_{\mathrm{eff}}/g_{*,S})\,(m/\mathrm{eV})$ [44], which in this case yields $\Omega_{\chi'^{(1)}} h^2 \gtrsim m_{\chi'^{(1)}}/35$ eV and requiring a negligible contribution, e.g. $\Omega_{\chi'^{(1)}} h^2 < 0.02$, implies the constraint $m_{\chi'}^{(1)} < 0.68$ eV.

3.5.2 Coupling to the Standard Model

Constraints on the scalar portal between the Dark Sector and the Standard Model apply [45]. Indeed, through the scalar portal with coupling a^2 the Standard Model Higgs particle gets a slightly different mass. After diagonalizing the mass matrix, the variation of the Standard Model Higgs mass M_h up to orders of a^2 is $\Delta M_h^2 = a^2 v_{\mathrm{d}}^2$. This, together with the assumption $v_{\mathrm{d}} \gtrsim M_h$ (as by assumption (5.)) and the experimental error on the Higgs mass $\Delta M_h \lesssim 0.17$ GeV [46], implies the constraint $a \lesssim 10^{-3}$ on the bridge coupling a.

3.5.3 Dark charges

The condition that the Dark Matter particles must have been thermally produced can be formulated as

$$\left\langle \sigma_{\chi'^{(j)}\chi'^{(j)}\to\chi^{(i)}\chi^{(i)}} v_{\mathrm{rel}} \right\rangle n_{\chi'^{(j)}} \left(m_{\chi^{(j)}}\right) > H\left(m_{\chi^{(i)}}\right) \;, \tag{3.5.1}$$

since $T = m_{\chi^{(i)}}$ is the temperature at which production of $\chi^{(i)}$ stops. This condition must apply to all Dark Matter particles which contribute significantly to the final Dark Matter relic density. With the relevant part in the cross section in Eq. (3.4.11) and using $H(T) = 1.66\sqrt{106.75}T^2/M_{\mathrm{Pl}}$ and $n_{\chi'^{(j)}}(T) = (3\zeta(3)/4\pi^2)4T^3$, the condition

$$\alpha'_{ij} > 3.87\sqrt{\frac{m_{\chi^{(i)}}}{M_{\mathrm{Pl}}}} \quad \text{for all } j \in \{1, \ldots, N\} \tag{3.5.2}$$

is derived, where M_{Pl} is the Planck mass.

3.5.4 Effective degrees of freedom

Within the Standard Model the energy density of radiation can be parametrized as

$$\rho_{\mathrm{rad}} = \rho_\gamma + \frac{\pi^2}{30}\frac{7}{4}N_\nu T_\nu^4 \;, \tag{3.5.3}$$

where the effective number of neutrinos is $N_\nu = 3.046$. The presence of the newly postulated Dark Sector modifies this expression to

$$\rho_{\mathrm{rad}} = \rho_\gamma + \frac{\pi^2}{30}\frac{7}{4}N_{\mathrm{eff}} T_\nu^4 \;, \tag{3.5.4}$$

where $N_{\mathrm{eff}} = N_\nu + \Delta N_{\mathrm{eff}}$ and

$$\Delta N_{\mathrm{eff}} = N_\nu \frac{\rho_{\mathrm{rel}}^{(\mathrm{DS})}}{\rho_\nu} \;. \tag{3.5.5}$$

Here, $\rho_{\mathrm{rel}}^{(\mathrm{DS})}$ is the energy density of all relativistic particles in the Dark Sector.

From Eq. (3.5.5) it is clear that the ratio between the temperatures of the Dark Sector T_{DS} and that of neutrinos T_ν plays a crucial role in determining ΔN_{eff}. Assuming that the Dark Sector and the Standard Model are in thermal contact until some temperature T_{D}, the ratio $\varepsilon \equiv (T_{\mathrm{DS}}/T_\nu)^3$ can be computed by requiring the entropy densities of the two sectors to be conserved separately,

$$\frac{s_{\rm SM}}{s_{\rm DS}} = \text{const.}\ . \tag{3.5.6}$$

Immediately after the decoupling of the two sectors, i.e. right after $T_{\rm D}$, the temperature of the Standard Model and the one of the Dark Sector are still the same. This means

$$\frac{g_{\rm S,\,SM}\,(T_D)}{g_{\rm S,\,DS}\,(T_{\rm D})} = \text{const.}\ , \tag{3.5.7}$$

where $g_{\rm S,\,\mathit{DS}}$ are the entropy degrees of freedom of the Dark Sector and $g_{\rm S,\,\mathit{SM}}$ are the ones of the Standard Model. At some different time, characterized by a temperature $T_{\rm DS}$ in the Dark Sector and T_ν for the neutrinos in the Standard Model, the above ratio becomes

$$\frac{g_{\rm S,\,\mathit{SM}}\,(T_\nu)}{g_{\rm S,\,\mathit{DS}}\,(T_{\rm DS})}\frac{T_\nu^3}{T_{\rm DS}^3} = \text{const.}\ . \tag{3.5.8}$$

Note that the effective number of degrees of freedom is given with respect to the temperature of the neutrinos and not to the temperature of the photons.

The explicit expression for $\varepsilon\,(T_{\rm DS})$ is thus finally

$$\varepsilon\,(T_{\rm DS}) = \frac{g_{\rm S,\,\mathit{DS}}\,(T_{\rm D})}{g_{\rm S,\,\mathit{SM}}\,(T_{\rm D})}\frac{g_{\rm S,\,\mathit{SM}}\,(T_\nu)}{g_{\rm S,\,\mathit{DS}}\,(T_{\rm DS})}\ . \tag{3.5.9}$$

It should be noted, that assumption (2.) was necessary to obtain the above expression for ε.

The value of $\Delta N_{\rm eff}$ at the time of neutron-proton freeze-out is highly constrained by Big Bang Nucleosynthesis. Indeed, the effect on the ^{4}He abundance can be quantified in the following way. The presence of extra degrees of freedom increases the neutron-proton freeze-out temperature $T_\gamma^{\rm fr}$ by

$$\Delta T_\gamma^{\rm fr} \simeq T_\gamma^{\rm fr}\frac{1}{6}\frac{7}{4}\frac{\Delta N_{\rm eff}}{g_{\rm SM}\left(T_\gamma^{\rm fr}\right)}\ , \tag{3.5.10}$$

where $g_{\rm SM}\left(T_\gamma^{\rm fr}\right)$ are the relativistic energy degrees of freedom of the Standard Model at the time of freeze-out [47]. This, in turn, modifies the neutron-to-proton ratio at the time of Big Bang Nucleosynthesis by

$$\Delta\left(\frac{n_n}{n_p}\right)_{\rm BBN} \simeq \frac{m_n - m_p}{T_\gamma^{\rm fr}}\left(\frac{n_n}{n_p}\right)_{\rm BBN}\frac{\Delta T_\gamma^{\rm fr}}{T_\gamma^{\rm fr}}\ , \tag{3.5.11}$$

where n_n and n_p are the neutron and proton number densities, respectively. The ^{4}He mass fraction $Y_p \simeq (2n_n/(n_n+n_p))_{BBN}$ thus increases as well by

$$\Delta Y_p \simeq Y_p \left(1-\frac{Y_p}{2}\right)\frac{1}{6}\frac{m_n-m_p}{T_\gamma^{\mathrm{fr}}}\frac{7}{4}\frac{\Delta N_{\mathrm{eff}}}{g_{\mathrm{SM}}\left(T_\gamma^{\mathrm{fr}}\right)} \,. \tag{3.5.12}$$

Therefore, measurements of the ^{4}He mass fraction implicitly impose a constraint on ΔN_{eff} at the time of neutron-proton freeze-out. The first case considered is the one with $N=1$. Since by assumption (5.) the temperature of decoupling between the Dark Sector and the Standard Model is in the $\mathcal{O}(100)$ GeV range and by assumption (3.) $m_\chi^{(1)} \approx 1$ TeV, the only relativistic particles at T_D are the mediator X and the light scattering partner $\chi'^{(1)}$, i.e. $g_{\mathrm{S},DS}(T_{\mathrm{D}}) = 7/2+3 = 6.5$. At the neutron-proton freeze-out temperature by assumption (3.) only the light fermions $\chi'^{(1)}$ are still relativistic and thus $g_{\mathrm{S},DS}\left(T_\gamma^{\mathrm{fr}}\right) = 3.5$. The entropy degrees of freedom of the Standard Model are $g_{\mathrm{S},SM}(T_{\mathrm{D}}) = 106.5$ and $g_{\mathrm{S},SM}\left(T_\gamma^{\mathrm{fr}}\right) = 2\times\ +3\times 7/4 + 2\times\frac{7}{4} = 10.75$. It should be noted that at this time, the electron-positron annihilation has not happened yet and thus neutrinos and photons still have the same temperature. In consequence, the deviation of the effective number of degrees of freedom is given by

$$\Delta N_{\mathrm{eff}} = N_\nu \frac{\rho_{\chi'}}{\rho_\nu} = 2\varepsilon^{\frac{4}{3}}\left(T_\gamma^{\mathrm{fr}}\right) \approx 0.214 \,. \tag{3.5.13}$$

In an analogous way, the value of ΔN_{eff} at the time of neutron-proton freeze-out can be calculated for the case of two generations, i.e. $N=2$. The main difference is simply that more possibilities are available depending on the mass scale of the extra particles. The results are summarized in Table 3.1. The constraint $\Delta Y_p \lesssim 0.004$ [48] implies a constraint $\Delta N_{\mathrm{eff}} \lesssim 0.36$ at the time of neutron-proton freeze-out [47]. This allows only scenarios I and IV from Table 3.1. For $N>2$ only the equivalent of scenario I in Table 3.1 is acceptable, which has the same phenomenology of the scenario of $N=1$.

The deviation of the effective number of neutrinos at the time of recombination is constrained as well. Indeed, an increase in the energy density at the temperature of recombination implies a larger expansion rate which would cause noticeable effects on the CMB power spectrum: the first peak would be higher and the other peaks would be shifted towards higher multipoles [47]. Within this model, at the temperature of recombination ($T_{\mathrm{rec}} \approx 0.3$ eV) only the lightest fermions in the Dark Sector satisfying $m_{\chi'}^{(j)} < T_{\mathrm{rec}}$ can still be relativistic and can contribute to the expression in Eq. 3.5.5.

	$N=1$	$N=2$					
		I	II	III	IV	V	VI
T	$m_{\chi}^{(1)}$	$m_{\chi'}^{(1)}, m_{\chi}^{(2)}, m_{\chi}^{(1)}$	$m_{\chi}^{(1)}, m_{\chi}^{(2)}$	$m_{\chi}^{(1)}$	$m_{\chi}^{(1)}, m_{\chi}^{(2)}$	$m_{\chi}^{(1)}$	$m_{\chi}^{(1)}$
T_{D}			$m_{\chi'}^{(1)}$	$m_{\chi'}^{(1)}, m_{\chi}^{(2)}$			$m_{\chi}^{(2)}$
T_{γ}^{fr}	$m_{\chi'}^{(1)}$	$m_{\chi'}^{(2)}$	$m_{\chi'}^{(2)}$	$m_{\chi'}^{(2)}$	$m_{\chi'}^{(1)}, m_{\chi'}^{(2)}$	$m_{\chi'}^{(1)}, m_{\chi}^{(2)}, m_{\chi'}^{(2)}$	$m_{\chi'}^{(1)}, m_{\chi'}^{(2)}$
$\Delta N_{\mathrm{eff}}\left(T_{\gamma}^{\mathrm{fr}}\right)$	0.21	0.21	0.38	0.57	0.30	0.39	0.45

Table 3.1: Mass spectra of dark fermions in accordance with the assumptions. Masses written in the first row lie well above the temperature of decoupling between the Dark Sector and the Standard Model, T_{D}. Masses in the third row lie well below the temperature of neutron-proton freeze-out T_{γ}^{fr}.

The generic expression for the energy density of each species $\chi'^{(j)}$ is

$$\rho_{\chi'^{(j)}}^{\mathrm{DS}}\left(T_{\chi'^{(j)}}\right) = \frac{g_{\chi'^{(j)}}}{2\pi^2}\int_{m_{\chi'}^{(j)}}^{\infty} \frac{\sqrt{E^2-\left(m_{\chi'}^{(j)}\right)^2}}{\exp\left(\frac{E}{T_{\chi'^{(j)}}}\right)+1} E^2 \mathrm{d}E \ . \tag{3.5.14}$$

It should be noted here that the temperature $T_{\chi'^{(j)}}$ is that of the particles in the Dark Sector. After recombination, $T_{\chi'^{(j)}}$ is related to the photon temperature by

$$T_{\chi'^{(j)}} = \varepsilon\left(T_{\mathrm{rec}}\right)^{\frac{1}{3}}\left(\frac{4}{11}\right)^{\frac{1}{3}} T_{\gamma} \ . \tag{3.5.15}$$

Thus, after using the reparametrization $z = E/T_{\chi'^{(j)}}$ and inserting $\rho_{\nu} = (7\pi^2/120)\, N_{\nu} T_{\nu}^4$ in Eq. (3.5.5), the deviation at recombination becomes

$$\frac{\Delta N_{\mathrm{eff}}\left(T_{\mathrm{rec}}\right)}{\varepsilon\left(T_{\mathrm{rec}}\right)^{\frac{4}{3}}} = \frac{60}{7\pi^4}\sum_j g_{\chi'^{(j)}} \int_{x_{\mathrm{rec}}'^{(j)}}^{\infty} \frac{z^2\sqrt{z^2-\left(x_{\mathrm{rec}}'^{(j)}\right)^2}}{\exp(z)+1}\mathrm{d}z \ , \tag{3.5.16}$$

where $x_{\mathrm{rec}}'^{(j)} = m_{\chi'}^{(j)}\varepsilon\left(T_{\mathrm{rec}}\right)^{-1/3}(4/11)^{-1/3}/T_{\mathrm{rec}}$ was introduced and the sum runs over all j's such that the corresponding particles still give a non-negligible contribution to the energy density at the time of recombination.

For the case $N = 1$, Eq. (3.5.16) can be computed univocally and the result only depends on the mass of the only remaining particle. This is represented in Fig. 3.4. The maximal deviation from the Standard Model value is obtained for

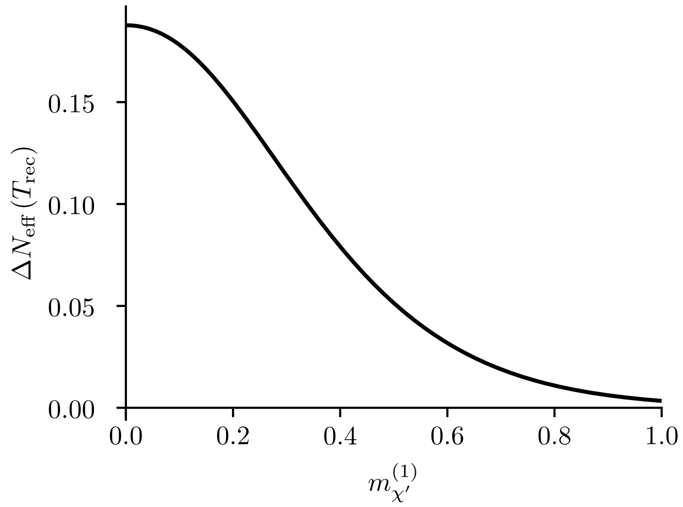

Figure 3.4: The value of ΔN_{eff} at the time of recombination as a function of the mass $m^{(1)}_{\chi'}$ for the case of $N = 1$.

the case of massless particles, while already for values of approximately 1 eV the deviation is negligible, although the constraint $m^{(1)}_{\chi'} \lesssim 0.65$ eV from Sec. 3.5.1 should also be taken into account. If one chooses $m^{(1)}_{\chi'} = 0.6$ eV, satisfying this constraint, the corresponding value for ΔN_{eff} at recombination is $\Delta N_{\text{eff}} \approx 0.03$ which lies well within the range expected by observations [1]. Even the limiting case $m^{(1)}_{\chi'} \approx 0$ yields values of $\Delta N_{\text{eff}} \approx 0.188$ which still lie within the constraints [1]. Furthermore, since $\Delta N_{\text{eff}}\left(T^{\text{fr}}_{\gamma}\right) \approx 0.214$ is larger than $\Delta N_{\text{eff}}\,(T_{\text{rec}})$, this provides a possible explanation for the decrease of the effective number of degrees of freedom between BBN- and CMB-based measurements [1].

For the case $N = 2$ the situation is less straightforward. For example, if $m^{(2)}_{\chi'}$ is much larger than the temperature of recombination, then its contribution to Eq. 3.5.16 is effectively negligible and ΔN_{eff} remains unchanged. However, if it has a mass similar to $m^{(1)}_{\chi'}$, the deviation increases approximately by a factor of two. For example, the case $m^{(1)}_{\chi'} = m^{(2)}_{\chi'} = 0.6$ eV yields $\Delta N_{\text{eff}} \approx 0.06$ which is still comfortably within the bounds given by Planck [1], while the case $m^{(1)}_{\chi'} = m^{(2)}_{\chi'} = 0$, yielding $\Delta N_{\text{eff}} \approx 0.38$, is excluded.

3.6 Cosmological observables

The most important cosmological observables are discussed in this section: the relic abundance, the temperature of kinetic decoupling with the corresponding damping masses, and the cross section for self-interactions.

3.6.1 The relic abundance

The relic abundance of the Dark Matter particles is determined by the Boltzmann equation,

$$(L - C)\left[f_{\chi^{(i)}}\right](\vec{p}) = 0 \,, \tag{3.6.1}$$

which describes the evolution of the Dark Matter distribution function, $f_{\chi^{(i)}}$. The operator L is the Liouville operator, which is defined by

$$L\left[f_{\chi^{(i)}}\right] = \frac{\mathrm{d}f_{\chi^{(i)}}}{\mathrm{d}\lambda} = m_\chi^{(i)} \frac{\mathrm{d}p^i}{\mathrm{d}\tau} \frac{\partial f_{\chi^{(i)}}}{\partial p^i} \,, \tag{3.6.2}$$

where τ denotes the proper time of the particles and the affine parameter $\lambda = \tau / m_{\chi^{(i)}}$ has been used. In a flat Friedmann-Robertson-Walker universe, the geodesic equation allows the Liouville operator to be rewritten as

$$L\left[f_{\chi^{(i)}}\right] = E\left(\partial_t - H p^i \frac{\partial}{\partial p^i}\right) f_{\chi^{(i)}} \,, \tag{3.6.3}$$

where $H = \dot{a}/a$ is the Hubble parameter. As discussed in Section 3.4.1, any dark fermion $\chi^{(j)}$ has three possible annihilation channels: some lighter (but still heavy) fermions $\chi^{(i)}$, the much lighter $\chi'^{(i)}$ and the mediator X. For this reason, the collision term in Eq. (3.6.1) is given by the sum of the contributions of these three processes,

$$C\left[f_{\chi^{(j)}}\right](\vec{p}) = C_1\left[f_{\chi^{(j)}}\right](\vec{p}) + C_2\left[f_{\chi^{(j)}}\right](\vec{p}) + C_3\left[f_{\chi^{(j)}}\right](\vec{p}) \,, \tag{3.6.4}$$

where

$$\begin{aligned} C_1\left[f_{\chi^{(j)}}\right](\vec{p}) \;\; = \;\; & \sum_i \Theta\left(m_{\chi^{(j)}} - m_\chi^{(i)}\right) \int \frac{\mathrm{d}^3\vec{p}_2}{E_2} \frac{\mathrm{d}^3\vec{p}_3}{E_3} \frac{\mathrm{d}^3\vec{p}_4}{E_4} \delta^4\left(p_1 + p_2 - p_3 - p_4\right) |\mathcal{M}_1|^2 \\ & \times \Big[f_{\chi^{(i)}}(\vec{p}_3) f_{\chi^{(i)}}(\vec{p}_4) \left(1 - f_{\chi^{(j)}}(\vec{p}_2)\right)\left(1 - f_{\chi^{(j)}}(\vec{p})\right) \\ & - f_{\chi^{(j)}}(\vec{p}) f_{\chi^{(j)}}(\vec{p}_2) \left(1 - f_{\chi^{(i)}}(\vec{p}_3)\right)\left(1 - f_{\chi^{(i)}}(\vec{p}_4)\right) \Big] \,, \end{aligned} \tag{3.6.5}$$

$$\begin{aligned} C_2\left[f_{\chi^{(j)}}\right](\vec{p}) \;=\; & \sum_i \int \frac{\mathrm{d}^3\vec{p}_2}{E_2}\frac{\mathrm{d}^3\vec{p}_3}{E_3}\frac{\mathrm{d}^3\vec{p}_4}{E_4}\delta^4\left(p_1+p_2-p_3-p_4\right)\left|\mathcal{M}_2\right|^2 \\ & \times\Big[f_{\chi'^{(i)}}\left(\vec{p}_3\right)f_{\chi'^{(i)}}\left(\vec{p}_4\right)\Big(1-f_{\chi^{(j)}}\left(\vec{p}_2\right)\Big)\Big(1-f_{\chi^{(j)}}\left(\vec{p}\right)\Big) \\ & -f_{\chi^{(j)}}\left(\vec{p}\right)f_{\chi^{(j)}}\left(\vec{p}_2\right)\Big(1-f_{\chi'^{(i)}}\left(\vec{p}_3\right)\Big)\Big(1-f_{\chi'^{(i)}}\left(\vec{p}_4\right)\Big)\Big] \end{aligned} \tag{3.6.6}$$

and

$$\begin{aligned} C_3\left[f_{\chi^{(j)}}\right](\vec{p}) \;=\; & \int \frac{\mathrm{d}^3\vec{p}_2}{E_2}\frac{\mathrm{d}^3\vec{p}_3}{E_3}\frac{\mathrm{d}^3\vec{p}_4}{E_4}\delta^4\left(p_1+p_2-p_3-p_4\right)\left|\mathcal{M}_3\right|^2 \\ & \times\Big[f_X\left(\vec{p}_3\right)f_X\left(\vec{p}_4\right)\Big(1-f_{\chi^{(j)}}\left(\vec{p}_2\right)\Big)\Big(1-f_{\chi^{(j)}}\left(\vec{p}\right)\Big) \\ & -f_{\chi^{(j)}}\left(\vec{p}\right)f_{\chi^{(j)}}\left(\vec{p}_2\right)\left(1-f_X\left(\vec{p}_3\right)\right)\left(1-f_X\left(\vec{p}_4\right)\right)\Big]\ . \end{aligned} \tag{3.6.7}$$

Here, $\mathcal{M}_1$, $\mathcal{M}_2$ and $\mathcal{M}_3$ are the scattering amplitudes for annihilation into heavy dark fermions, lighter dark fermions and the mediator, respectively.

Using the diluted-gas approximation, $1-f_{\chi^{(i)}}\approx 1$, $1-f_{\chi'^{(i)}}\approx 1$ and $1-f_X\approx 1$, and the fact that all particles other than $\chi^{(j)}$ are in thermal equilibrium (e.g. $f_X\left(\vec{p}_3\right)f_X\left(\vec{p}_4\right)=f^{(\mathrm{eq})}_{\chi^{(j)}}\left(\vec{p}\right)f^{(\mathrm{eq})}_{\chi}\left(\vec{p}_2\right)$) the collision term can be rewritten as

$$C\left[f_{\chi^{(j)}}\right](\vec{p})=\int\frac{\mathrm{d}^3\vec{p}_2}{(2\pi)^3}\sigma_{\mathrm{ann}}v_{\mathrm{rel}}\left[f^{(\mathrm{eq})}_{\chi^{(j)}}\left(\vec{p}\right)f^{(\mathrm{eq})}_{\chi^{(j)}}\left(\vec{p}_2\right)-f_{\chi^{(j)}}\left(\vec{p}\right)f_{\chi^{(j)}}\left(\vec{p}_2\right)\right]\ . \tag{3.6.8}$$

It should be noted that this is the whole collision term, since the information about the different annihilation channels is now contained in the total annihilation cross section from Eq. (3.4.11).

From $f_{\chi^{(i)}}=\left(n_{\chi^{(i)}}/n^{(\mathrm{eq})}_{\chi^{(i)}}\right)f^{(\mathrm{eq})}_{\chi^{(i)}}$ follows

$$f^{(\mathrm{eq})}_{\chi^{(i)}}\left(\vec{p}\right)f^{(\mathrm{eq})}_{\chi^{(i)}}\left(\vec{p}_2\right)-f_{\chi^{(i)}}\left(\vec{p}\right)f_{\chi^{(i)}}\left(\vec{p}_2\right)=f^{(\mathrm{eq})}_{\chi^{(i)}}\left(\vec{p}\right)f^{(\mathrm{eq})}_{\chi^{(i)}}\left(\vec{p}_2\right)\left(1-\frac{n^2_{\chi^{(i)}}}{n^{(\mathrm{eq})}_{\chi^{(i)}}}\right)\ , \tag{3.6.9}$$

where $n_{\chi^{(i)}}$ is the number density of the $\chi^{(i)}$ particles. Dividing Eq. (3.6.1) by E and integrating over $\vec{p}$ finally yields

$$\dot{n}_{\chi^{(i)}}+3Hn_{\chi^{(i)}}=\left(n^{(\mathrm{eq})}_{\chi^{(i)}}n^{(\mathrm{eq})}_{\chi^{(i)}}-n_{\chi^{(i)}}n_{\chi^{(i)}}\right)\left\langle\sigma_{\mathrm{ann}}v_{\mathrm{rel}}\right\rangle\ . \tag{3.6.10}$$

The derivative of the *particle yield* $Y_{\chi^{(i)}}$, defined as $Y_{\chi^{(i)}}=n_{\chi^{(i)}}/s$ where s is the

Universe's entropy density, is then

$$\begin{aligned}
\dot{Y}_{\chi^{(i)}} &= \frac{\dot{n}_{\chi^{(i)}}}{s} - \frac{\dot{s}}{s^2} n_{\chi^{(i)}} && (3.6.11)\\
&= \frac{\dot{n}_{\chi^{(i)}}}{s} + 3H \frac{n_{\chi^{(i)}}}{s} && (3.6.12)\\
&= \frac{1}{s} \langle \sigma_{\text{ann}} v_{\text{rel}} \rangle \left(n^{(\text{eq})}_{\chi^{(i)}} n^{(\text{eq})}_{\chi^{(i)}} - n_{\chi^{(i)}} n_{\chi^{(i)}} \right) && (3.6.13)\\
&= \langle \sigma_{\text{ann}} v_{\text{rel}} \rangle \, s \left(Y^{(\text{eq})}_{\chi^{(i)}} Y^{(\text{eq})}_{\chi^{(i)}} - Y_{\chi^{(i)}} Y_{\chi^{(i)}} \right) \ , && (3.6.14)
\end{aligned}$$

where the Boltzmann equation was used in the last step and $Y^{(\text{eq})}_{\chi^{(i)}} \equiv n^{(\text{eq})}_{\chi^{(i)}}/s$.

After defining $x = m_{\chi^{(i)}}/T$, the time derivative can be rewritten as $d/dt = Hx\, d/dx$. This allows to express the change of $Y_{\chi^{(i)}}$ w.r.t. x as

$$\frac{\mathrm{d}Y_{\chi^{(i)}}}{\mathrm{d}x} = -\frac{\lambda}{x^2} \left(Y_{\chi^{(i)}} Y_{\chi^{(i)}} - Y^{(\text{eq})}_{\chi^{(i)}} Y^{(\text{eq})}_{\chi^{(i)}} \right) \tag{3.6.15}$$

with the efficiency $\lambda \equiv \langle \sigma_{\text{ann}} v_{\text{rel}} \rangle \, s\,(x=1)\,/H\,(x=1)$.

Since at late times, i.e. at large values of x, the equilibrium particle yield is exponentially suppressed, the differential equation can be solved by separation of variables. The integration is done between the time of freeze-out x_{f}, when the $\chi^{(i)}$'s departed from the equilibrium distribution, and the asymptotic value $x \to \infty$. This yields

$$\frac{1}{\lambda Y_\infty} - \frac{1}{\lambda Y_{\text{f}}} = \frac{1}{x_f} \ , \tag{3.6.16}$$

which can be further simplified to

$$Y_\infty = \frac{x_{\text{f}}}{\lambda}, \tag{3.6.17}$$

when using the approximation $Y_{\text{f}} \gg Y_\infty$. Using Y_∞, the relic density today is given by

$$\Omega_{\chi^{(i)}} h^2 = \frac{Y_\infty s_0 m_{\chi^{(i)}}}{\rho_c/h^2} \ , \tag{3.6.18}$$

where s_0 is the entropy density today, ρ_c is the critical energy density today and $h = 0.674 \pm 0.005$ is the Hubble parameter today in units of $100\,\text{km/s}\,\text{Mpc}$[1].

The time of freeze-out x_{f} appearing in Y_∞ is obtained from the condition

$$\langle v_{\text{rel}} \sigma_{\text{ann}} \rangle \, n^{(\text{eq})}_{\chi^{(i)}}(x_{\text{f}}) \stackrel{!}{=} H(x_{\text{f}}) \ . \tag{3.6.19}$$

Since $H(x_\mathrm{f}) = H(x=1)\, x_\mathrm{f}^{-2}$ and $n^{(\mathrm{eq})}_{\chi^{(i)}}(x_\mathrm{f}) = n^{(eq)}_{\chi^{(i)}}(x=1)\, x_f^{-3/2} e^{-x_\mathrm{f}+1}$, this condition can be rewritten as

$$C = x_\mathrm{f}^{-\frac{1}{2}} e^{x_\mathrm{f}} \,, \tag{3.6.20}$$

with

$$C = \frac{\langle v_\mathrm{rel}\sigma_\mathrm{ann}\rangle|_{x=1}\, n^{(eq)}_{\chi^{(i)}}(x=1)\, e}{H(x=1)} \,. \tag{3.6.21}$$

The exact solution of Eq. (3.6.20) is $x_f = W_0(2C^2)/2$, where W_0 is the principal branch of the Lambert W function. A sufficiently good approximation for large values of C is

$$x_\mathrm{f} \approx \ln(C) - \frac{\frac{1}{2}\ln(\ln(C))}{1 + \frac{1}{2}\ln^{-1}(C)} \,. \tag{3.6.22}$$

Introducing $\alpha = \sum_j \alpha_{ij} \Theta\left(m_\chi^{(i)} - m_{\chi^{(j)}}\right) + \alpha'_{ij}\Theta\left(m_\chi^{(i)} - m_{\chi'^{(j)}}\right) + \Theta\left(m_\chi^{(i)} - m_X\right)$ and choosing $\alpha \approx 0.1$ and $m_{\chi^{(i)}} \approx 10$ TeV, $x_f \approx 30$ is obtained. This choice of parameters is in accordance with the values which will later be found to be the most phenomenologically desirable ones in this model.

Using this value of x_f and the other parameters of this model the relic density from Eq. (3.6.18) can be written as

$$\Omega_{\chi^{(i)}} h^2 \approx 0.06 \left(\frac{\alpha}{0.1}\right)^{-2} \left(\frac{m_{\chi^{(i)}}}{10\mathrm{TeV}}\right)^2 \,. \tag{3.6.23}$$

Taking into account the Dark-Matter antiparticles, $\overline{\chi^{(i)}}$, the total relic density is then $\Omega_{\chi^{(i)}\overline{\chi^{(i)}}} h^2 \approx 0.12$ for $\alpha \approx 0.1$ and $m_{\chi^{(i)}} \approx 10\,\mathrm{TeV}$, in agreement with ΛCDM predictions.

3.6.2 Self-interactions

Self-interactions are well known to be able to solve the cusp vs core, too big to fail and diversity problems [41, 49, 50, 51]. To maintain the large-scale success of collisionless Dark Matter, self-interactions should only become relevant at small scales, i.e. towards the center of the halo. These collisions increase the entropy of the Dark Matter phase-space distribution near the center and thus create a flattened density profile and a Dark Matter distribution which is more spherical rather than elliptical [52]. Furthermore, since the inner regions of subhalos have a shallower density profile, their velocity profiles are modified as well: the rotational velocity is smaller at smaller radii compared to simulations within the ΛCDM model. This has been shown to solve the too big to fail problem [41]. Finally, due to these self-interactions in the inner regions of halos, the Dark Matter density behaves like an ideal gas and must satisfy the hydrodynamic equilibrium condition, $\sigma_0^2 \nabla^2 \ln(\rho_{\rm dm}) = -4\pi G (\rho_{\rm dm} + \rho_{\rm b})$, where σ_0 is the one-dimensional Dark Matter velocity dispersion. Thus, the Dark Matter density profile near the center, $\rho_{\rm dm}$, is highly dependent on the baryonic density, $\rho_{\rm b}$, which can vary greatly depending on the formation history of each galaxy. This provides a solution to the diversity problem [51].

To address all the small-scale problems mentioned above, the value of $\left\langle \sigma_T / m_{\chi^{(i)}} \right\rangle_{v_0}$ should lie between 0.1 $\mathrm{cm}^2\ \mathrm{g}^{-1}$ and 1 $\mathrm{cm}^2\ \mathrm{g}^{-1}$ at small scales. Specifically, at the scale of dwarf galaxies, where $v_{\rm therm} \approx 30\,\mathrm{km/s}$, $\left\langle \sigma_T / m_{\chi^{(i)}} \right\rangle_{30} \approx 1\,\mathrm{cm}^2\,\mathrm{g}^{-1}$ should hold; at large scales, where $v_{\rm therm} \approx 1000\,\mathrm{km/s}$, the condition $\left\langle \sigma_T / m_{\chi^{(i)}} \right\rangle_{100} < 0.1\,\mathrm{cm}^2\,\mathrm{g}^{-1}$ should be satisfied. Here, the average is taken over a Maxwell-Boltzmann distribution centered around the most probable velocity v_0,

$$\frac{\langle \sigma_T \rangle_{v_{\rm therm}}}{m_{\chi^{(i)}}} = \frac{1}{m_X^{(i)}} \int \mathrm{d}^3 v \frac{1}{(2\pi v_{\rm therm})^{3/2}} e^{-\frac{v^2}{v_{\rm therm}^2}} \sigma_T \ . \tag{3.6.24}$$

Since in this case both attractive ($\chi^{(i)}\overline{\chi^{(i)}}$) and repulsive ($\chi^{(i)}\chi^{(i)}$ and $\overline{\chi^{(i)}\chi^{(i)}}$) interactions are present, σ_T must be taken as the average over the cross section of these two kinds of interactions. The cross section for self-interactions in the classical regime ($m_{\chi^{(i)}} v / m_X \ll 1$) for a repulsive potential is

$$\sigma_T^{\rm clas} = \begin{cases} \frac{2\pi^2}{m_X^2} \beta^2 \log\left(1 + \beta^{-2}\right) & \beta \lesssim 1 \\ \frac{\pi^2}{m_X^2} \left(\log(2\beta) - \log(\log(2\beta))\right)^2 & \beta \gtrsim 1 \end{cases} , \tag{3.6.25}$$

while for an attractive potential it is

$$\sigma_T^{\rm clas} = \begin{cases} \frac{4\pi}{m_X^2} \beta^2 \log\left(1 + \beta^{-1}\right) & \beta \lesssim 10^{-1} \\ \frac{8\pi}{m_X^2} \frac{\beta^2}{1 + 1.5\beta^{1.65}} & 10^{-1} \lesssim \beta \lesssim 10^3 \end{cases} \tag{3.6.26}$$

where $\beta = 2\alpha_{ii} m_X / \left(m_{\chi^{(i)}} v^2\right)$. Both cross sections are taken from Ref. [42]. With the final choice of parameters presented in Sec. 3.7, $\left\langle \sigma_T / m_{\chi^{(i)}} \right\rangle_{30} \approx 1\,\mathrm{cm}^2/\,\mathrm{g}$ and $\left\langle \sigma_T / m_{\chi^{(i)}} \right\rangle_{30} \approx 8 \times 10^{-3}\,\mathrm{cm}^2/\,\mathrm{g}$ are obtained.

3.6.3 Damping masses

The mass of the smallest protohalos within this model is determined by the temperature of kinetic decoupling between the Dark Matter particles and their last relativistic scattering partner. Indeed, as long as the Dark Matter particles are in thermal equilibrium with relativistic particles, any overdensities which might begin to form are washed out by these interactions with high momentum transfer. This ceases to happen at kinetic decoupling and thus the masses of the smallest structures are given by the total mass contained within the Hubble radius at that time,

$$M_{\mathrm{d}} = \frac{4}{3}\pi\rho_{\mathrm{m}}\frac{1}{H\left(T_{\mathrm{kd}}\right)^3} \ . \tag{3.6.27}$$

In principle, the largest between the above expression and the free-streaming cut-off mass should be taken, but the latter is negligible in this case, being proportional to $1/T_{\mathrm{kd}}^{3/2}$.

The analytic expression for the temperature of kinetic decoupling T_{kd} given a specific particle model is

$$\frac{T_{\mathrm{kd}}}{m_{\chi^{(i)}}} = \left(\left(\frac{a}{n+2}\right)^{\frac{1}{n+2}}\Gamma\left(\frac{n+1}{n+2}\right)\right)^{-1} \ , \tag{3.6.28}$$

as given in Ref. [53]. In the above expression n is the exponent appearing in the elastic-scattering amplitude, $|\mathcal{M}|^2 \propto \left(E/m_{\chi^{(i)}}\right)^n$, and a is defined as

$$a = \sqrt{\frac{5}{2\left(2\pi\right)^9 g_{\mathrm{eff}}}}\,(n+4)!\zeta\left(n+4\right)\left(\frac{T_{\mathrm{DS}}}{T}\right)^{n+4} c_n\frac{M_{\mathrm{Pl}}}{m_{\chi^{(i)}}}\left(1-2^{-(n+3)}\right) \ . \tag{3.6.29}$$

g_{eff} is the effective number of heat-bath degrees of freedom immediately after the kinetic decoupling and c_n is defined by $\left\langle |\mathcal{M}|^2_{t=0}\right\rangle = c_n\left(E/m_{\chi^{(i)}}\right)^n$. Comparison with Eq. (3.4.19) shows that in this case $n = 2$. The temperature of kinetic decoupling of the particles $\chi^{(i)}$ from the particles $\chi'^{(j)}$ is then given by

$$\frac{T_{\mathrm{kd}}}{m_{\chi^{(i)}}} = \left(\left(\left(\frac{5}{2\left(2\pi\right)^9 g_{\mathrm{eff}}}\right)^{\frac{1}{2}}\frac{124}{21}\pi^6\frac{\left(g_i g_j'\right)^2}{m_X^4}M_{\mathrm{Pl}}m^3_{\chi^{(i)}}\varepsilon^3\frac{T_\nu}{T}\right)^{\frac{1}{4}}\Gamma\left(\frac{3}{4}\right)\right)^{-1} \ . \tag{3.6.30}$$

This can be brought to a much simpler form for the case $N = 1$,

$$T_{\text{kd}} \approx 147\,\text{eV}\,\varepsilon|_{T_{\text{kd}}}^{-1/2} \left(\frac{10\,\text{TeV}}{m_{\chi}^{(i)}}\right)^{\frac{1}{4}} \left(\frac{\Omega_{\chi^{(i)}\overline{\chi^{(i)}}}h^2}{0.12}\right)^{1/4} \left(\frac{Q_{\tilde{H}}}{2\times10^{-8}}\right)\left(\frac{v_{\text{d}}}{40\,\text{TeV}}\right)\left(\frac{T}{T_{\nu}}\right)^{3/2}, \tag{3.6.31}$$

by making use of the fact that $g_1 g_1'$ is fully determined by the relic density in Eq. (3.6.23) for $N = 1$ and that $m_X = \sqrt{2}Q_{\tilde{H}}v_{\text{d}}$. The parameters with the strongest influence on the temperature of kinetic decoupling are $Q_{\tilde{H}}$ and v_{d}. Here, it was assumed that the elastic scattering between the Dark Matter candidates and the mediator X ceases to be efficient at much earlier times, since the X particles are much heavier.

Having computed the temperature of kinetic decoupling and using $\rho_{\text{m}}(T_{\text{kd}}) = (\Omega_{\text{m},0}\rho_{\text{crit.},0}/s(T_0))\,s(T_{\text{kd}})$, Eq. (3.6.27) can be explicitly written as [54]

$$M_{\text{d}} \approx 4.67\times10^9 \frac{g_{*,\text{S}}(T_{\text{kd}})}{g_*^{\frac{3}{2}}(T_{\text{kd}})}\left(\frac{\text{keV}}{T_{\text{kd}}}\right)^3 M_{\odot}\,. \tag{3.6.32}$$

Here $M_{\odot}$ is the solar mass, $g_{*,\text{S}}$ is the number of effective degrees of freedom in entropy and g_* the number of effective relativistic degrees of freedom. For example, for the case of $N = 1$, i.e. with $\varepsilon|_{T_{\text{kd}}} = 0.187$ and with all other parameters as in Eq. (3.6.31), a damping mass value of $M_{\text{d}} \approx 3\times10^{10}\,M_{\odot}$ is obtained. Contrary to $M_{\text{d}} \approx M_{\oplus}$ which is usually obtained in the ΛCDM Model, the suppression of small structures is significant within this model. Indeed, the damping mass should lie in the range between $10^9\,M_{\odot}$ and $5\times10^{10}\,M_{\odot}$ in order to successfully address the missing satellites problem [35, 36].

3.7 Results

The final choice of parameters is highly constrained for the case $N = 1$. Requiring the correct relic density imposes a relation between $m_{\chi^{(1)}}$ and the coupling between light and heavy particles, α. Furthermore, the self-interaction cross-section depends strongly on the mass of the mediator, m_X. Finally, all of these parameters play a role in determining the temperature of kinetic decoupling. A complete parameter set solving all small-scale problems simultaneously is presented in Table 3.2. With this choice, a temperature of kinetic decoupling of $T_{\text{kd}} \approx 0.456$ keV is obtained, which then corresponds to a damping mass of $M_{\text{d}} \approx 3\times10^{10}M_{\odot}$. Furthermore, the cross section for self-interaction is approximately $\left\langle\sigma_T/m_{\chi^{(1)}}\right\rangle_{30} \approx 1\,\text{cm}^2/\,\text{g}$ at small scales.

Parameter	Approximate value
$m_{\chi^{(1)}}$	10 TeV
m_X	1.1 MeV
$m_{\chi',(1)}$	$< 0.65\,\mathrm{eV}$
g_1	1.3
g_1'	1.3
$Q_{\tilde{h}}$	2×10^{-8}
v_d	40 TeV

Table 3.2: The parameters of this model which solve all the small-scale problems simultaneously for the case $N = 1$.

The case of $N = 2$ is more flexible. Indeed, the presence of more masses and couplings gives a larger choice of parameter values yielding the desired phenomenology. The scenario I given in Table 3.1 is equivalent to the case $N = 1$. This is because the heavier particles can annihilate into the lightest among them before the decoupling of the Dark Sector from the Standard Model, leaving a heavy particle and a light scattering partner like in the case $N = 1$. Within scenario II the ratio ε between the temperatures of the Dark Sector and the Standard Model increases. As can be seen from Eq. (3.6.31), this implies that slightly larger masses for the mediator and smaller couplings can be chosen leading to the same value of the temperature of kinetic decoupling. In particular, smaller couplings mean that the mass of the Dark Matter candidate can be smaller (see Eq. (3.6.23)). In this special case masses of around 2 TeV can be obtained easily while still satisfying the small- and large-scale requirements simultaneously. The scenario III is in principle equivalent to scenario II. However, it should be noted that the values of ΔN_eff which can be seen in Table 3.1 lie well outside the range expected by Planck measurements [1] and thus, this scenario is disfavored compared to scenario II. Scenario IV represents a mixed Dark Matter scenario which is in principle equivalent to scenario I and the case $N = 1$. It should be noted that it has the best possible values of ΔN_eff among all possibilities with $N = 2$, except of course for scenario I. Finally, scenarios V and VI are equivalent to I and II respectively but have larger values of ΔN_eff which renders them unfavorable due to Planck measurements.

4 Neutrinophilic Dark Matter

In this Chapter, a different model is presented, which considers the idea of neutrinos as the last scattering partners of Dark Matter particles. The model successfully satisfies all bounds that were previously thought to exclude the possibility of neutrinos as scattering candidates and, at the same time, gives a valid explanation to all small-scale problems of ΛCDM.

4.1 Standard Model particles as relativistic scattering partners

The question of whether the relativistic scattering partner of the Dark Matter particles can be a Standard Model particle is crucial for experiments and has been discussed at great lengths in the literature.

The number density of hadrons is highly suppressed after the QCD phase transition and thus, if one is interested in a late kinetic decoupling, only leptons and photons can be considered as relativistic scattering partners.

There are a lot of constraints on the interactions between such particles and Dark Matter. In particular, even though charged leptons have been considered [55] for the role of relativistic scattering partners of Dark Matter, they must be discarded because they would yield protohalo masses in the range of $10^{-6} - 10^{-1} M_{\odot}$, which are incompatible with the missing satellites problem [56]. While some models with neutrinos as the last scattering partners and a vector mediator have been presented in the past [57], they have been later ruled out by constraints coming from the Z, W, and kaon decays as well as electron-neutrino scattering [58]neutrinophilic models with scalar mediators have been ruled out by the constraints given in Refs. [59] and [60] Sommerfeld enhancement and constraints coming from CMB measurements [61]. The conclusion in the literature was that the elastic scattering partner of Dark Matter should be dark [61]. The work described in this chapter is a proof of concept showing that neutrinophilic models are in fact still possible, if one allows for two mediators providing the correct relic density and cross sections for self-interaction [32]. Furthermore, this model is UV-complete, has no dark-photon/photon mixing at one loop [61, 62] and is compatible with BBN and all other cosmological constraints.

4.2 The Lagrangian of the theory

The particle content of the Dark Sector is assumed to consist of two Majorana fields ψ and n and three real scalar fields ϕ, Φ, and X. The roles played by these particles are summarized in Table 4.1. Before discussing each new field in detail, the full Lagrangian is presented below.

Particle	Role
ψ	DM candidate
n	Late kinetic decoupling
ϕ	Self-interactions
Φ	Symmetry breaking
X	Freeze-in

Table 4.1: A summary of the roles played by each particle in the neutrinophilic model.

The proposed Lagrangian consists of a completely dark sector $\mathcal{L}_{\text{ds}}$ and a bridge into the Standard Model via a coupling to sterile neutrinos $\mathcal{L}_{\text{nb}}$,

$$\mathcal{L} = \mathcal{L}_{\text{ds}} + \mathcal{L}_{\text{nb}} \ . \tag{4.2.1}$$

The dark sector Lagrangian can be again separated into kinetic terms and interactions,

$$\mathcal{L}_{\text{ds}} = \mathcal{L}_{\text{kin}} + \mathcal{L}_{\text{int}} \ . \tag{4.2.2}$$

The kinetic terms of the theory are given by

$$\begin{aligned} \mathcal{L}_{\text{kin}} \quad &= \quad \frac{1}{2}\overline{\psi}\left(i\partial\!\!\!/ - m_\psi\right)\psi + \frac{1}{2}\overline{n}\left(\mathrm{i}\partial\!\!\!/ - m_n\right)n - \frac{1}{2}\phi\left(\Box + m_\phi^2\right)\phi \\ &\quad -\frac{1}{2}\Phi\Box\Phi - \frac{1}{2}X\left(\Box + m_X^2\right)X \ . \end{aligned} \tag{4.2.3}$$

m_ψ, m_n, and m_ϕ are the real and positive mass parameters. Note that since ψ is a

Majorana field, the spinor ψ has the form

$$\psi = \psi_L + \psi_L^C \ , \tag{4.2.4}$$

where ψ_L^C denotes the charge-conjugated ψ_L. The kinetic part of the Lagrangian for ψ can then be written out explicitly as

$$\mathcal{L}_{\mathrm{kin}}^{\mathrm{Maj}} = \frac{1}{2}\overline{\psi_L} i\partial\!\!\!/ \psi_L + \frac{1}{2}\overline{\psi_L^C} i\partial\!\!\!/ \psi_L - \frac{1}{2} m_\psi \left(\overline{\psi_L^C}\psi_L + \overline{\psi_L}\psi_L^C\right) \ . \tag{4.2.5}$$

The same is of course valid for the other Majorana field n.

The relevant interaction terms are

$$\mathcal{L}_{\mathrm{int}} = \frac{1}{2} g_{\phi\psi}\overline{\psi}\phi\psi + \frac{1}{2} g_{\phi n}\overline{n}\phi n + \frac{1}{2} g_X \overline{\psi} X \psi - \mathcal{V}\left[\phi, \Phi\right] \ . \tag{4.2.6}$$

Only the cosmologically relevant dimension-four interaction terms have been considered. While other terms could be present too, it was assumed that their couplings are negligible when compared to the ones presented here. The potential $\mathcal{V}\left[\phi, \Phi\right]$ in Eq. (4.2.6) is given by

$$\mathcal{V}\left[\phi, \Phi\right] = \frac{\ell}{4}\left(\Phi^2 - v_\Phi^2\right)^2 + \frac{x}{4}\Phi^2\phi^2 \ , \tag{4.2.7}$$

where v_Φ, ℓ and x are real parameters. This potential allows for a spontaneous symmetry breaking which modifies the mass of the field ϕ, as will be explained later.

The neutrino bridge between the dark sector and the Standard Model is given by

$$\mathcal{L}_{\mathrm{nb}} = \mathrm{i} y \overline{L} \sigma_2 H^* n + H.c. \quad . \tag{4.2.8}$$

Here, L denotes the Standard Model lepton doublet $L = (\nu_L, e_L)$ and H is the Standard Model Higgs doublet. n is a *sterile* neutrino, since it is a right-handed version of the Standard Model neutrino which does not transform under the $SU\left(3\right)_C \times SU\left(2\right)_L$ symmetry and has hypercharge $Y = 0$. For simplicity, it is assumed that it is only coupled to the first generation of neutrinos, but a generalization to all three generations is straightforward. Neutrino oscillations and the Pontecorvo-Maki-Nakagawa-Sakata matrix are neglected as well. The precise origin of the mass of the sterile neutrino is beyond the scope of this study. For example, a dark Higgs model could be introduced: a dark Higgs field with expectation value v_{d} could couple to some heavy fermion field $\tilde{\psi}$ and give a mass of $m_{\mathrm{n}} \sim v_{\mathrm{d}}^2/m_{\tilde{\psi}}$ to the sterile neutrino. After the spontaneous symmetry breaking of the SM Higgs boson a term of the form $\frac{yv}{\sqrt{2}}\overline{\nu}n$ appears in the

Lagrangian, where v is the vacuum expectation value of the Higgs field. Assuming the existence of a Majorana mass term for the SM neutrino of the form $-m_\nu \overline{\nu}\nu$ and taking into account the mass term for the sterile neutrino in Eq. (4.2.3), the mass matrix

$$m_{n\nu} = \begin{pmatrix} m_n & \frac{yv}{\sqrt{2}} \\ \frac{yv}{\sqrt{2}} & m_\nu \end{pmatrix} \tag{4.2.9}$$

is obtained. With the approximation $yv \ll m_n$ and $m_\nu \ll m_n$ the eigenvalues of $m_{n\nu}$ are m_n and $m_\nu - y^2v^2/2m_n$. The mass of the SM neutrino would thus be slightly changed due to the presence of this sterile neutrino. From here on the eigenstates corresponding to these masses will be called n and ν, substituting the initial definitions of these fields.

The motivation behind each term in the Lagrangian can now be presented. The Majorana fermion ψ is assumed to be the Dark Matter candidate and a singlet of the symmetries of the Standard Model. It should be noted that the Lagrangian is invariant under the transformation $\psi \to -\psi$. This accidental $\mathbb{Z}_2$ symmetry ensures the stability of the Dark Matter particles. A coupling between Dark Matter and sterile neutrinos is mediated by the scalar ϕ in Eq. (4.2.6). ϕ is furthermore responsible for self-interactions between Dark Matter particles.

The neutrino bridge in Eq. (4.2.8) creates an effective coupling (discussed in more detail below) between the Dark Matter particles and SM neutrinos. It is a necessary ingredient which makes it possible for Dark Matter to couple only to SM neutrinos and not charged leptons while still respecting all gauge symmetries. It will be shown, that it is possible to choose the parameters of the theory in such a way that this coupling lasts until temperatures below the keV range, making SM neutrinos the last elastic scattering partners of Dark Matter.

As will be discussed in detail in Section 4.6.1, the mediator ϕ cannot be responsible for a late kinetic decoupling and the correct Dark Matter relic density at the same time. Indeed, to ensure a late kinetic decoupling, the coupling between ϕ and ψ will have to be chosen in such a way that the annihilation process $\psi\psi \to \phi\phi$ depletes the Dark Matter population before becoming ineffective due to the expansion of the Universe. For this reason, another Yukawa coupling between some new scalar field X and Dark Matter must be present as well. The decay of X into two ψ's after the freeze-out of ψ from ϕ restores the Dark Matter population and ensures a correct relic density.

Finally, a scalar field Φ must also be postulated. This field is coupled to the scalar mediator ϕ and undergoes a spontaneous symmetry breaking through the potential in

Event	Temperature
m_X	$\mathcal{O}(1)$ PeV
m_ψ	$\mathcal{O}(1)$ TeV
decoupling of ϕ from the Standard Model	~ 0.5TeV
baryogenesis	~ 100 GeV
QCD phase transition	~ 150 MeV
$m_\phi^{(\mathrm{SSB})}$	$\mathcal{O}(10)$ MeV
neutrino decoupling	~ 1 MeV
Big Bang Nucleosynthesis	~ 100 keV
freeze-in of ϕ and Φ	$\lesssim 30$ keV
kinetic decoupling	~ 0.6keV
spontaneous symmetry breaking of Φ	$\mathcal{O}(100)$ eV
m_ϕ	$\mathcal{O}(10-100)$ eV
recombination	$0.26-0.33$ eV

Table 4.2: A preview of the thermal evolution of the Universe and the relevant energy scales within the neutrinophilic Dark Matter model.

Eq. (4.2.7). This allows to change the mass of ϕ after the phase transition, which is required to tune the cross section for self-interaction to the desired values. This will be explained in more detail in Section 4.2.2.

Table 4.2 summarizes the thermal evolution of this neutrinophilic model.

Having motivated the role of each particle, the rest of this Section is devoted to more quantitative details about the Lagrangian and the new fields.

4.2.1 Effective coupling

The neutrino bridge mediates an effective coupling between the scalar boson ϕ and the Standard Model neutrinos ν. In particular the coupling represented in Fig. 4.1a can be summarized as an effective coupling g_ν with

$$g_\nu = \frac{Y^2 g_{\phi n}}{2m_n^2} , \tag{4.2.10}$$

where $Y = y\sqrt{2}v$, resulting in the effective diagram represented in Fig. 4.1b.

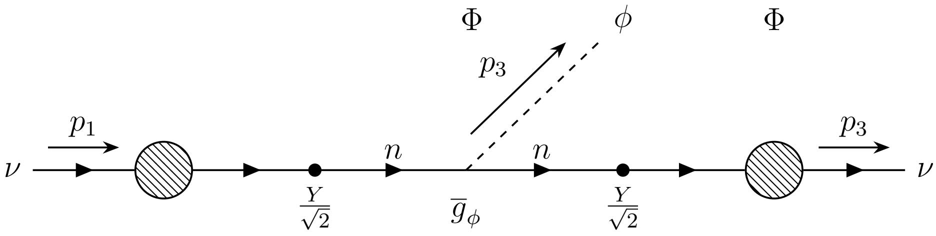

(a) The coupling between the Dark Sector and the Standard Model at high energies.

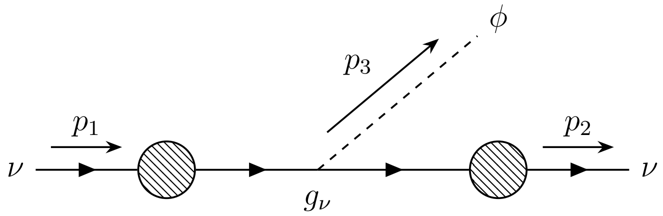

(b) The effective coupling between the Dark Sector and the Standard Model.

Figure 4.1: The diagrams representing the coupling of the Dark Sector to the Standard Model.

4.2.2 Symmetry breaking

The field Φ undergoes a spontaneous symmetry breaking thanks to the potential in Eq. (4.2.7). After attaining its minimal value v_Φ, it can be expanded around it as

$$\Phi = v_\Phi + \tilde{\Phi} \; . \tag{4.2.11}$$

Inserting this expansion in the potential in Eq. (4.2.7) leads to

$$\mathcal{V}\left[\tilde{\Phi}, \phi\right] = -\frac{\ell}{4}\left(\tilde{\Phi}^4 + 4v_\Phi\tilde{\Phi}^2 + 4v_\Phi a^3\right) - \frac{x}{2}v_\Phi^2\phi^2 - \frac{x}{2}\tilde{\Phi}^2\phi^2 - xv_\Phi\tilde{\Phi}\phi^2 \; . \tag{4.2.12}$$

Clearly, the quadratic term in $\tilde{\Phi}$ corresponds to a mass of $m_{\tilde{\Phi}} = \sqrt{2\ell}v_\Phi$, while the term $-(x/2)\, v_\Phi \phi^2$ represents a correction to the mass of the scalar ϕ which now becomes $m_\phi^{(\mathrm{SSB})} = \sqrt{m_\phi^2 + xv_\Phi^2}$. The superscript in $m_\phi^{(\mathrm{SSB})}$ signifies that the mass is the one after the spontaneous symmetry breaking.

It is this spontaneous symmetry breaking which allows the mediator of self-interactions ϕ to yield the correct values of the cross section at late times, while bypassing neutrinophilic constraints at earlier times [58, 59, 60].

4.2.3 Mass hierarchy

Finally, the assumed mass hierarchy of the model is presented and motivated here. The assumed relation between the masses of the particles is

$$m_X \gg m_n > m_\psi,\, m_h \gg m_\phi^{(\mathrm{SSB})} \gg m_\phi,\, m_{\tilde{\Phi}},\, m_\nu\,. \tag{4.2.13}$$

The field X is postulated to be the most massive one. It will be shown that its mass can be as high as PeV in order to yield the correct relic density.

The mass of the scalar field ϕ is originally very small (in the eV range) to allow a late kinetic decoupling. However, after the spontaneous symmetry breaking of the field Φ, it increases to values into the MeV range. The field $\tilde{\Phi}$ has a negligible mass too, such that it does not contribute to the Dark Matter relic density.

The Dark Matter particles are assumed to have a mass in the TeV range. This is necessary to resolve the small-scale problems and satisfy all constraints, as will be explained in more detail later. The sterile neutrino n has a mass in the TeV range as well.

4.3 Relevant cross sections and decay rates

In this section the relevant cross sections and decay rates are discussed. The cross section for the annihilation process $\psi\psi \to \phi\phi$ and the decay rate of $X \to \psi\psi$ will be relevant for computing the relic density of Dark Matter. The cross section for the elastic scattering process $\psi\nu \to \psi\nu$ determines the time of kinetic decoupling. The self-interaction $\psi\psi \to \psi\psi$, mediated by the light scalar mediator ϕ, is important to resolve the cusp vs. core problem.

4.3.1 Annihilation cross-section for the Dark Matter candidates

The cross section for the process

$$\psi + \overline{\psi} \to \phi + \phi \tag{4.3.1}$$

is given by the two diagrams in Figure 4.2. The amplitudes for the two diagrams are

$$\mathcal{M}_1 = -\mathrm{i}\overline{v_L}\,(p_2)\,\frac{\not{p}_1 - \not{p}_3 + m_\psi}{(p_1 - p_3)^2 - m_\psi^2} u_L\,(p_1)\, g_{\phi\psi}^2 \tag{4.3.2}$$

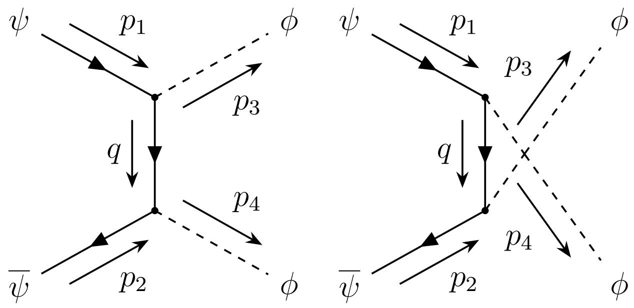

Figure 4.2: The diagrams contributing to the annihilation cross section for the Dark Matter candidates.

and

$$\mathcal{M}_2 = -\mathrm{i}\overline{v_L}\left(p_2\right) \frac{\not{p}_1 - \not{p}_4 + m_\psi}{\left(p_1 - p_4\right)^2 - m_\psi^2} u_L\left(p_1\right) g_{\phi\psi}^2 \,. \tag{4.3.3}$$

They must be added, squared and averaged over all possible spins in order to obtain the amplitude of the whole process, $\left\langle \left|\mathcal{M}\right|^2 \right\rangle = \left\langle \left(\mathcal{M}_1 + \mathcal{M}_2\right)^* \left(\mathcal{M}_1 + \mathcal{M}_2\right) \right\rangle$. In the center-of-mass frame, using the approximations $p_1 = (m_\psi, m_\psi \vec{v}_{\mathrm{rel}}/2)$ and $p_2 = (m_\psi, -m_\psi \vec{v}_{\mathrm{rel}}/2)$, and neglecting m_ϕ, the average of the squared amplitude is

$$\left\langle \left|\mathcal{M}\right|^2 \right\rangle \approx \frac{1}{2} g_{\phi\psi}^4 v_{\mathrm{rel}}^2 \tag{4.3.4}$$

neglecting terms of order v_{rel}^4 and higher.

The resulting cross section for this annihilation process is

$$\left\langle v_{\mathrm{rel}} \sigma_{\mathrm{ann}} \right\rangle = \frac{\pi}{4} \frac{\alpha^2}{m_\psi^2} v_{\mathrm{rel}}^2, \tag{4.3.5}$$

where $\alpha \equiv g_{\phi\psi}^2/4\pi$ was introduced.

4.3.2 Decay of the mediator X

The heavy mediator X can decay into two Dark Matter particles due to the interaction term in the Lagrangian

$$\frac{1}{2} g_X \overline{\psi} X \psi. \tag{4.3.6}$$

The amplitude for this process is given by

$$\mathcal{M} = \frac{g_X}{2} \overline{u}_L\left(p_2\right) v_L\left(p_3\right) \,. \tag{4.3.7}$$

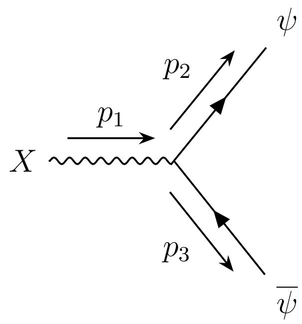

Figure 4.3: The diagram for the decay of the X mediator into Dark Matter particles.

All momenta are indicated in Fig. 4.3. The average over all spins of the square of this amplitude can be computed as

$$\left\langle |\mathcal{M}|^2 \right\rangle = \frac{g_X^2}{2} (p_2 \cdot p_3) \ . \tag{4.3.8}$$

This amplitude can be further simplified after inserting the momenta $p_1 = (m_X, \vec{0})$, $p_2 = (m_X/2, \vec{p})$ and $p_3 = (m_X/2, -\vec{p})$ in Eq. (4.3.8),

$$\left\langle |\mathcal{M}|^2 \right\rangle = \frac{g_X^2}{4} m_X^2 \ . \tag{4.3.9}$$

Note that $|\vec{p}|^2 = m_X^2/4 - m_\psi^2$ has been approximated by $|\vec{p}|^2 \approx m_X^2/4$, because to $m_X \gg m_\psi$.

The decay rate in the rest frame of the mediator X is related to the amplitude by

$$\Gamma = \frac{|\vec{p_2}|}{8\pi m_X^2} \left\langle |\mathcal{M}|^2 \right\rangle \ . \tag{4.3.10}$$

The final decay rate is

$$\Gamma_{X\to\psi\psi} = \frac{g_X^2}{64\pi} m_X \ . \tag{4.3.11}$$

4.3.3 Elastic scattering $\psi + \nu \to \psi + \nu$

The Dark Matter particles remain in thermal equilibrium with the Standard Model for a long time thanks to the efficient momentum transfer between the ψ's and the neutrinos. Indeed the temperature of kinetic decoupling is determined by the moment in time when the scattering $\psi + \nu \to \psi + \nu$ ceases to be efficient, i.e. when $\Gamma_{\psi+\nu\to\psi+\nu} <$

H.

The amplitude for this process is given by

$$\mathcal{M} = -\frac{g_{\phi\psi} g_\nu}{m_\phi^2} g_{\mu\nu} \left[\overline{u}\left(p_3\right) \gamma^\mu u\left(p_1\right)\right] \left[\overline{u}\left(p_4\right) \gamma^\nu u\left(p_2\right)\right] \ , \tag{4.3.12}$$

as can be seen from Fig. (4.4). Here, the massive ϕ propagator around has been approximated as $-\mathrm{i}\left(g_{\mu\nu} - q_\mu q_\mu / m_\phi^2\right) / \left(q^2 - m_\phi^2\right) \approx \left(\mathrm{i}/m_\phi^2\right) g_{\mu\nu}$ since $q^2 \ll m_\phi^2$ is assumed. The average of the squared amplitude can be simplified as

$$\begin{aligned} \left\langle \left|\mathcal{M}\right|^2 \right\rangle &= 8 g_{\phi\psi}^2 g_\nu^2 \frac{1}{m_\phi^4} \left[\left(p_1 \cdot p_2\right)\left(p_3 \cdot p_4\right) + \left(p_1 \cdot p_4\right)\left(p_2 \cdot p_3\right)\right. \\ &\quad \left. - m_\nu^2 \left(p_1 \cdot p_3\right) - m_\psi^2 \left(p_2 \cdot p_4\right) + 2 m_\nu^2 m_\phi^2 \right] \ . \end{aligned} \tag{4.3.13}$$

Using $m_\nu \approx 0$ and $p_1 \cdot p_2 = m_\psi E = p_3 \cdot p_4$, where E is the energy of the neutrino, the averaged squared amplitude can be further simplified to

$$\left\langle \left|\mathcal{M}\right|^2 \right\rangle = 16 \cdot 8 G_D^2 m_\psi^2 E^2 \ , \tag{4.3.14}$$

where the Fermi constant $G_D^2 = 2 g_{\phi\psi}^2 g_\nu^2 / 16 m_\phi^4$ has been introduced.

This leads to the cross section

$$\sigma v_{\mathrm{rel}} = \frac{8}{\pi} G_D E^2 \ , \tag{4.3.15}$$

where the fact that $E \ll m_\psi$ was used to approximate the final result. The thermal average is defined by

$$\left\langle \sigma v_{\mathrm{rel}} \right\rangle = \frac{1}{\int f\left(\vec{p}\right) \frac{\mathrm{d}^3 \vec{p}}{(2\pi)^3}} \int \sigma v_{\mathrm{rel}} f\left(\vec{p}\right) \frac{d^3 \vec{p}}{(2\pi)^3} \ , \tag{4.3.16}$$

where $f\left(\vec{p}\right)$ is the Fermi-Dirac distribution

$$f\left(E\right) = \frac{1}{1 + \exp\left(\frac{E}{T}\right)} \ . \tag{4.3.17}$$

Eq. (4.3.16) can be rewritten as an integral over the energy by using the spherical symmetry of the expression

$$\left\langle \sigma v_{\mathrm{rel}} \right\rangle = \frac{1}{\int_0^\infty E^2 f\left(E\right) \mathrm{d}E} \int_0^\infty \mathrm{d}E E^2 \sigma v_{\mathrm{rel}} f\left(E\right) \ . \tag{4.3.18}$$

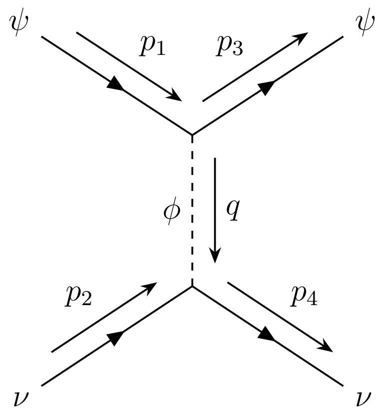

Figure 4.4: The diagram for the elastic scattering of Dark Matter particles with Standard Model neutrinos.

These are known integrals that yield the following result containing the Riemann-Zeta function ζ,

$$\langle \sigma v_{\mathrm{rel}} \rangle = \frac{15 \cdot 8\zeta(5)}{\pi\zeta(3)} G_D^2 T^2 \,. \tag{4.3.19}$$

4.3.4 Cross section for self-interactions

The dark fermions ψ can interact with each other thanks to a force mediated by the scalar ϕ. The numerical solution for the cross section for these purely repulsive self-interactions in the classical limit $m_\psi v/m_\phi \gg 1$ is found in Ref. [42],

$$\sigma_T \approx \frac{2\pi}{m_\phi^2} \beta^2 \ln\left(1 + \beta^{-2}\right) \tag{4.3.20}$$

Here, the definition $\beta \equiv 2\alpha m_\phi / \left(m_\psi v_{\mathrm{rel}}^2\right)$ was used. This expression is valid for the case $\beta \lesssim 1$, which is realized within this model as will be explained later.

4.4 Constraints from particle physics

4.4.1 Constraints on the masses

The Dark Matter particles ψ are assumed to be stable and produced in local thermal equilibrium. By requiring partial-wave unitarity of the scattering matrix, the bound $m_\psi < \mathcal{O}(300)$ TeV follows [43] (see also Section 3.5.1).

A lower bound on the mass of the Dark Matter particles, $m_\psi > \mathcal{O}(1)$MeV, can furthermore be inferred from the Planck measurements of the effective number of neutrinos [1], since the considered Dark Matter particles are assumed to remain in thermal contact with neutrinos until late times.

In principle, m_n, m_ϕ, and m_X are not bounded in any way other than by the assumed mass hierarchy in Eq. (4.2.13). Constraints would arise if, for example, the X's or n's were to remain in thermal equilibrium with with the neutrinos after the time of neutrino decoupling [56].

4.4.2 Constraints on the couplings

The couplings $g_{\phi\psi}$, $g_{\phi n}$, and g_X are assumed to lie in the perturbative regime. Furthermore, bounds on the Yukawa bridge to SM neutrinos constrain Y to satisfy $Y^2/2m_n \lesssim 5\,\text{GeV}$ [63].

Since there is no coupling between the Dark Sector and charged leptons, the only decays providing constraints on the effective neutrino coupling g_ν are those of Z^0, $W^\pm$, and $K^\pm$.

For $m_\phi^{(\text{SSB})} \approx 10\,\text{MeV}$ the additional decay channel $Z^0 \to \nu\,\nu\,\phi$ has a rate $\Gamma_{Z^0\to\nu\,\nu\,\phi} \approx 0.18\,\text{GeV}\,g_\nu^2 N_\nu/3$. Here, a specific value for the mass of ϕ after the symmetry breaking was chosen, educated by the optimal value described later. However, it should be noted that the value of the decay rate does not depend strongly on $m_\phi^{(\text{SSB})}$. The error on the Z^0 decay is 0.0023 Gev [46]. This implies a bound $g_\nu \lesssim 0.2/\sqrt{N_\nu}$. Since the elastic scattering rate Γ_{el} is proportional to $N_\nu g_\nu^2$, its upper bound is independent of the number of neutrinos N_ν. Note that this is only relevant if ϕ has not decayed earlier, in which case the decay $Z^0 \to \nu\,\nu\,\nu\,\nu$ would be dominant and the constraint would be relaxed.

The error on the decay of the charged electroweak boson $W^\pm$ is 0.042 Gev [46]. The contribution coming from the new possible decay $W \to \nu\,e\,\phi$ must then lie within this error. Assuming again $m_\phi^{(\text{SSB})} \approx 10$ MeV, this implies $g_\nu \leq \mathcal{O}(1)$, which is weaker than the previous constraint.

Finally, the last decay affected by the Dark Sector is the decay of $K^\pm$. The new decay channel $K \to \mu\nu\phi$ is now added to the most common one, $K \to \nu\mu$. The ratio between these two decay rates is almost constant for energies of the outgoing muon in the range $165.5 - 205.5\,\mathrm{MeV}$ [46],

$$\frac{\Gamma_{K\to\mu\nu\phi}}{\Gamma_{K\to\nu\mu}} \approx 7.4\times 10^{-4} g_\nu^2\,. \tag{4.4.1}$$

Here, $m_\phi^{(\mathrm{SSB})} \approx 10\,\mathrm{MeV}$ was assumed as well. The decay rate $\Gamma_{K\to\mu\nu\phi}$ is bounded from above by the decay rate $\Gamma_{K\to\mu\nu\nu\nu} \lesssim 2.7\times 10^{-6}\Gamma_{\mathrm{total}}$ [64]. This implies the strongest constraint yet on the coupling between the dark scalar and Standard-Model neutrinos, $g_\nu \lesssim 7\times 10^{-2}$. Note that much stronger constraints will be derived in the following section due to cosmological restrictions.

This concludes the discussion about the constraints on the new couplings. It must be noted that the process $\nu e \to \nu e$ is not affected at tree level by the presence of the Dark Sector, which only couples to neutrinos and not charged leptons [58]. Furthermore, constraints coming from lepton number violation and decays into mesons [59] are negligible compared to other constraints discussed here. Finally, while this is not relevant to this specific model, it is interesting to remark that if there were N_ϕ copies of the dark scalar ϕ, the coupling to neutrinos would behave as $g_\nu \propto 1/\sqrt{N_\phi}$ and the constraints given above would have to be adjusted accordingly.

4.5 Constraints from cosmology

4.5.1 Equilibrium condition for the scalar fields ϕ and Φ

The condition that the ϕ particles must have been in thermal equilibrium with the Φ particles before the spontaneous symmetry breaking at T_{SSB} must be imposed. This condition can be formulated as

$$\langle \sigma_{\phi\phi\to\Phi\Phi} v_{\mathrm{rel}} \rangle\, n_\phi\left(T_{\mathrm{SSB}}\right) \gtrsim H\left(T_{\mathrm{SSB}}\right)\ , \tag{4.5.1}$$

where H is the Hubble parameter. Using $\langle \sigma_{\phi\phi\to\Phi\Phi} v_{\mathrm{rel}} \rangle = (1/32\pi m_\phi^2)x^2$, $n_\phi\left(T_{\mathrm{SSB}}\right) = \left(m_\phi T/2\pi\right)^{3/2}\exp\left(-m_\phi/T_{\mathrm{SSB}}\right)$ and $H\left(T_{\mathrm{SSB}}\right) \approx 3.05 T_{\mathrm{SSB}}^2/M_{\mathrm{Pl}}$, the condition on the coupling x between the ϕ's and the Φ's becomes

$$x \gtrsim 10^{-13}\left(\frac{m_\phi}{100\ \mathrm{eV}}\right)^{\frac{1}{4}}\left(\frac{T_{\mathrm{SSB}}}{100\ \mathrm{eV}}\right)^{\frac{1}{4}}\ . \tag{4.5.2}$$

The fact that the mass m_ϕ should be approximately 100 eV was already used here for the non-relativistic number density n_ϕ. The reason behind $m_\phi \approx 100$ eV will be shown in Sec. 4.6.2.

4.5.2 Constraints on g_ν

The particles ϕ and Φ are very light before the spontaneous symmetry breaking and would violate constraints coming from Big Bang Nucleosynthesis. The deviation of the effective number of neutrino degrees of freedom at the time of neutron-proton freeze-out T_γ^{fr} is

$$\Delta N_{\mathrm{eff}}\left(T_\gamma^{\mathrm{fr}}\right) = N_\nu \frac{\rho_\phi\left(T_\gamma^{\mathrm{fr}}\right) + \rho_\Phi\left(T_\gamma^{\mathrm{fr}}\right)}{\rho_\nu\left(T_\gamma^{\mathrm{fr}}\right)} \,. \tag{4.5.3}$$

This is only within the bounds coming from measurements of the ^{4}He abundance if the ratio T_ϕ^4/T_ν^4 is well below 1. For this reason, the ϕ and Φ particles must be produced out of equilibrium through a freeze-in mechanism [65]. This is the case if the condition

$$\Gamma_{\mathrm{eq}}\left(T_\gamma^{\mathrm{fr}}\right) < H\left(T_\gamma^{\mathrm{fr}}\right) \tag{4.5.4}$$

is satisfied, where Γ_{eq} is the equilibrium annihilation rate of the particles ϕ, i.e. $\Gamma_{\mathrm{eq}} = \langle \sigma_{\phi\phi\to\overline{\nu}\nu} v_{\mathrm{rel}} \rangle\, n_\phi^{(\mathrm{eq})}$. This implies the constraint on the coupling $g_\nu < 10^{-6}$. The produced ϕ's should have a temperature $T_\phi \approx (0.1)^{1/3}\, T_\nu$ in order to yield $\Delta N_{\mathrm{eff}}\left(T_\gamma^{\mathrm{fr}}\right) \approx 0.05$, satisfying the Big Bang Nucleosynthesis constraints.

A lower bound on g_ν is given by deleptonization arguments regarding the observation of SN1987A [60]. In particular this implies $g_\nu \gtrsim 1.6 \times 10^{-6}\,\mathrm{MeV}/m_\phi^{(\mathrm{SSB})}$. As will be explained later, a value of $m_\phi^{(\mathrm{SSB})} \approx 10\,\mathrm{MeV}$ is particularly favored in order to obtain the desired self-interactions. This implies $g_\nu \gtrsim 10^{-7}$.

Combining the lower and the upper bound, $10^{-7} \lesssim g_\nu \lesssim 10^{-6}$, a value of $g_\nu \approx 10^{-7}$ will be assumed throughout the rest of the discussion of this model without loss of generality.

4.5.3 Lower bound on m_n

The ratio $T_\phi \approx (0.1)^{1/3}\, T_\nu$ described above at the time of neutrino decoupling is achieved if the ϕ particles freeze-out from the Standard Model plasma at early temperatures, before the QCD phase transition. At those temperatures the number of degrees of freedom is still high enough to generate such a difference of temperatures between the two sectors. Indeed, for a freeze-out at the temperautre of the QCD phase transition, the ratio at the time of neutrino decoupling is

$$\frac{T^3_{\phi,\,\nu_D}}{T^3_{\nu,\nu_D}} = \frac{g_{\mathrm{S,\,SM}}\left(T_{\nu_D}\right)}{g_{\mathrm{S,\,SM}}\left(T_{\mathrm{QCD}}\right)} \approx 0.17\ . \tag{4.5.5}$$

The condition for a freeze-out before the temperature of the QCD phase transition is

$$\Gamma_{\phi\phi\to n\nu} < H\left(T_{\mathrm{QCD}}\right)\ , \tag{4.5.6}$$

where $\Gamma_{\phi\phi\to n\nu}$ is the annihilation rate of the ϕ's. This condition implies a lower bound on the mass m_n,

$$\left(\frac{g_\nu}{10^{-6}}\right)\left(\frac{g_{\phi n}}{1}\right)\left(\frac{\mathrm{TeV}}{m_n}\right) \leq \mathcal{O}\left(1\right)\ . \tag{4.5.7}$$

4.5.4 Relic density of $\tilde{\Phi}$

After the spontaneous symmetry breaking, the remaining field $\tilde{\Phi}$ contributes to the energy density of the Universe. It is a hot relic with relic density [47]

$$\Omega_{\tilde{\Phi}} h^2 \approx \frac{m_{\tilde{\Phi}}}{150\,\mathrm{eV}}\ . \tag{4.5.8}$$

Since $m_{\tilde{\Phi}}$ can be chosen to be arbitrarily small, the condition that this particle does not contribute significantly to the relic density of the universe is easily satisfied.

4.5.5 Cosmic Microwave Background

The deviation of the effective number of neutrinos at the time of recombination is given by

$$\Delta N_{\mathrm{eff}}\left(T_{\mathrm{rec}}\right) = \frac{8}{7}\left(\frac{4}{11}\right)^{-\frac{4}{3}}\left[\frac{\rho_{\mathrm{rad}}\left(T_{\mathrm{rec}}\right)}{\rho_\gamma\left(T_{\mathrm{rec}}\right)} - 1\right] - N_\nu\ . \tag{4.5.9}$$

At recombination the scalar field ϕ has already decayed and the radiation energy density consists of $\rho_{\mathrm{rad}} = \rho_\gamma + \rho_\nu + \rho_{\tilde{\Phi}}$. With this the variation of the effective number of degrees of freedom becomes becomes

$$\Delta N_{\mathrm{eff}}\left(T_{\mathrm{rec}}\right) = N_\nu\left[\left(\frac{11}{4}\right)^{\frac{4}{3}}\frac{T^4_{\nu,\,\mathrm{rec}}}{T^4_{\gamma,\,\mathrm{rec}}} - 1\right] + \frac{4}{7}\left(\frac{11}{4}\right)^{\frac{4}{3}}\frac{T^4_{\tilde{\Phi},\,\mathrm{rec}}}{T^4_{\gamma,\,\mathrm{rec}}}\ . \tag{4.5.10}$$

Using the fact that the ratio of entropy densities

$$\frac{s_\gamma + s_\phi + s_{\tilde{\Phi}}}{s_\gamma} = \text{const.} \tag{4.5.11}$$

is constant during the evolution of the Universe, the following relation between temperatures right after neutrino decoupling (denoted by the index "ν_D") and temperatures right after CMB (denoted by the index "rec") can be derived,

$$\left(\frac{T_{\nu,\,\nu_\mathrm{D}}}{T_{\gamma,\,\nu_\mathrm{D}}}\right)^3 \left(1 + \frac{8}{7}\frac{1}{N_\nu}\left(\frac{T_{\phi,\,\nu_\mathrm{D}}}{T_{\nu,\,\nu_\mathrm{D}}}\right)^3\right) = \left(\frac{T_{\nu,\,\mathrm{rec}}}{T_{\gamma,\,\mathrm{rec}}}\right)^3 \left(1 + \frac{s_{\tilde{\Phi},\,\mathrm{rec}}}{s_{\nu,\,\mathrm{rec}}}\right) . \tag{4.5.12}$$

Since the $\tilde{\Phi}$'s and the neutrinos are in thermal equilibrium at recombination, the ratio of their entropy densities is

$$\frac{s_{\tilde{\Phi},\,\mathrm{rec}}}{s_{\nu,\,\mathrm{rec}}} = \frac{4}{7}\frac{1}{N_\nu} , \tag{4.5.13}$$

which implies

$$\left(\frac{T_{\nu,\,\mathrm{rec}}}{T_{\gamma,\,\mathrm{rec}}}\right)^4 = \left(\frac{T_{\nu,\,\nu_\mathrm{D}}}{T_{\gamma,\,\nu_\mathrm{D}}}\right)^4 \frac{\left(1 + \frac{8}{7}\frac{1}{N_\nu}\left(\frac{T_{\phi,\,\nu_\mathrm{D}}}{T_{\nu,\,\nu_\mathrm{D}}}\right)^3\right)^{\frac{4}{3}}}{\left(1 + \frac{4}{7}\frac{1}{N_\nu}\right)^{\frac{4}{3}}} . \tag{4.5.14}$$

Inserting this in Eq. (4.5.10) and using again the assumption due to the freeze-in $T_{\phi,\nu_\mathrm{D}} \approx (0.1)^{1/3}\, T_{\nu,\nu_\mathrm{D}}$ and $N_\nu = 3.046$ yields

$$\Delta N_\mathrm{eff}\,(T_\mathrm{rec}) \approx\, -0.02 . \tag{4.5.15}$$

This result is well within the existing experimental bounds [1]. It should be noted that such a value could potentially explain the tension about the decrease of the effective number of neutrinos between BBN- and CMB-based measurements [1].

4.5.6 Decay channel for X

The decay of the X particles repopulates the Dark Matter relic abundance after the chemical decoupling from the ϕ particles as will be discussed in Section 4.6.1. For this reason, two conditions can be imposed on the coupling g_X. The first one is that this freeze-in of the X particles should happen after the Dark Matter freeze-out, i.e. $\Gamma_{X\to\psi\psi} < H\,(T_f)$, where T_f is the temperature of freeze-out. The second one is that this decay should stop before Big Bang Nucleosynthesis, i.e. $\Gamma_{X\to\psi\psi} > H\,(T_{\nu\,\mathrm{D}})$.

Using $H(T) = \sqrt{(8\pi G/3)\ (\pi^2/30)\ g_*(T)}T^2$, where $g_*(T)$ is the effective number of relativistic degrees of freedom, the resulting constraints on the coupling g_X are

$$\begin{aligned} 4\times 10^{-5}\left(\frac{T_{\nu D}}{2.3\,\mathrm{MeV}}\right)\left(\frac{g_*(T_{\nu_\mathrm{D}})}{10.75}\right)^{1/4} &\lesssim \left(\frac{g_X}{3\times 10^{-10}}\right)\left(\frac{m_X}{\mathrm{PeV}}\right)^{1/2} \\ &\lesssim \left(\frac{30}{x_\mathrm{f}}\right)\left(\frac{g_*(T_\mathrm{f})}{108.75}\right)^{1/4}\left(\frac{m}{\mathrm{TeV}}\right)\ . \end{aligned} \tag{4.5.16}$$

4.6 Cosmological observables

The relevant cosmological observables of this model are discussed in this section: the Dark-Matter relic density, the temperature of kinetic decoupling, the damping masses and finally the cross section for self-interactions.

4.6.1 Relic abundance

As discussed in Section 3.6.1, the relic abundance of the Dark Matter particles is determined by the Boltzmann equation

$$(L-C)\left[f_\psi\right](\vec{p}) = 0\ , \tag{4.6.1}$$

which describes the evolution of the Dark Matter distribution function. In this case, the collision term is given by

$$\begin{aligned} C\left[f_\psi\right](\vec{p}) \;=\; & \int \frac{\mathrm{d}^3\vec{p}_2}{E_2}\frac{\mathrm{d}^3\vec{p}_3}{E_3}\frac{\mathrm{d}^3\vec{p}_4}{E_4}\delta^4\left(p_1+p_2-p_3-p_4\right)|\mathcal{M}|^2 \\ & \times\left[f_\phi(\vec{p}_3)\,f_\phi(\vec{p}_4)\left(1-f_\psi(\vec{p}_2)\right)\left(1-f_\psi(\vec{p})\right)\right. \\ & \left. -f_\psi(\vec{p})\,f_\psi(\vec{p}_2)\left(1-f_\phi(\vec{p}_3)\right)\left(1-f_\phi(\vec{p}_4)\right)\right]\ , \end{aligned} \tag{4.6.2}$$

since $g_{\phi\psi} \gg g_\nu$ is assumed, which implies that the main process responsible for the freeze-out of the Dark Matter particles is given by $\psi\psi \to \phi\phi$.

Analogously to the discussion in Section 3.6.1, the Boltzmann equation can be rewritten as

$$\frac{\mathrm{d}Y_\psi}{\mathrm{d}x} = -\frac{\lambda}{x^2}\left(Y_\psi Y_\psi - Y_\psi^{(\mathrm{eq})}Y_\psi^{(\mathrm{eq})}\right) \tag{4.6.3}$$

with the efficiency $\lambda \equiv \langle\sigma_\mathrm{ann}v_\mathrm{rel}\rangle\, s\,(x=1)\,/H\,(x=1)$, the particle yield $Y_\psi = n_\psi/s$ and $Y_\psi^{(\mathrm{eq})} = n_\psi^{(\mathrm{eq})}/s$, and the unitless quantity $x = m_\psi/T$.

This differential equation implies a constant value at large values of x of

$$Y_\infty = \frac{x_\mathrm{f}}{\lambda}\,, \tag{4.6.4}$$

where $x_\mathrm{f} = m_\psi/T_\mathrm{f}$ marks the time of freeze-out of the Dark Matter particles, when they started departing from the equilibrium distribution. The relic density today and Y_∞ are related by

$$\Omega_\psi h^2 = \frac{Y_\infty s_0 m_\psi}{\rho_c/h^2}\,, \tag{4.6.5}$$

where s_0 is the entropy density today, ρ_c is the critical energy density today and $h = 0.674 \pm 0.005$ [1].

The time of freeze-out x_f appearing in Y_∞ is obtained from the condition

$$\langle v_\mathrm{rel}\sigma_\mathrm{ann}\rangle\, n_\psi^{(\mathrm{eq})}(x_\mathrm{f}) \overset{!}{=} H(x_\mathrm{f}) \tag{4.6.6}$$

and has the exact solution $x_f = W_0\left(2C^2\right)/2$, where W_0 is the principal branch of the Lambert W function.

Using this value of x_f and the other parameters of this model, the relic density from Eq. (4.6.5) is calculated to be

$$\Omega_\psi h^2 \approx 0.12 \left(\frac{\alpha}{0.1}\right)^{-2} \left(\frac{m_\psi}{\mathrm{TeV}}\right)\,. \tag{4.6.7}$$

In particular, it should be noted that $\alpha \approx 0.1$ is required to recover the expected relic density. However, larger values of α are needed for a late kinetic decoupling as will be shown in the next section. The two requirements are in contradiction. To solve this problem, another mechanism is needed to generate the correct relic density: the out-of-equilibrium decay of the X boson at late times. The particle yield of the X scalar is

$$\frac{\mathrm{d}Y_X}{\mathrm{d}x} = \frac{3}{8\pi^5}\frac{M_\mathrm{Pl}\Gamma_{X\to\psi\psi}}{g_*^{3/2}\left(T_\mathrm{f}\right) m_X^2}\left(\frac{m_X}{m_\psi}x\right)^3 K_1\left(\frac{m_X}{m_\psi}x\right)\,, \tag{4.6.8}$$

where $K_1\left(\frac{m_X}{m_\psi}x\right)$ is the first Bessel function of the second kind. This late freeze-in repopulates the Dark Matter density and yields

$$\Omega_\psi h^2 \approx 0.12 \left(\frac{g_X}{8\times 10^{-11}}\right)^2 \left(\frac{114}{g_*\left(T_\mathrm{f}\right)}\right)^{3/2} \left(\frac{m_\psi}{\mathrm{TeV}}\right)\left(\frac{\mathrm{PeV}}{m_X}\right)\,. \tag{4.6.9}$$

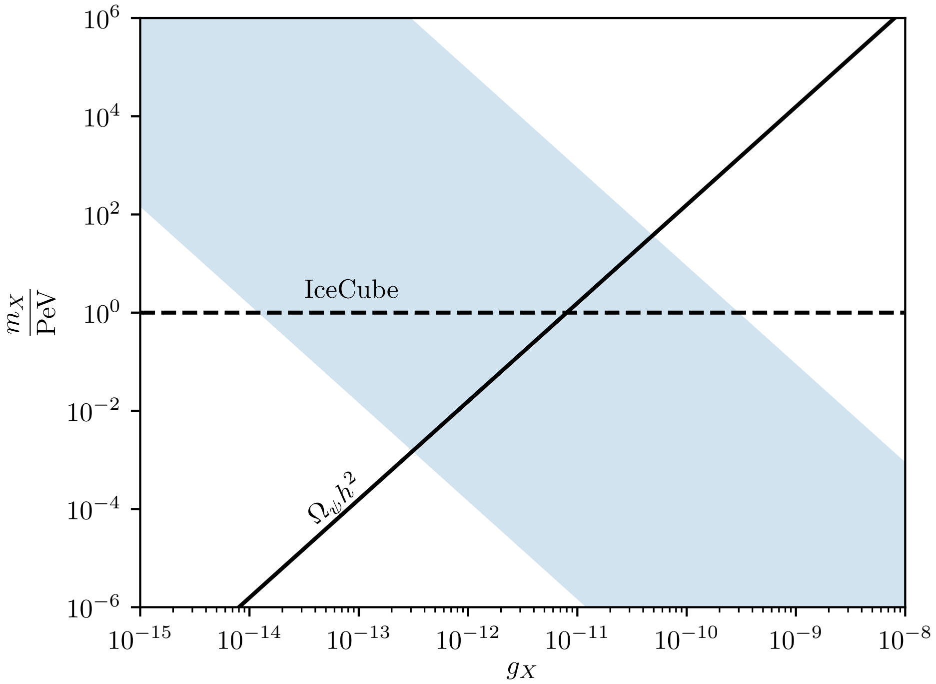

Figure 4.5: Constraints on the relation between the coupling constant g_X and the mass of the heavy scalar X. The shaded region represents the parameter space allowed by Eq. (4.5.16), while the solid line comes from the condition for the correct relic density in Eq. (4.6.9). The dashed line represents the IceCube measurements of ultra-energetic neutrinos in the PeV regime. Dark Matter with mass $m_\psi = 1$ TeV is assumed.

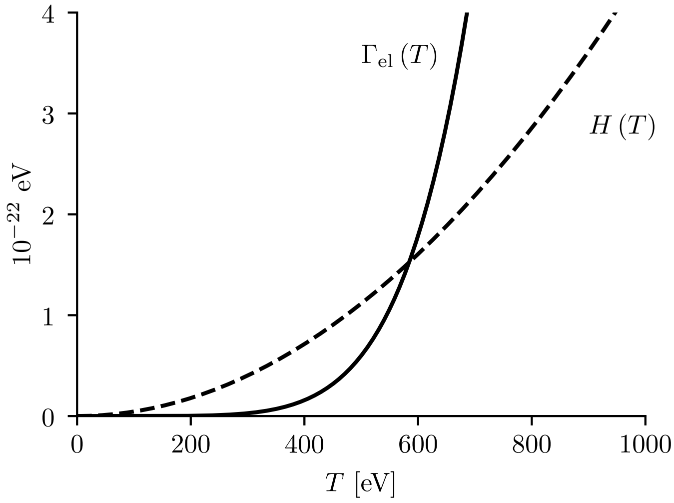

Figure 4.6: The intersection between the Hubble expansion rate (dashed line) and the rate of elastic scattering (solid line) gives a good approximation for the temperature of kinetic decopuling.

4.6.2 Kinetic decoupling

The temperature of kinetic decoupling marks the moment in time when the momentum exchange between the Dark Matter particles and the SM neutrinos is no longer efficient at maintaining thermal equilibrium between the two. In order to solve the missing satellites problem, this should happen at late times, preferably after Big Bang Nucleosynthesis and before recombination. A lower bound of $T_{\mathrm{kd}} \gtrsim 100$ eV is given by Lyman-α measurements [66, 67]. A sufficient approximation for T_{kd} is obtained after imposing the condition

$$\langle \sigma_{\mathrm{el}} v_{\mathrm{rel}} \rangle \, n_\nu \left(T_{\mathrm{kd}}\right) = H\left(T_{\mathrm{kd}}\right) \ , \tag{4.6.10}$$

i.e. by determining the temperature at which the expansion of the universe is faster than the rate of the elastic scattering (see also Figure 4.6). A more precise calculation of T_{kd}, which yields very similar results in this case, can be done following Ref. [53]. For $m_\phi \approx \mathcal{O}(1)$ keV and $m_\psi \approx \mathcal{O}(1)$ TeV values of $T_{\mathrm{kd}} \approx 0.6$ keV are obtained, which allow to solve the missing satellites problem.

4.6.3 Damping scales

The temperature of kinetic decoupling determines the size of the smallest Dark Matter structures in the Universe. Indeed, any structure contained within the set of points which can be reached by neutrinos before T_{kd} will be destroyed by them. This set of points is a sphere with radius $H^{-1}(T_{\mathrm{kd}})$ and the mass contained within it is

$$M_{\mathrm{d}} = \frac{4\pi}{3}\rho_{\mathrm{m}}(T_{\mathrm{kd}})\frac{1}{H^3(T_{\mathrm{kd}})} \,. \tag{4.6.11}$$

Using $\rho_{\mathrm{m}}(T_{\mathrm{kd}}) = (\Omega_{\mathrm{m},0}\rho_{\mathrm{crit.},0}/s(T_0))\, s(T_{\mathrm{kd}})$, this can be explicitly written as [54]

$$M_{\mathrm{d}} \approx 4.67\times 10^{9}\frac{g_{*,\mathrm{S}}(T_{\mathrm{kd}})}{g_*^{\frac{3}{2}}(T_{\mathrm{kd}})}\left(\frac{\mathrm{keV}}{T_{\mathrm{kd}}}\right)^3 M_\odot \,. \tag{4.6.12}$$

Here, $M_\odot$ is the solar mass, $g_{*,\mathrm{S}}$ is the number of effective degrees of freedom in entropy and g_* the number of effective relativistic degrees of freedom. This is precisely at the scale of dwarf galaxies which is required to solve the missing satellites problem [35, 56, 68, 66]. This result strongly departs from the values obtained with WIMPs within the ΛCDM model [69, 70],

$$M_{\mathrm{d,WIMP}} \approx 30 M_\oplus \left(\frac{10\,\mathrm{MeV}}{T_{\mathrm{kd}}}\right)^3 \,, \tag{4.6.13}$$

where $M_\oplus$ is the mass of the Earth.

In principle, between the damping mass due to free streaming and the one due to acoustic damping, the larger one should be taken. Here, however, free streaming is negligible, since the corresponding damping masses are proportional to $1/T_{\mathrm{kd}}^{3/2}$ which is subdominant to $1/T_{\mathrm{kd}}^3$ for late kinetic decouplings [70].

It should be noted how requiring such a kinetic decoupling highly constrains the parameters α and m_ϕ. While it is in principle possible to choose m_ϕ freely and adjust α accordingly in order to obtain the correct value of T_{kd}, this is not always compatible with the requirements about self-interactions which will be explained in Section 4.6.4. Indeed, it will be shown that only a value of m_ϕ in the sub-keV range is acceptable

4.6.4 Self-interactions

Self-interactions are mediated by the ϕ scalar and are crucial to successfully address the cusp vs. core, too-big-to-fail and diversity problems. For this purpose, the elastic cross section should be approximately $\langle\sigma_T/m_\psi\rangle_{v_{\mathrm{therm}}} \approx 1\,\mathrm{cm}^2\,\mathrm{g}^{-1}$ [71]. Here, the angled brackets denote an average over a Maxwell-Boltzmann distribution with mean value

v_{therm},

$$\frac{\langle\sigma_T\rangle_{v_{\text{therm}}}}{m_\psi} = \frac{1}{m_\psi}\int \mathrm{d}^3v \frac{1}{(2\pi v_{\text{therm}})^{3/2}} e^{-\frac{v^2}{v_{\text{therm}}^2}} \sigma_T \; . \tag{4.6.14}$$

More specifically, the cross section should be velocity dependent in order to address the small-scale problems and leave the situation unchanged at large scales. At the scales of dwarf galaxies ($\lesssim \mathcal{O}(1)$ keV) it should have an approximate value of $\langle\sigma_T\rangle_{30}/m_\psi \approx 1.0\ \mathrm{cm}^2\,\mathrm{g}^{-1}$ [61, 50, 41], where the average velocity is 30km/s. At large scales, i.e. at the scale of galaxy clusters ($\gtrsim \mathcal{O}(10)$ Mpc), it should have a value satisfying $\langle\sigma_T\rangle_{1000}/m_\psi \lesssim 0.1\ \mathrm{cm}^2\,\mathrm{g}^{-1}$. Using Eq. (4.3.20), values of $m_\phi \approx \mathcal{O}(1)$ MeV are needed to obtain values of $\langle\sigma_T\rangle/m_\psi$ in the desired range [42]. However, values of $m_\phi \lesssim 1000$ eV are required to have a late kinetic decoupling. This is solved within this model thanks to the phase transition taking place after kinetic decoupling ($T_{\text{SSB}} < T_{\text{kd}}$) and gives a new much larger mass to the scalar ϕ. An example of a choice of parameters yielding the correct self-interaction cross sections would be $m_\psi \approx 1$ TeV and $m_\phi^{(\text{SSB})} \approx 5$ MeV.

4.7 Results

Having discussed each single cosmological observable on its own, it is now possible to present an explicit choice of parameters which solve all small-scale problems at once. It is summarized in Table 4.3.

As discussed in Section 4.5.2, the effective coupling between ϕ and SM neutrinos is highly constrained and must satisfy $g_\nu \approx 10^{-7}$. The other couplings should lie in the perturbative regime as well, but are not subject to such stringent bounds. A good choice for $g_{\phi n}$ is $g_{\phi n} \approx 0.02$. Then $Y^2/(2m_n^2) \approx 4\times10^{-3}$ follows immediately from the relation between g_ν and $g_{\phi n}$ (see Eq. (4.2.10)). Remembering that $Y = y\sqrt{2}\langle H\rangle$ and the fact that the sterile neutrinos are here supposed to have a mass approximately in the TeV range, an estimate $y \approx 0.1$ can be calculated, using $\langle H\rangle \approx 246$ GeV for the expectation value of the Higgs field. These tiny couplings make the field ϕ chemically decouple at early temperatures (at $T \approx$ TeV) from the SM-neutrinos in order to evade Big Bang Nucleosynthesis constraints. The acceptable values for α (and thus $g_{\phi\psi}$) depend on the choice for the parameter m_ϕ. For example, $\alpha \approx 10^{-2}$ (i.e. $g_{\phi\psi} \approx 0.3$) is needed if $m_\phi \approx 10$ keV, while $\alpha \approx 10^{-1}$ (i.e. $g_{\phi\psi} \approx 1$) is required in the case $m_\phi \approx 30$ eV. The coupling g_X is also dependent on the mass of the heaviest boson X, as seen in Fig. (4.5). In view of the Ice Cube measurements of ultra-energetic neutrinos [19], the preferred value is $g_X \approx 10^{-11}$, as can also be seen from Fig. 4.5. Finally, concluding the presentation of the couplings, the couplings in the scalar potential x and ℓ are fully determined by the choice of the masses $m_{\tilde{\Phi}}$ and $m_{\phi}^{(\mathrm{SSB})}$ discussed below as well as by the condition that the spontaneous symmetry breaking happens at a temperature $T_{\mathrm{SSB}} \approx 100$ eV.

The mass of the Dark Matter particles is $m_{\psi} \approx 0.3-1$ TeV, although lower masses would be allowed if there were more than one copy of the boson X. Similarly, the sterile neutrinos should have $m_n \approx 20$ TeV. It is due to these large masses of ψ and n that the cubic interactions between them and the light boson ϕ are suppressed. The value of the mass of the ϕ boson after the spontaneous symmetry breaking in the Dark Sector can be chosen to be $m_{\phi}^{(\mathrm{SSB})} \approx 1-5$ MeV. This allows to obtain the correct cross sections for self-interactions. Before the symmetry breaking, the mass parameter should lie in the range $m_{\phi} \approx 30-1000$ eV for a late kinetic decoupling solving the missing satellites problem. The heavy boson X should have a mass $m_X \approx \mathcal{O}(1)$ PeV in order to yield the correct relic density by decaying after the freeze-out between Dark Matter and the light bosons ϕ. Furthermore, rare decays of the X particle could possibly explain the observation of three neutrinos with energies in the PeV range by the IceCube collaboration [19]. Regardless of these measurements, Fig. 4.5 clearly indicates that the mass of X should lie in the range between $\mathcal{O}(1)$ TeV and $\mathcal{O}(100)$ PeV. Finally, the mass of the scalar field $\tilde{\Phi}$ after the spontaneous symmetry breaking should be $m_{\tilde{\Phi}} \approx \mathcal{O}(1)$ μeV in order to give only a negligible contribution to the DM relic density. It should be noted here that the other fields ϕ, X and n have decayed earlier, such that the relic density is only given by the Dark Matter particles ψ.

With this parameter set, all constraints presented in Sections 4.4 and 4.5 are satisfied, while at the same time the cosmological observables discussed in Section 4.6 are such that the small-scale problems are resolved.

Parameter	Approximate Value
m_ψ	$0.3 - 1$ TeV
m_n	20 TeV
m_ϕ	$30 - 1000$ eV
$m_\phi^{(\mathrm{SSB})}$	$1 - 5$ MeV
m_X	1 PeV
$m_{\tilde{\Phi}}$	$\ll 1$ eV
g_ν	10^{-7}
$g_{\phi n}$	0.02
$g_{\phi\psi}$	$0.3 - 1$

Table 4.3: A summary of all the parameters able to solve the small-scale problems within the neutrinophilic Dark-Matter model.

5 Leptophilic Dark Matter

5.1 Introduction

The final model considered studies the possibility of a Dark Matter annihilation channel into positrons and electrons [33]. A particle model is constructed which simultaneously addresses all small-scale problems of ΛCDM and could lead to Dark Matter detection as electron-positron excesses in cosmic rays. Indeed, a large number of experiments have been looking for electron or positron excesses (e.g. ATIC [72], CALET [73], PAMELA [74]). In particular, the DAMPE collaboration [75] claimed to have measured a peak in the cosmic rays positron spectrum at energies of approximately 1.4 TeV. Even though the validity of those results has since been challenged [73], a leptophilic Dark Matter model remains an interesting possibility to analyze, for its aptness to be experimentally verified.

The model assumes a fermionic Dark Matter candidate, which annihilates through some mediator into electrons and positrons. The mass of the Dark Matter candidate is assumed to lie above the TeV range, i.e. the region which has only recently been reached by experiment detectors. Of course, such an annihilation into Standard-Model particles means that a lot of constraints must be taken into account: for example, the modification to the electron's anomalous magnetic moment due to these new interactions should lie within the current experimental error.

At the same time, the other goal of this model is to resolve the cusp vs core, too-big-to-fail, missing satellites and diversity problems. This poses further constraints on the new parameters of the theory and even requires the introduction of an extra mediator to ensure a late kinetic decoupling which would otherwise be impossible together with annihilations at $E \gtrsim 1$ TeV into electrons and positrons.

5.2 Lagrangian

The Lagrangian of the theory consists of three terms, $\mathcal{L}_{\mathrm{DS}} = \mathcal{L}_{\mathrm{kin}} + \mathcal{L}_{\mathrm{lept}} + \mathcal{L}_{\mathrm{int}}$. $\mathcal{L}_{\mathrm{kin}}$ contains the kinetic terms for the new particles. $\mathcal{L}_{\mathrm{lept}}$ describes the coupling of the Dark Matter candidates to all charged leptons in the Standard Model. $\mathcal{L}_{\mathrm{int}}$ describes all other interaction operators up to dimension-4 which are allowed by the symmetries of the model.

The kinetic part of the Lagrangian is

$$\mathcal{L}_{\mathrm{kin}} = \overline{\chi}\left(\mathrm{i}\not{\partial} - m_\chi\right)\chi + \left(D^*_\mu \Delta^{+*}\right)\left(D^\mu \Delta^+\right) - m^2_{\Delta^+}\Delta^{+*}\Delta^+ - \frac{1}{2}\Delta^0\left(\Box + m^2_{\Delta^0}\right)\Delta^0 \tag{5.2.1}$$

with $D_\mu = \partial_\mu - \mathrm{i}g' B_\mu$. This can be written more explicitly as

$$\begin{aligned}\mathcal{L}_{\mathrm{kin}} \;=\;& \overline{\chi}\left(\mathrm{i}\not{\partial} - m_\chi\right)\chi - \Delta^{+*}\left(\Box + m^2_{\Delta^+}\right)\Delta^+ + \mathrm{i}g' B_\mu\left[\left(\partial^\mu \Delta^{+*}\right)\Delta^+ - \Delta^{+*}\left(\partial^\mu \Delta^+\right)\right] \\ & + g'^2 B_\mu B^\mu \left|\Delta^+\right|^2 - \frac{1}{2}\Delta^0\left(\Box + m^2_{\Delta^0}\right)\Delta^0 \,.\end{aligned} \tag{5.2.2}$$

The fields introduced in the above expressions are the following. The Dark Matter candidate χ is a Dirac field, Δ^+ is a complex scalar field, Δ^0 is a real scalar field and B is the gauge boson of the $\mathrm{U}(1)_Y$ hypercharge symmetry of the Standard Model. g' is the corresponding coupling.

The Yukawa interaction between Dark Matter particles and charged leptons is given by

$$\mathcal{L}_{\mathrm{lept}} = -g_i \overline{\chi}\Delta^+ l^i_R - g_i \overline{l^i_R}\left(\Delta^+\right)^* \chi \;\; . \tag{5.2.3}$$

Here, l_R is the right-handed charged lepton triplet, $l_R = (e_R, \mu_R, \tau_R)^T$, and g_i for $i \in \{e,\, \mu,\, \tau\}$ distinguishes the couplings between the different leptons. From this interaction, it is clear that the complex scalar field Δ^+ must carry a U(1) charge as well. Dark Matter particles are assumed to couple only to right-handed charged leptons. This is necessary in order to satisfy constraints on the lepton anomalous magnetic moment, as will be shown in Sec. 5.4.3.

Finally, the other interactions of the theory are described by

$$\mathcal{L}_{\mathrm{int}} = -a_1\left(\Delta^+\right)^*\Delta^+\left(\Delta^0\right)^2 - \mu_+\left(\Delta^+\right)^*\Delta^+\Delta^0 - \frac{1}{6}\mu_0\left(\Delta^0\right)^3 + g_0\overline{\chi}\Delta^0\chi \,. \tag{5.2.4}$$

All the new parameters a_1, g_0, μ_+ and μ_0 are real. Each term plays a specific role for the phenomenology of the theory. The first one is responsible for the depletion of the Δ^+ particles. The second one allows the Δ^0 particles to decay. The third one enables IR-dominant, purely uncharged interactions. Finally the last one facilitates self-interactions between the Dark Matter particles. All these features will be discussed in great detail in the rest of this Section.

5.2.1 Mass hierarchy

As mentioned in the introduction, the mass of the Dark Matter candidate is assumed to lie in the TeV range. This was originally motivated by the DAMPE collaboration's claim of having measured a peak in the positron's cosmic ray excess at energies of approximately 1.4 TeV [75]. However, the TeV range is an interesting one regardless of such claims, being at the frontier of the current experiments.

A mass degeneracy between the charged scalar fields and Dark Matter is assumed in order to suppress annihilations of the charged mediator into Dark Matter particles and allow an enhanced elastic scattering with electrons as will be discussed in Sec. 5.5.2. This mass degeneracy is parametrized as

$$m_{\Delta^+} - m_\chi \equiv d > 0 \quad \text{with} \quad \delta \equiv \frac{d}{m_\chi} \ll 1 \, . \tag{5.2.5}$$

The condition $m_e < d < m_\mu, m_\tau$ is also imposed, where $m_e \approx 0.5$ MeV, $m_\mu \approx 105$ MeV, and $m_\tau \approx 1.7$ GeV are the masses of the electron, muon, and tau, respectively. This particular condition enables a resonance in the elastic scattering between electrons and Dark Matter which might reestablish thermal equilibrium between the two at temperatures below 1 keV (see Sec. 5.5.2 for more details).

Finally, the mass of the uncharged scalar Δ^0 is assumed to be significantly smaller, namely in the keV range. As will be discussed in Secs. 5.5.2 and 5.5.3, this allows for the resolution of the Dark Matter small-scale problems.

5.3 Relevant cross sections and decay rates

All relevant scatterings and decays are calculated and discussed in this section.

5.3.1 Annihilation into charged leptons

The Yukawa coupling in Eq. (5.2.3) creates an annihilation channel for Dark Matter into charged leptons, as depicted in Fig. 5.1. This annihilation could potentially be observed as a Cosmic Ray Excess from different experiments. Furthermore, this process is responsible for the freeze-out of Dark Matter as will be discussed in Sec. 5.5.1, where the Dark Matter relic density is computed.

The average of the squared amplitude for the process in Fig. 5.1 is

$$\begin{aligned}\left\langle |\mathcal{M}|^2 \right\rangle &= \sum_{\text{spins}} \frac{1}{4} \frac{g_{\mathrm{i}}^4}{\left[(p_1 - p_3)^2 - m_{\Delta^+}^2\right]^2} \left[\overline{u}_R(p_3)\, u(p_1)\right]^* \left[\overline{u}_R(p_3)\, u(p_1)\right] \\ &\quad \times \left[\overline{v}(p_2)\, v_R(p_4)\right]^* \left[\overline{v}(p_2)\, v_R(p_4)\right] \ , \end{aligned} \tag{5.3.1}$$

which, with the identity $\mathrm{tr}\left\{\gamma^\mu \gamma^\nu\right\} = 4g^{\mu\nu}$, can be written explicitly as

$$\left\langle |\mathcal{M}|^2 \right\rangle = \frac{g_i^4}{\left[(p_1 - p_3)^2 - m_{\Delta^+}^2\right]^2} (p_1 \cdot p_3)(p_2 \cdot p_4) \ . \tag{5.3.2}$$

Assuming highly non-relativistic Dark Matter particles, $m_{\Delta^+} \approx m_\chi \gg m_e$, and in the center-of-mass frame, i.e. $p_1 = p_2 = \left(m_\chi, \vec{0}\right)$, $p_3 = (m_\chi, \vec{p})$ and $p_4 = (m_\chi, -\vec{p})$ with $|\vec{p}| = \sqrt{m_\chi^2 - m_i^2}$, the squared amplitude is $\left\langle |\mathcal{M}|^2 \right\rangle \approx g_i^4/4$. This can be inserted in the expression for the cross section,

$$\sigma = \frac{1}{4\pi v_{\mathrm{rel}}} \frac{1}{2E_1 2E_2} \frac{|\vec{p}|}{(E_1 + E_2)} \left\langle |\mathcal{M}|^2 \right\rangle \ , \tag{5.3.3}$$

and yields

$$\langle \sigma v_{\mathrm{rel}} \rangle_{\chi\overline{\chi} \to l_{R,\,i} \overline{l_{R,\,i}}} = \frac{\pi \alpha_i^2}{8} \frac{1}{m_\chi^2} \sqrt{1 - \delta_i'^{\,2}} \ . \tag{5.3.4}$$

Here, the notation $\alpha_i = g_i^2/4\pi$ and $\delta_i' = m_i/m_\chi$ with $i \in \{e, \mu, \tau\}$ has been introduced. Furthermore, the angled brackets $\langle \dots \rangle$ denote the thermal average using relative velocities, which is trivial in this case, since there is no energy dependence in this non-relativistic limit.

5.3.2 Annihilation of the charged mediator

The principal annihilation channel for the charged mediator is the four-point interaction with coupling strength a_1 in Eq. (5.2.4). The averaged squared amplitude is

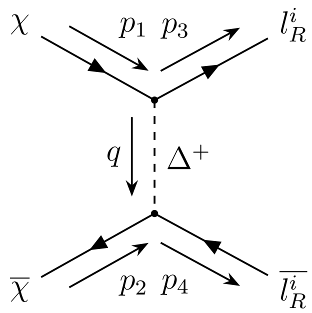

Figure 5.1: The annihilation channel for Dark Matter into charged leptons.

$\left\langle |\mathcal{M}|^2 \right\rangle = a_1^2$. In the center-of-mass frame and in the non-relativistic limit, i.e. with $p_1 = p_2 = \left(m_{\Delta^+}, \vec{0}\right)$, $p_3 = (m_{\Delta^+}, \vec{p})$ and $p_4 = (m_{\Delta^+}, -\vec{p})$ with $|\vec{p}| = \sqrt{m_{\Delta^+}^2 - m_{\Delta^0}^2}$, the cross section is

$$\langle v_{\rm rel}\sigma_{\Delta^+\Delta^+\to\Delta^0\Delta^0}\rangle = \frac{\pi\alpha_1^2}{4\left(m_{\Delta^+}\right)^2}\sqrt{1 - \frac{m_{\Delta^0}^2}{m_{\Delta^+}^2}}\ , \tag{5.3.5}$$

where $\alpha_1 = a_1/4\pi$ has been introduced. In principle, s-channel annihilations mediated by Δ^0 are also possible. In this case, the cross section is proportional to $\mu_0^2\mu_+^2/m_{\Delta^+}^4$ under the assumption $m_{\Delta^+} \gg m_{\Delta^0}$. Thus, this channel is negligible compared to the four-point interaction described above if $\mu_0^2\mu_+^2/m_{\Delta^+}^4 \ll a_1^2$.

It should be also noted that annihilations into the Dark Matter particles χ have a cross section which is proportional to $\left(1 - m_\chi^2/m_{\Delta^+}^2\right)^{5/2}$. By the assumed mass degeneracy, m_χ/m_{Δ^+} is close to one and thus, this annihilation channel is kinematically suppressed. Furthermore, the annihilation process of the Δ^+'s into right-handed electrons is p-wave suppressed, since in the center-of-mass frame the final state has a total angular momentum of +1.

5.3.3 Elastic scattering with electrons

Electrons are a long lasting elastic scattering partner of the Dark Matter candidates through the diagrams in Fig. 5.2.

The average of the squared amplitude for the process $\chi e \to \chi e$ in Fig. 5.2a is

$$\left\langle |\mathcal{M}|^2 \right\rangle = \frac{g_i^4}{\left[\left(p_1 - p_3\right)^2 - m_{\Delta^+}^2\right]^2} 2\left(p_1 \cdot p_3\right) 2\left(p_2 \cdot p_4\right)\ . \tag{5.3.6}$$

In the non-relativistic approximation, $p_1 \approx \left(m_\chi, \vec{0}\right)$, $p_2 \approx \left(m_e\left(1 + v^2/2\right), m_e\vec{v}\right)$, valid

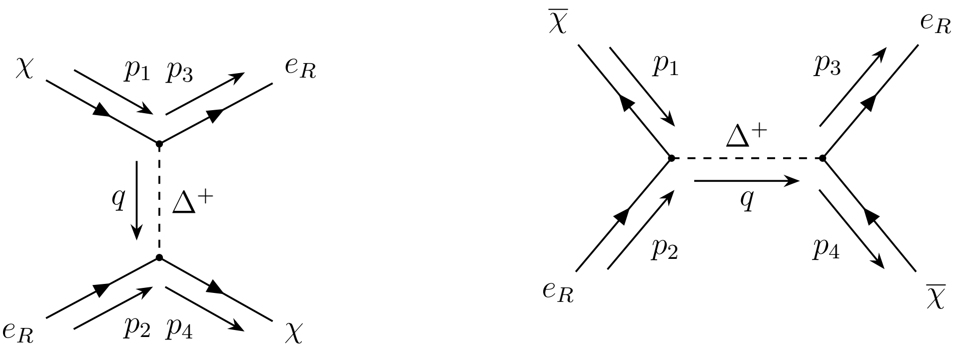

(a) Elastic scattering of χ with electrons. (b) Elastisc scattering of $\overline{\chi}$ with electrons.

Figure 5.2: The diagrams responsible for the elastic scattering of Dark Matter with electrons.

at temperatures $T \ll m_e$, and assuming that only the direction of the electron's momentum is changed after the scattering, the differential cross section becomes

$$\frac{d\sigma}{d\Omega} = \frac{1}{4\pi^2} \frac{m_e}{m_\chi + m_e\left(1+\frac{v^2}{2}\right)} m_\chi m_e \left(1+\frac{v^2}{2}\right) \frac{g_i^4}{\left[m_\chi^2 + m_e^2 - 2m_\chi m_e\left(1+\frac{v^2}{2}\right) - m_{\Delta^+}^2\right]^2} \,. \tag{5.3.7}$$

Using again the definitions $\delta = (m_{\Delta^+} - m_\chi)/m_\chi$ and $\delta'_e = m_e/m_\chi$, the momentum-transfer cross section $\sigma_T = \int \mathrm{d}\Omega\,(1-\cos(\theta))\,d\sigma/d\Omega$ can finally be written as

$$\sigma_T^{\chi e} \approx \frac{g_i^4}{16\pi}\frac{m_e^2}{4m_\chi^4}\frac{1}{\left[-\delta - \delta'_e\left(1+\frac{v^2}{2}\right) + \frac{1}{2}\left(-\delta^2 + \delta_e'^2\right)\right]^2} \,. \tag{5.3.8}$$

The average of the squared amplitude of the process described by Fig. 5.2b is very similar,

$$\left\langle |\mathcal{M}|^2 \right\rangle = \frac{g_i^4}{\left[(p_1-p_2)^2 - m_{\Delta^+}^2\right]^2} 2\,(p_1\cdot p_2)\,2\,(p_3\cdot p_4) \;, \tag{5.3.9}$$

and leads to the momentum-transfer cross section

$$\sigma_T^{\overline{\chi} e} \approx \frac{g_i^4}{16\pi}\frac{m_e^2}{4m_\chi^4}\frac{1}{\left[-\delta + \delta'_e\left(1+\frac{v^2}{2}\right) + \frac{1}{2}\left(-\delta^2 + \delta_e'^2\right)\right]^2} \,. \tag{5.3.10}$$

The behavior of these two cross sections is quite different. Both have a divergence for some specific value of δ. The divergences are located at

$$\delta_{\mathrm{div}}^{\chi} = \sqrt{\delta_e'^2 - \delta'_e\,(2+v^2) + 1} - 1 \;, \tag{5.3.11}$$

$$\delta^{\overline{\chi}}_{\rm div} = \sqrt{\delta'^2_e + \delta'_e\left(2+v^2\right)+1} - 1 \; . \tag{5.3.12}$$

However, for the scattering of χ with electrons the assumption $m_{\Delta^+} - m_\chi > m_e$ implies that the divergence in Eq. (5.3.11) can never be attained, since $\delta^{\chi}_{\rm div} \leq \delta'_e$ for all values of v. Indeed, the corresponding cross section is always bounded from above by

$$\sigma^{\chi e}_T \leq \frac{g_e^4}{16\pi}\frac{1}{16 m_\chi^2} \; . \tag{5.3.13}$$

On the other hand, the elastic scattering between $\overline{\chi}$ and e is divergent. For small velocities the cross section is enhanced a lot when $\delta \approx \delta'_e$. A more precise choice for the value of δ will be given in Sec. 5.7, where the possibility of a late kinetic decoupling thanks to this resonant behavior is discussed.

5.3.4 Elastic scattering with Δ^0

The Dark Matter particles χ can scatter elastically with the light dark mediators Δ^0 as well. The process is represented in Fig. 5.3. The amplitude is given by

$$\mathrm{i}\mathcal{M} = \left(\mathrm{i}g_0\right)\left(\mathrm{i}\mu_0\right)\frac{\mathrm{i}}{\left(p_1 - p_3\right)^2 - m^2_{\Delta^0}}\overline{u}\left(p_3\right)u\left(p_1\right) \; . \tag{5.3.14}$$

With the average of the square of this amplitude

$$\left\langle \left|\mathcal{M}\right|^2\right\rangle = \frac{2 g_0^2 \mu_0^2}{\left[\left(p_1 - p_3\right)^2 - m^2_{\Delta^0}\right]^2}\left(p_1\cdot p_3 + m_\chi^2\right) , \tag{5.3.15}$$

the differential cross section in the center-of-mass frame is

$$\frac{\mathrm{d}\sigma}{\mathrm{d}\Omega} = \frac{g_0^2\mu_0^2}{32\pi^2 E_{\rm cm}}\frac{p_1\cdot p_3 + m_\chi^2}{\left[\left(p_1 - p_3\right)^2 - m^2_{\Delta^0}\right]^2} \; . \tag{5.3.16}$$

It should be noted that all spatial momenta have the same magnitude in this reference frame and thus $p_1 \cdot p_3 = m_\chi^2 + \left|\vec{p}\right|^2\left(1-\cos\left(\theta\right)\right)$, where θ is the angle between the ingoing and the outgoing momenta. Analogously, $\left(p_1 - p_3\right)^2 = -2\left|\vec{p}\right|^2\left(1-\cos\left(\theta\right)\right)$.

The momentum-transfer cross section for this elastic scattering is then

$$\sigma_T = \int_0^{2\pi} \mathrm{d}\varphi \int_0^{\pi} \mathrm{d}\theta \sin(\theta)\left(1-\cos(\theta)\right) \frac{g_0^2 \mu_0^2}{32\pi^2 E_{\mathrm{cm}}^2} \frac{2m_\chi^2 + |\vec{p}|^2 \left(1-\cos(\theta)\right)}{\left[2|\vec{p}|^2 \left(2-\cos(\theta)\right) + m_{\Delta^0}^2\right]^2} . \tag{5.3.17}$$

While the integral over φ is immediate and simply gives a factor of 2π, the integral over θ requires the change of variables $y = 1-\cos(\theta)$. This yields

$$\sigma_T = \frac{g_0^2 \mu_0^2}{16\pi E_{\mathrm{cm}}^2} \frac{1}{4|\vec{p}|^4} \left\{ 2m_\chi^2 \int_0^2 \mathrm{d}y \frac{y}{\left(y + \frac{m_{\Delta 0}^2}{2|\vec{p}|^2}\right)^2} + |\vec{p}|^2 \int_0^2 \mathrm{d}y \frac{y^2}{\left(y + \frac{m_{\Delta 0}^2}{2|\vec{p}|^2}\right)^2} \right\} . \tag{5.3.18}$$

Both integrals are solvable by splitting the fractions into sums of multiple, lower order fractions. The result is

$$\begin{aligned} \sigma_T &= \frac{g_0^2 \mu_0^2}{16\pi E_{\mathrm{cm}}^2} \frac{1}{4|\vec{p}|^4} \left\{ 2m_\chi^2 \left[\log\left(\frac{m_{\Delta^0}^2 + 4|\vec{p}|^2}{m_{\Delta^0}^2}\right) - \frac{4|\vec{p}|^2}{4|\vec{p}|^2 + m_{\Delta^0}^2} \right] \right. \\ &\quad \left. + |\vec{p}|^2 \left[-\frac{m_{\Delta^0}^2}{|\vec{p}|^2} \log\left(\frac{m_{\Delta^0}^2 + 4|\vec{p}|^2}{m_{\Delta^0}^2}\right) + \frac{8|\vec{p}|^2 + 4m_{\Delta^0}^2}{4|\vec{p}|^2 + m_{\Delta^0}^2} \right] \right\} \qquad (5.3.19) \\ &= \frac{g_0^2 \mu_0^2}{16\pi E_{\mathrm{cm}}^2} \frac{1}{4|\vec{p}|^4} \left\{ \left(2m_\chi^2 - m_{\Delta^0}^2\right) \log\left(\frac{m_{\Delta^0}^2 + 4|\vec{p}|^2}{m_{\Delta^0}^2}\right) \right. \\ &\quad \left. + \left(-4m_\chi^2 + 4|\vec{p}|^2 + 2m_{\Delta^0}^2\right) \frac{2|\vec{p}|^2}{4|\vec{p}|^2 + m_{\Delta^0}^2} \right\} . \qquad (5.3.20) \end{aligned}$$

This can be brought to a much simpler form in the low-energy regime, i.e. when most of the energy of the Dark Matter candidates is their rest energy. This is indeed the relevant regime for elastic scattering, which is still expected to happen at low temperatures $T \ll m_\chi$. The center-of-mass energy is thus dominated by $E_{\mathrm{cm}}^2 \approx m_\chi^2$. Furthermore, $m_\chi^2 \gg m_{\Delta^0}^2$ is assumed within this model and can be used to simplify the result even more. The result is finally expressed as a function of the energy of the Δ^0's, $E^2 = m_{\Delta^0}^2 + |\vec{p}|^2$. With these assumptions the momentum-transfer cross section for the elastic scattering between χ and Δ^0 is

$$\sigma_T = \frac{g_0^2 \mu_0^2}{16\pi} \frac{\log\left(\frac{4E^2 - 3m_{\Delta 0}^2}{m_{\Delta 0}^2}\right) - \frac{E^2 - m_{\Delta 0}^2}{E^2 - \frac{3}{4}m_{\Delta 0}^2}}{2\left(E^2 - m_{\Delta^0}^2\right)^2} . \tag{5.3.21}$$

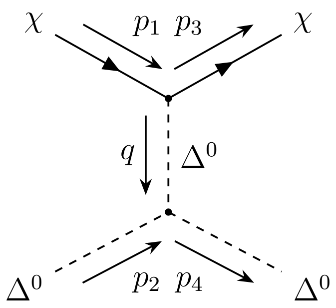

Figure 5.3: The elastic scattering between Dark Matter and the uncharged Δ^0's.

Thus, this elastic scattering is particularly dominant at temperatures close to the mass of Δ^0.

5.3.5 Self-interactions

The last term in Eq. (5.2.4) mediates self-interactions between the Dark Matter particles. In this model, the self-interactions are purely attractive, since they are mediated by a scalar particle.

In order to address the small-scale problems, a velocity-dependent cross section is required: this allows to modify Dark Matter structures at small scales, where the velocity is smaller, while leaving them unchanged at large scales, where the velocity is larger. Such a behavior is obtained in the regime where non-perturbative effects are relevant, i.e. outside of the Born regime when $\alpha_0^2 m_\chi / m_{\Delta^0} > 1$, with $\alpha_0 = g_0^2/4\pi$. An analytic fit for the cross section in the classical limit, $m_\chi v_{\rm rel}/m_{\Delta^0} \gg 1$, can be found in Refs. [42, 76] and is

$$\sigma_T = \frac{8\pi}{m_{\Delta^0}^2} \frac{\beta^2}{1 + 1.5\beta^{1.65}} \,. \tag{5.3.22}$$

Here, $\beta = \alpha_0 m_{\Delta^0} / \left(m_\chi v_{\rm rel}^2\right) \lesssim 10^3$ is assumed. This assumption is warranted as will become clear later, once the most favored values for the masses of the theory have been presented.

5.3.6 Decay of Δ^+

The charged scalars Δ^+ can decay into electrons and Dark Matter via the Yukawa coupling in Eq. (5.2.3). It should be remarked that Δ^+ cannot decay into other leptons, i.e. muons and taus, due to the assumption $m_{\Delta^+} - m_\chi < m_\mu, m_\tau$. The process is represented in Fig. 5.4 and the corresponding amplitude is

$$\mathrm{i}\mathcal{M} = \overline{u}\left(q_1\right)\frac{1+\gamma_5}{2}g_e v\left(q_2\right)\ . \tag{5.3.23}$$

With the usual trace identities, the average of the amplitude squared is

$$\left\langle \left|\mathcal{M}\right|^2 \right\rangle = 2g_e^2\left(q_1\cdot q_2\right)\ . \tag{5.3.24}$$

In the center-of-mass frame, the decay rate is then

$$\Gamma_{\Delta^+\to\chi\bar{e}_R} = \frac{|\vec{q}_1|}{8\pi m_{\Delta^+}^2}2g_e^2\left(q_1\cdot q_2\right)\ . \tag{5.3.25}$$

In this reference frame, i.e. with $p=\left(m_{\Delta^+},\vec{0}\right)$, $q_1=(E_\chi,\vec{q}_1)$, and $q_2=(E_e,-\vec{q}_1)$, the magnitude of the outgoing momentum can be written as

$$|\vec{q}_1| \;=\; \sqrt{\left(m_{\Delta^+}-\sqrt{m_\chi^2+|\vec{q}_1|^2}\right)^2-m_e^2}\ . \tag{5.3.26}$$

This can be solved for $|\vec{q}_1|$ and yields

$$|\vec{q}_1| = \sqrt{\frac{\left(m_{\Delta^+}^2-m_\chi^2\right)^2-2m_e^2\left(m_\chi^2+m_{\Delta^+}^2\right)+m_e^4}{4m_{\Delta^+}^2}}\ . \tag{5.3.27}$$

Using the definition $\delta=\left(m_{\Delta^+}-m_\chi\right)/m_\chi$, the first term under the square root can be written as $\left(m_{\Delta^+}^2-m_\chi^2\right)^2=\delta^2m_\chi^2\left(m_{\Delta^+}+m_\chi\right)^2$. Furthermore, using the valid approximations $m_\chi+m_{\Delta^+}\approx 2m_\chi$ and $m_\chi/m_{\Delta^+}\approx 1$, the final expression for $|\vec{q}_1|$ is

$$|\vec{q}_1| \approx m_\chi\sqrt{\delta^2-\delta_e'^2+\frac{1}{4}\delta_e'^4}\ , \tag{5.3.28}$$

where $\delta_e'=m_e/m_\chi$ has been used again. It should be noted that the last term under the square root could easily be neglected, since in this model $\delta_e'\ll 1$.

With $\left(q_1\cdot q_2\right)=\left[\left(q_1+q_2\right)^2-q_1^2-q_2^2\right]/2$, the product $\left(q_1\cdot q_2\right)$ can be simplified as

$$\left(q_1\cdot q_2\right) \;\approx\; m_\chi^2\left(\delta-\frac{\delta_e'^2}{2}\right)\ , \tag{5.3.29}$$

where the approximation $m_\chi+m_{\Delta^+}\approx 2m_\chi$ has been used once more. Here, again,

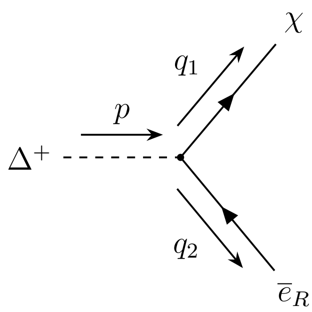

Figure 5.4: The decay channel for the charged scalar.

the second term in the parenthesis is negligible, since $\delta_e'^2 \ll \delta_e' < \delta$.

Putting everything all back together yields

$$\Gamma_{\Delta^+ \to \chi \overline{e}_R} \approx \frac{1}{4\pi} g_e^2 m_\chi \sqrt{\delta^2 - \delta_e'^2}\,\delta \ . \tag{5.3.30}$$

As an example, this corresponds to a lifetime of $\tau_{\Delta^+} = 1/\Gamma \approx 4 \times 10^{-13}$ s if $g_e^2/4\pi = 0.1$, $m_\chi = 2.2$ TeV and $m_{\Delta^+} - m_\chi = 1.01\, m_e$.

5.4 Parameters and constraints

A number of constraints on the parameters of this theory must be taken into consideration. In particular, a lot of particle constraints are necessary, since the Dark Sector is directly in contact with the Standard Model. Constraints coming from cosmological observations are present as well.

5.4.1 μ_0 and μ_+

All new couplings are assumed to allow perturbative expansions. In particular, for the dimensionful couplings μ_0 and μ_+ this translates to $\mu_+ \lesssim m_{\Delta^+}$ and $\mu_0 \lesssim m_{\Delta^0}$. The first constraint, $\mu_+ \lesssim m_{\Delta^+}$, comes from the one-loop correction of the $\mu_+ \Delta^0 \left(\Delta^+\right)^* \Delta^+$ interaction represented in Fig. 5.5a. The corresponding amplitude is proportional to

$$\mathcal{M} \propto \mu_+^3 \int \frac{\mathrm{d}^4 k}{(2\pi)^4} \frac{1}{k^2 - m_{\Delta^0}^2} \frac{1}{(q_1 - k)^2 - m_{\Delta^+}^2} \frac{1}{(q_2 - k)^2 - m_{\Delta^+}^2} \ , \tag{5.4.1}$$

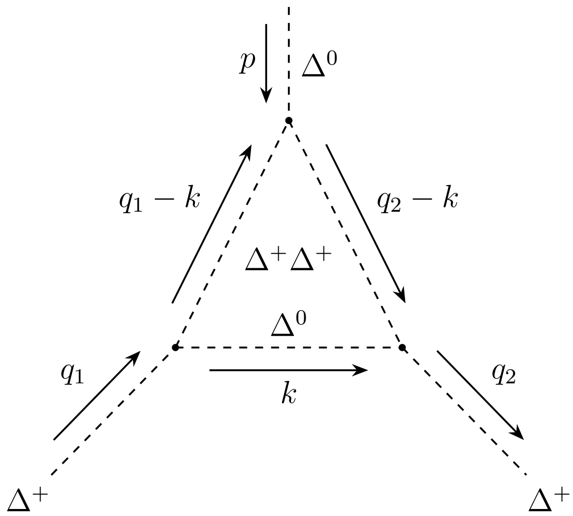

(a)

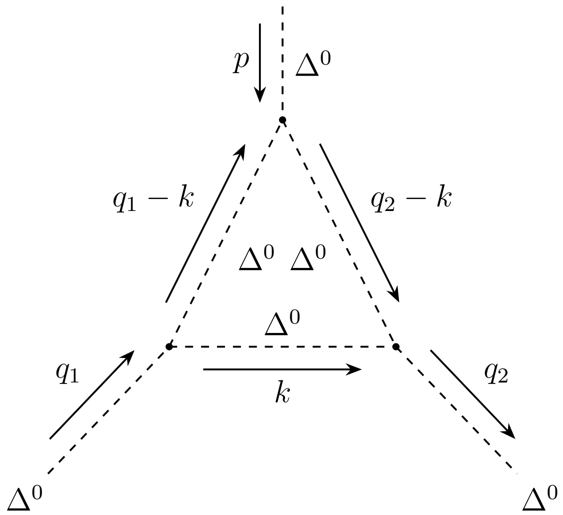

(b)

Figure 5.5: The diagrams responsible for $\mu_+ \ll m_{\Delta^+}$ and $\mu_0 \ll m_{\Delta^0}$.

which can be rewritten as

$$\mathcal{M} \propto \mu_+^3 \int_0^1 \mathrm{d}x\mathrm{d}y\mathrm{d}z\delta\left(x+y+z-1\right)\int \frac{\mathrm{d}^4k}{\left(2\pi\right)^4}\frac{1}{\left[k^2-\Delta\right]^3} \tag{5.4.2}$$

using Feynman parameters. Here, Δ is given by

$$\Delta = -zyp^2 + \left(1-x\right)^2 m_{\Delta^+}^2 + xm_{\Delta^0}^2 \; . \tag{5.4.3}$$

Neglecting factors of π and i and performing the integration over d^4k, the amplitude can be written as

$$\mathcal{M} \propto \frac{\mu_+^3}{m_{\Delta^+}^2}\int_0^1 \mathrm{d}x\mathrm{d}y\mathrm{d}z\delta\left(x+y+z-1\right)\frac{1}{-zy\frac{p^2}{m_{\Delta^+}^2}+\left(1-x\right)^2+x\frac{m_{\Delta^0}^2}{m_{\Delta^+}^2}} \; . \tag{5.4.4}$$

The result is proportional to $\mu_+(\mu_+/m_{\Delta^+})^2$ up to a large but finite numerical factor dependent on $p^2/m_{\Delta^+}^2$ and $m_{\Delta^0}^2/m_{\Delta^+}^2$ coming from the integral. Thus $\mu_+ \ll m_{\Delta^+}$ must hold to allow perturbative expansions.

The condition $\mu_0 \ll m_{\Delta^0}$ can be derived completely analogously from the vertex correction in Fig. 5.5b. In this case, the amplitude for the correction to the vertex is proportional to

$$\mathcal{M} \propto \mu_0^3 \int \frac{\mathrm{d}^4k}{\left(2\pi\right)^4}\frac{1}{k^2-m_{\Delta^0}^2}\frac{1}{\left(q_1-k\right)^2-m_{\Delta^0}^2}\frac{1}{\left(q_2-k\right)^2-m_{\Delta^0}^2} \tag{5.4.5}$$

and can be rewritten as

$$\mathcal{M} \propto \mu_0^3 \int_0^1 \mathrm{d}x\mathrm{d}y\mathrm{d}z\delta\left(x+y+z-1\right)\int \frac{\mathrm{d}^4k}{\left(2\pi\right)^4}\frac{1}{\left[k^2-\Delta\right]^3} \tag{5.4.6}$$

using Feynman parameters with $\Delta = m_{\Delta^0}^2\left(1+x^2-x+zy\right)$. Again, up to factors of i and π the amplitude is then

$$\mathcal{M} \propto \mu_0\frac{\mu_0^2}{m_{\Delta^0}^2}\int_0^1 \mathrm{d}x\mathrm{d}y\mathrm{d}z\delta\left(x+y+z-1\right)\frac{1}{1+x^2-x+zy} \; . \tag{5.4.7}$$

Since the integral is finite and only yields a numerical factor, it is clear that the condition $\mu_0 \ll m_{\Delta^0}$ must hold to allow for a perturbative theory.

5.4.2 Thermal production

Another constraint comes from the following requirements. The Dark Matter candidates should have been thermally produced and have been in thermal equilibrium with the Standard Model at some point in time. In this model, the process governing Dark Matter annihilation and production is $\overline{\chi}\chi \leftrightarrow l_{R,i}\overline{l_{R,i}}$. At a temperature $T \approx m_\chi$, Dark Matter production stops and the number density of χ starts to decrease right up until the moment when the expansion of the universe is faster than the annihilation rate, i.e. at the temperature of freeze-out. Requiring that Dark Matter was thermally produced means that the condition

$$\langle \sigma v_{\text{rel}} \rangle_{\chi\overline{\chi}\to l_{R,i}\overline{l_{R,i}}} n_\chi(m_\chi) > H(m_\chi) \tag{5.4.8}$$

must be fulfilled. With Eq. (5.3.4) this can be rewritten as

$$\frac{\pi\alpha_i^2}{8}\frac{1}{m_\chi^2}\sqrt{1-\delta_i'^2}\frac{2m_\chi^3}{(2\pi)^{\frac{3}{2}}}e^{-1} > \frac{\pi}{3}\left(\frac{g_*}{10}\right)^{\frac{1}{2}}\frac{m_\chi^2}{M_{\text{Pl}}} . \tag{5.4.9}$$

With $\sqrt{1-\delta_i'^2} \approx 1$ and $g_* = 106.75$ at temperatures in the range of TeV, the constraint on the coupling α_i becomes

$$\alpha_i > 13.6\sqrt{\frac{m_\chi}{M_{\text{Pl}}}} . \tag{5.4.10}$$

5.4.3 Anomalous magnetic moment

Within this model, each charged lepton's vertex gets a new contribution coming from the interaction represented in Fig. 5.6. This modifies their anomalous magnetic moment. The amplitude corresponding to this new interaction is

$$\begin{aligned} \mathrm{i}\mathcal{M}_i^\mu &= -g_i^2 e\overline{u}(q_2)\frac{1-\gamma_5}{2}\int\frac{\mathrm{d}^4k}{(2\pi)^4}\frac{\not{k}+m_\chi}{k^2-m_\chi^2}\frac{1}{(q_1-k)^2-m_{\Delta^+}^2}\frac{1}{(q_2-k)^2-m_{\Delta^+}^2} \\ &\quad \times\left(q_1^\mu+q_2^\mu-2k^\mu\right)\frac{1+\gamma_5}{2}u(q_1) , \end{aligned} \tag{5.4.11}$$

where $i \in \{e, \mu, \tau\}$. Using Feynman parameters this can be rewritten as

$$\begin{aligned} \mathrm{i}\mathcal{M}_i^\mu &= -g_i^2 e\overline{u}(q_2)\frac{1-\gamma_5}{2}\int_0^1 \mathrm{d}x\mathrm{d}y\mathrm{d}z\delta(1-x-y-z)\int\frac{\mathrm{d}^4k}{(2\pi)^4}\frac{\not{k}+y\not{q}_1+z\not{q}_2+m_\chi}{[k^2-\Delta]^3} \\ &\quad \times\left(q_1^\mu+q_2^\mu-2k^\mu-2yq_1^\mu-2zq_2^\mu\right)\frac{1+\gamma_5}{2}u(q_1) , \end{aligned} \tag{5.4.12}$$

where $\Delta = (1-x)^2 m_i^2 - yzp^2 + xm_\chi^2 - (1-x)\, m_e^2 + (1-x)\, m_{\Delta^+}^2$ and the substitution $k \to k + yq_1 + zq_2$ was performed. The numerator of the quantity to be calculated can be reformulated as

$$N^\mu = \frac{1}{4}\overline{u}(q_2)\left[\not{k}(1+\gamma_5) + ym_i(1-\gamma_5) + zm_i(1+\gamma_5)\right]u(q_1) \tag{5.4.13}$$
$$\times\left[(1-2y)\,q_1^\mu + (1-2z)\,q_2^\mu - 2k^\mu\right] \ , \tag{5.4.14}$$

after using the Dirac equation on the on-shell spinors $u(q_1)$ and $\overline{u}(q_2)$. All terms linear in k will vanish after the d^4k integration and can thus be neglected. Furthermore, the correction to the anomalous magnetic moment will be proportional to the prefactor of $\mathrm{i}\sigma^{\mu\nu}p_\nu$, while terms proportional to γ^μ and γ_5 are irrelevant [77]. This allows to rewrite the numerator in a simpler way by keeping only the relevant terms,

$$\begin{aligned} N^\mu \sim\ & \frac{1}{4}\overline{u}(q_2)\left[-2k^\mu\not{k}(1+\gamma_5) + ym_i(1-\gamma_5)\left((1-2y)\,q_1^\mu + (1-2z)\,q_2^\mu\right)\right. \\ & \left.+zm_i(1+\gamma_5)\left((1-2y)\,q_1^\mu + (1-2z)\,q_2^\mu\right)\right]u(q_1) \end{aligned} \tag{5.4.15}$$
$$\sim \frac{1}{4}\overline{u}(q_2)\,m_i(1-x)\left[(1-2y)\,q_1^\mu + (1-2z)\,q_2^\mu\right]u(q_1) \ . \tag{5.4.16}$$

The Gordon identity, which can be rewritten both as

$$\overline{u}(q_2)\,q_1^\mu u(q_1) = \overline{u}(q_2)\left[m_i\gamma^\mu - \frac{1}{2}p^\mu - \frac{\mathrm{i}}{2}\sigma^{\mu\nu}p_\nu\right]u(q_1) \tag{5.4.17}$$

and

$$\overline{u}(q_2)\,q_2^\mu u(q_1) = \overline{u}(q_2)\left[m_i\gamma^\mu + \frac{1}{2}p^\mu - \frac{\mathrm{i}}{2}\sigma^{\mu\nu}p_\nu\right]u(q_1) \ , \tag{5.4.18}$$

makes it possible to finally obtain the relevant terms in the numerator of the amplitude,

$$N^\mu \sim \frac{1}{2}m_i x(1-x)\,\overline{u}(q_2)\left(-\frac{\mathrm{i}}{2}\sigma^{\mu\nu}p_\nu\right)u(q_1) \ . \tag{5.4.19}$$

The second form factor is defined as the proportionality factor appearing in

$$\mathrm{i}\mathcal{M}^\mu = -ie\overline{u}(q_2)\left[\text{other form factors } + \frac{\mathrm{i}\sigma^{\mu\nu}p_\nu}{2m_i}F_2\left(\frac{p^2}{m_i^2}\right)\right]u(q_1) \ , \tag{5.4.20}$$

and thus, in this case, the new contribution to it is

$$\delta F_2\left(p^2=0\right) = \mathrm{i}g_i^2\frac{m_i^2}{2}\int \mathrm{d}x\mathrm{d}y\mathrm{d}z\,\delta(1-x-y-z)\int\frac{\mathrm{d}^4k}{(2\pi)^4}\frac{x(1-x)}{\left[k^2-\Delta\right]^3} \ . \tag{5.4.21}$$

The integration over d^4k yields $-\mathrm{i}/\left(32\pi^2\Delta\right)$ and with the approximation $m_\chi \approx m_{\Delta^+}$ and $m_i^2 \ll m_\chi^2$ the contribution to the second form factor for each charged lepton's vertex is

$$\begin{aligned}
\delta F_2\left(p^2=0\right) &\approx \frac{g_e^2 m_i^2}{64\pi^2}\int \mathrm{d}x\mathrm{d}y\mathrm{d}z\delta\left(1-x-y-z\right)\frac{x\left(1-x\right)}{m_\chi^2} && (5.4.22)\\
&= \frac{g_e^2 m_i^2}{64\pi^2}\frac{1}{12m_\chi^2} && (5.4.23)\\
&= \frac{\alpha_e}{144\pi}\delta_i'^2\ . && (5.4.24)
\end{aligned}$$

The corresponding values for each charged lepton are presented in Table 5.1 and lie within the experimental errors for the observed anomalous magnetic moments [46].

It should be noted, that this is the reason why the assumption of a Yukawa coupling with only right-handed leptons as in Eq. 5.2.3 is crucial for the viability of this theory. This can be seen as follows. If the coupling in Eq. (5.2.3) would not to discriminate between right- and left-handed particles, the amplitude for the one-loop vertex correction would be

$$\begin{aligned}
\mathrm{i}\mathcal{M}_i^\mu &= -g_i^2 e\overline{u}\left(q_2\right)\int_0^1 \mathrm{d}x\mathrm{d}y\mathrm{d}z\delta\left(1-x-y-z\right)\int\frac{\mathrm{d}^4k}{\left(2\pi\right)^4}\frac{\not{k}+y\not{q}_1+z\not{q}_2+m_\chi}{\left[k^2-\Delta\right]^3}\\
&\quad\times\left(q_1^\mu+q_2^\mu-2k^\mu-2yq_1^\mu-2zq_2^\mu\right)u\left(q_1\right)\ , && (5.4.25)
\end{aligned}$$

where $i \in \{e,\, \mu,\, \tau\}$ and Δ is the same as for the purely right-handed interaction, since the denominator is not affected. The numerator is slightly modified. After using the Dirac equation and the Gordon identity analogously to the previous calculation, the numerator can be rewritten as

$$\tilde{N}^\mu \sim \overline{u}\left(q_2\right)2x\left[\left(1-x\right)m_i+m_\chi\right]\left(-\frac{\mathrm{i}}{2}\sigma^{\mu\nu}p_\nu\right)u\left(q_1\right) \qquad (5.4.26)$$

up to terms that are irrelevant for the anomalous magnetic moment. Comparison with

Lepton	experimental error	δF_2	$\delta\tilde{F}_2$
e	$\approx 3\times10^{-13}$	6×10^{-17}	7×10^{-10}
μ	$\approx 8\times10^{-9}$	2×10^{-12}	1.4×10^{-7}
τ	$\approx 2\times10^{-2}$	6×10^{-10}	2×10^{-6}

Table 5.1: The contribution to the anomalous magnetic moment of each charged lepton and the corresponding experimental error [46]. $\delta\tilde{F}_2$ for electrons and muons is too large and thus a coupling to both right- and left-handed particles is excluded. $\alpha_i = 0.1$ and $m_\chi \approx 1$ TeV was used to obtain these values.

Eq. (5.4.20) yields

$$\begin{aligned}
\delta\tilde{F}_2\left(p^2=0\right) &= \frac{g_i^2 m_i}{16\pi^2}\int_0^1 \mathrm{d}x\mathrm{d}y\mathrm{d}z\,\delta\left(1-x-y-z\right)\frac{x\left[\left(1-x\right)m_i+m_\chi\right]}{\Delta} \\
&\approx \frac{g_i^2 m_i}{16\pi^2}\frac{1}{m_\chi^2}\int_0^1 \mathrm{d}x\mathrm{d}y\mathrm{d}z\,\delta\left(1-x-y-z\right)x\left[\left(1-x\right)m_i+m_\chi\right] \\
&= \frac{g_i^2}{16\pi^2}\frac{m_i}{m_\chi^2}\left[\frac{1}{12}m_i+\frac{1}{6}m_\chi\right] \\
&= \frac{\alpha_i}{\pi}\left(\frac{1}{48}\delta_i'^2+\frac{1}{24}\delta_i'\right)\ ,
\end{aligned} \tag{5.4.27}$$

where the same approximations on Δ were used as in the previous calculation. The main difference with respect to the purely right-handed interaction is that here the variation on the anomalous magnetic moment is linear in δ_i' instead of quadratic. Since $\delta_i' \ll 1$, this renders this contribution much larger than the purely right-handed one. Table 5.1 includes these values as well as the experimental bounds on the anomalous magnetic moments for each charged lepton. From these it is clear that purely right-handed interactions are necessary to satisfy experimental constraints.

5.4.4 Effective number of neutrinos

The presence of new particles in the Dark Sector might modify processes like Big Bang Nucleosynthesis and recombination due to the added energy in the Universe. The relativistic energy of the Universe is parametrized through ΔN_{eff} as

$$\rho_{\mathrm{rad}}\left(T_\gamma\right) = \rho_\gamma\left(T_\gamma\right) + \frac{\pi^2}{30}\frac{7}{4}N_\nu\left(\frac{4}{11}\right)^{\frac{4}{3}}T_\gamma^4 + \frac{\pi^2}{30}\frac{7}{4}\left(\frac{4}{11}\right)^{\frac{4}{3}}\Delta N_{\mathrm{eff}}T_\gamma^4\ , \tag{5.4.28}$$

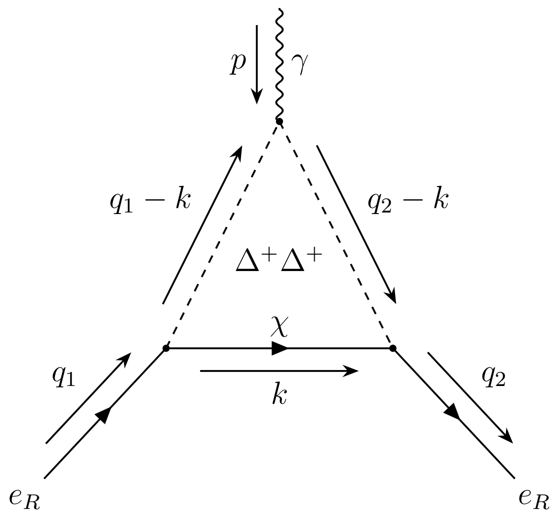

Figure 5.6: The new one-loop contribution to the anomalous magnetic moment of electrons.

where ρ_{rad} is the energy of all particles that are relativistic at a temperature T_γ. For this model, this can be rewritten as

$$\Delta N_{\mathrm{eff}}\left(T_\gamma\right) = \frac{\rho_{\mathrm{DS}}\left(T_{\mathrm{DS}}\right)}{\frac{\pi^2}{30}\frac{7}{4}\left(\frac{4}{11}\right)^{\frac{4}{3}} T_\gamma^4} \ , \tag{5.4.29}$$

where ρ_{DS} is the energy density of all relativistic particles in the Dark Sector and T_{DS} is the temperature in the Dark Sector at a given temperature T_γ in the Standard-Model plasma.

As discussed in Section 3.5.4, ΔN_{eff} should be smaller than 0.36 at the time of neutron-proton freeze-out (T_γ^{fr}) in order to be compatible with measurements of the abundances of light elements in the Universe [48, 47]. At that time ($T \approx 100$ keV), only the uncharged scalars, Δ^0's, were still relativistic and thus $\rho_{\mathrm{DS}} = \left(\pi^2/30\right) T_{\Delta^0}^4$. The ratio T_{Δ^0}/T_γ needed for computing Eq. (5.4.29) is obtained by making use of the fact that $g_{\mathrm{s},\,DS} T_{\Delta^0}^3$ and $g_{\mathrm{s},\,SM} T_\gamma^3$ are conserved separately after the decoupling of the Dark Sector from the Standard Model, which happens at energies in the TeV range. $g_{\mathrm{s,DS}}$ and $g_{\mathrm{s,SM}}$ are the degrees of freedom in entropy in the Dark Sector and the Standard Model respectively. This means,

$$\frac{T_{\Delta^0}^3}{T_\gamma^3} = \frac{g_{\mathrm{s,\,SM}}\left(T_\gamma^{\mathrm{fr}}\right)}{g_{\mathrm{s,\,SM}}\left(\mathrm{TeV}\right)}\frac{g_{\mathrm{s,\,DS}}\left(\mathrm{TeV}\right)}{g_{\mathrm{s,\,DS}}\left(T_\gamma^{\mathrm{fr}}\right)} = \frac{10.75}{106.75} \approx 0.1 \ . \tag{5.4.30}$$

With this, the deviation from the effective number of neutrinos, ΔN_{eff}, at the time of neutron-proton freeze-out is

$$\Delta N_{\text{eff}}\left(T_\gamma^{\text{fr}}\right) = \frac{4}{7}\left(\frac{11}{4}\right)^{\frac{4}{3}} \frac{T_{\Delta^0}^4}{T_\gamma^4} \approx 0.1 \,, \tag{5.4.31}$$

which is well within boundaries imposed by measurements of the ^{4}He abundance [48].

After the decay of the uncharged scalars into photons at $T_{\Delta^0} \approx 10$ keV, the photon temperature increases. Taking into account the fact that the Δ^0's were already colder than the photon plasma as described by Eq. (5.4.30), the temperature of the photons after this decay is

$$T_\gamma^3 = \frac{\left(2 + \left(\frac{T_{\Delta^0}}{T'_\gamma}\right)^3\right) T'^3_\gamma}{2} \approx 1.05\, T'^3_\gamma \,, \tag{5.4.32}$$

where T'_γ denotes the temperature of the photons right before the heating due to the Δ^0 decay. This changes the T_ν/T_γ ratio from $(T_\nu/T_\gamma)^3 = (4/11)$ to $(T_\nu/T_\gamma)^3 = (4/11) \times 0.95$ and thus the defining equation for ΔN_{eff} implies that

$$\frac{7}{4} N_\nu \left(\frac{4}{11}\right)^{\frac{4}{3}} (0.95)^{\frac{4}{3}}\, T_\gamma^4 \overset{!}{=} \frac{7}{4} N_\nu \left(\frac{4}{11}\right)^{\frac{4}{3}} T_\gamma^4 + \frac{7}{4}\Delta N_{\text{eff}} \left(\frac{4}{11}\right)^{\frac{4}{3}} T_\gamma^4 \tag{5.4.33}$$

at low temperatures. This corresponds to an effective number of neutrino degrees of freedom at recombination of

$$N_\nu + \Delta N_{\text{eff}} = N_\nu\, (0.95)^{\frac{4}{3}} \approx 2.85 \tag{5.4.34}$$

or equivalently $\Delta N_{\text{eff}} \approx -0.19$. This value is within the experimental constraints given in Ref. [1] for ΔN_{eff} at the time of recombination.

5.5 Cosmological observables

The most relevant cosmological observables are discussed in this section.

5.5.1 Relic density

Even though Δ^+ and χ have very similar masses, the total Dark Matter relic density at present times is dominated by the χ particles, since the Δ^+ particles decay before the freeze-out of the dark fermions. Analogously to Sec. 4.6.1, the relic density can be written as

$$\Omega_\chi h^2 = \frac{Y_\infty s_0 m_\chi}{\rho_c/h^2} \,, \tag{5.5.1}$$

where again $Y_\infty = x_f/\lambda$ is determined by

$$\lambda = \frac{\langle \sigma_{\mathrm{ann}} v_{\mathrm{rel}} \rangle \, s\,(x=1)}{H\,(x=1)} \tag{5.5.2}$$

and

$$x_f = -\frac{1}{2} W_0 \left(-\frac{2}{C^2} \right) \,. \tag{5.5.3}$$

Here, $C = n_\chi^{(\mathrm{eq})}\,(x=1)\,\langle \sigma_{\mathrm{ann}} v_{\mathrm{rel}} \rangle \, e/H\,(x=1)$ and W_0 is the principal branch of the Lambert W function. Thus, with the cross section from Eq. (5.3.4), the relic density can be written as

$$\Omega_\chi h^2 \approx 0.06 \left(\frac{\alpha_l}{0.06} \right)^{-2} \left(\frac{m_\chi}{1.4\,\mathrm{TeV}} \right)^2 \,, \tag{5.5.4}$$

where $\alpha_l = \sum_{i\in\{e,\mu,\tau\}} \alpha_i$ was introduced. To obtain this expression, $x_f \approx 30$ has been computed from Eq. (5.5.3), assuming $m_\chi \approx 1.4$ TeV and $\alpha_l \approx 0.06$. It should be noted that the factor $\sqrt{1-\delta_i'^2}$ appearing in the annihilation cross section is negligible when computing the relic density for Dark Matter masses in the range considered here.

Of course, $\Omega_{\overline{\chi}} h^2 = \Omega_\chi h^2$ holds, since there is no asymmetry between particles and antiparticles. The total Dark Matter relic density is easily consistent with the values required by the ΛCDM model.

5.5.2 Kinetic decoupling

The elastic scattering rate between the $\overline{\chi}$'s and the right-handed electrons is

$$\Gamma_{\overline{\chi}e,\,\mathrm{el}} = \left\langle \sigma_T^{\overline{\chi}e} v_{\mathrm{rel}} \right\rangle n_e \,. \tag{5.5.5}$$

Assuming a neutral Universe, the electron number density at temperatures in the 100 eV range is given by $n_e\,(T) \approx 0.89 \eta_b n_\gamma\,(T)$, where η_b is the baryon-to-photon ratio and the factor of 0.89 is due to the fact that approximately eightynine percent of the baryons are protons. This is the number density after the freeze-out of the electrons.

Since $\sigma_T^{\overline{\chi}e}$ does not depend on any momenta in this non-relativistic limit, the average over the thermal distribution, denoted by $\langle \ldots \rangle$, must be performed only on the relative velocity v_{rel},

$$\langle v_{\mathrm{rel}} \rangle = \frac{\int \frac{\mathrm{d}^3\vec{p}}{(2\pi)^3} v_{\mathrm{rel}} f(\vec{p})}{\int \frac{\mathrm{d}^3\vec{p}}{(2\pi)^3} f(\vec{p})} , \tag{5.5.6}$$

where $\vec{p}$ is the momentum of either the Dark Matter candidates or the electrons in the center-of-mass frame.

In this frame,

$$v_{\mathrm{rel}} = |\vec{p}| \frac{E_{\mathrm{CM}}}{E_\chi E_e} \approx |\vec{p}| \frac{m_\chi + m_e}{m_\chi m_e} . \tag{5.5.7}$$

The distribution function in the non-relativistic limit can be written as

$$f(\vec{p}) \approx \exp\left(- \frac{m_\chi + m_e + \frac{1}{2}\vec{p}^2 \frac{m_\chi + m_e}{m_\chi m_e}}{T} \right) \tag{5.5.8}$$

and thus the thermal average is

$$\langle v_{\mathrm{rel}} \rangle = \frac{2\sqrt{2}}{\sqrt{\pi}} \frac{\sqrt{T}}{\sqrt{m_e}} . \tag{5.5.9}$$

Inserting this in Eq. (5.5.5) yields the scattering rate,

$$\Gamma_{\overline{\chi}e,\mathrm{el}} \approx 4\sqrt{\frac{2}{\pi}} 0.89 \frac{\zeta(3)}{\sqrt{m_e}} \sqrt{1+\delta_e'} \sigma_{\mathrm{T}}^{\overline{\chi}e} T^{\frac{7}{2}} . \tag{5.5.10}$$

Due to the resonance of $\sigma_T^{\overline{\chi}e}$ for $\delta \approx \delta_e'$ it is possible to choose the masses of the theory in such a way that elastic scattering becomes again efficient at temperatures below keV's although only for a short period of time. This is represented in Fig. 5.7. For example, choosing $\delta = 1.001\, m_e/m_\chi$, $m_\chi = 2.2$ TeV and $\alpha_e = 0.02$ yields a temperature of kinetic decoupling of $T_{\mathrm{kd}} = 420$ eV. However, due to the divergent behavior, the $\overline{\chi}$'s and e's are not in thermal contact long enough to establish thermal equilibrium effectively. Indeed, with the mentioned parameter set they are in thermal contact for about fifteen daysfixed by choosing much lower masses, e.g. for $m_\chi \approx 10^{10}$ eV the time of thermal contact is approximately twenty years.

While this first kind of elastic scattering only involves the Dark Matter antiparticles $\overline{\chi}$ the scattering with the uncharged scalar Δ^0 involves both χ and $\overline{\chi}$. Starting from $\Gamma_{\chi\Delta^0,\mathrm{el}} = \left\langle \sigma_T^{\chi\Delta^0} v_{\mathrm{rel}} \right\rangle n_{\Delta^0}$ the scattering rate can be computed to be

$$\Gamma_{\chi\Delta^0,\mathrm{el}} \approx \frac{1}{3\pi^2 m_\chi} \int_{m_{\Delta^0}}^{\infty} \mathrm{d}E f_{\Delta^0}(E) \frac{\partial}{\partial E} \left(\left(E^2 - m_{\Delta^0}^2 \right)^2 \sigma_T^{\chi\Delta^0} \right) , \tag{5.5.11}$$

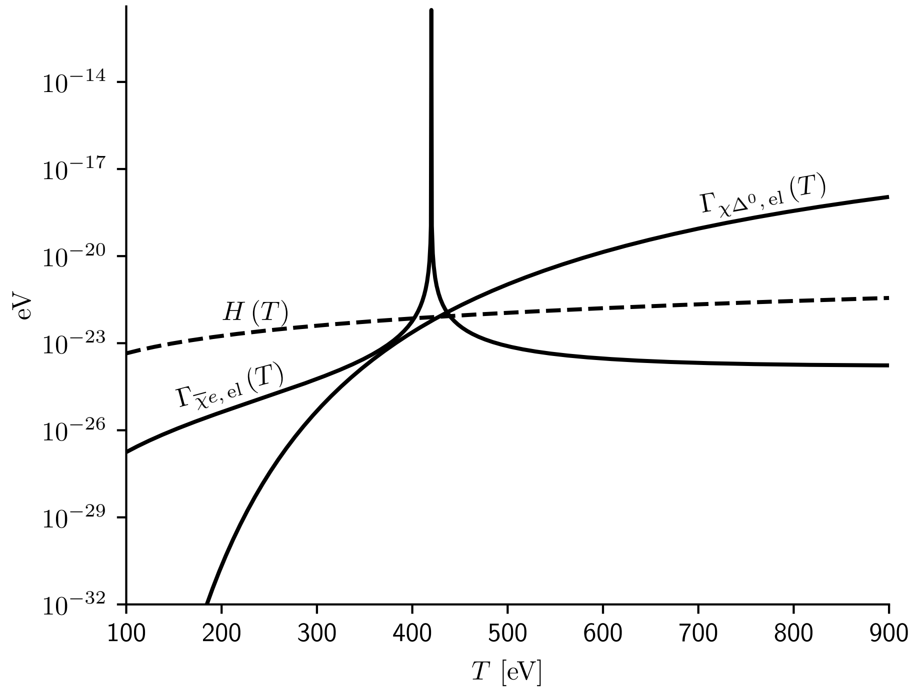

Figure 5.7: The late kinetic decoupling regime at sub-keV temperatures.

following Ref. [69]. This expression was used to numerically find the temperature at which the scattering rate becomes smaller than the Hubble rate. The result depends very strongly on the mass of Δ^0. A value of $T_{\mathrm{kd}} \approx 420$ eV is obtained for $m_\chi = 1.4$ TeV, $g_0 \approx 0.06$, $\mu_0/m_{\Delta^0} \approx 0.02$ and $m_{\Delta^0} \approx 7$ keV. Even a small change in the mass of the mediator, e.g. $m_{\Delta^0} \approx 1$ keV, requires a reduction by a factor of 100 in the product of the coupling constants $g_0\mu_0/m_{\Delta^0}$ in order to yield a similar temperature of kinetic decoupling. In general, smaller values of m_{Δ^0} result in a smaller T_{kd}. Moderate changes in the value of m_χ do not affect the temperature of this kinetic decoupling significantly.

Both elastic scattering rates and the expansion rate of the Universe are represented in Fig. 5.7.

5.5.3 Self-interactions

The exchange of the light scalar mediator Δ^0 mediates self-interactions between the Dark Matter particles with the cross section given in Eq. (5.3.22). As discussed in Section 3.6.2, the relevant quantity to alleviate the cups vs core problem is $\langle \sigma_T/m_\chi \rangle_{v_{\mathrm{therm}}}$, where $\langle \dots \rangle_{v_{\mathrm{therm}}}$ denotes the thermal average over a Maxwell-Boltzmann distribution with average velocity v_{therm},

$$\langle\sigma_T/m_\chi\rangle_{v_{\text{therm}}} = 4\pi \int \frac{\mathrm{d}v}{(2\pi v_{\text{therm}}^2)^{\frac{3}{2}}} v^2 e^{-\frac{1}{2}\frac{v^2}{v_{\text{therm}}^2}} \frac{\sigma_{\text{T}}}{m_\chi} \,. \tag{5.5.12}$$

In particular, the relevant values are $\langle\sigma_T/m_\chi\rangle_{30}$ and $\langle\sigma_T/m_\chi\rangle_{1000}$, where $v_{\text{therm}} = 30\,\text{km/s}$ and $v_{\text{therm}} = 1000\,\text{km/s}$ are the average velocities at the scales of dwarf galaxies and clusters respectively. The integral in Eq. (5.5.12) can be evaluated numerically. As an example, for $g_0 \approx 0.055$, $m_{\Delta^0} = 7\,\text{keV}$, and $m_\chi = 1.4\,\text{TeV}$ the values $\langle\sigma_T/m_\chi\rangle_{30} \approx 1\,\text{cm}^2/\text{g}$ and $\langle\sigma_T/m_\chi\rangle_{1000} \approx 3\times10^{-5}\,\text{cm}^2/\text{g}$ are obtained. The largest impact on this value comes from the choice of g_0: even a small decrease in this coupling strength produces much smaller values of $\langle\sigma_T/m_\chi\rangle_{30}$.

5.6 Small-scale structure

A late kinetic decoupling can successfully resolve the missing satellites problem. For this purpose, T_{kd} should lie below the temperature of Big Bang Nucleosynthesis [32, 33, 34] and above approximately 100 eV, as required by Lyman-α constraints [66, 78]. Indeed, for $T_{\text{kd}} \approx 420$ eV the mass of the smallest Dark Matter protohalos is (see also Sec. 3.6.3)

$$M_{\text{d}} \approx 4.67\times10^9 \frac{g_{*,\text{S}}(T_{\text{kd}})}{g_*^{\frac{3}{2}}(T_{\text{kd}})} \left(\frac{\text{keV}}{T_{\text{kd}}}\right)^3 M_\odot \;. \tag{5.6.1}$$

This lies precisely in the required range, suppressing structures at scales as large as those of dwarf galaxies [36, 35]. As discussed in the other models as well, free-streaming can be neglected here [70]. Furthermore, Dark Matter simulations where interactions with relativistic particles are present until late times show that the concentration parameter of small halos is reduced as well, decreasing the cusp/core discrepancy [79].

As discussed previously in Sec. 3.6.2, self-interacting Dark Matter is able to provide a solution to the cusp vs core, too-big-to-fail and diversity problems. Cross sections of approximately $\langle\sigma_T/m_\chi\rangle_{30} \approx 1\,\text{cm}^2/\text{g}$ are effective for flattening the density and velocity profiles and create cores that are highly dependent on the formation history of the galaxy [79, 51]. At the same time, the cross section should be much smaller at large scales: the bound $\langle\sigma_T/m_\chi\rangle_{1000} \lesssim 0.1\,\text{cm}^2/\text{g}$ can be inferred from cluster lensing surveys [80]. The values presented in Sec. 5.5.3 satisfy precisely these constraints and provide a solution to the cusp vs core, too-big-to-fail and diversity problems.

5.7 Results

The two main objectives of the model presented in this section were to provide a possible solution to the small-scale problems of ΛCDM and to include an annihilation channel of Dark Matter into electrons and positrons at the TeV scale which could potentially be detected by experiments. In order to reach both goals, the following particles were introduced in the Dark Sector:

- χ, the Dark Matter candidate,
- Δ^+, the mediator which allows annihilations into charged leptons, and
- Δ^0, which mediates self-interactions between the Dark Matter particles.

Two mediators are necessary, since one of them is charged under the Standard Model U(1) symmetry and thus could not possibly mediate self-interactions unless the Dark Matter particles where charged under this symmetry as well. Since this is highly constrained, a new neutral mediator Δ^0 had to be introduced.

The ideal choice for the parameters of this theory was presented in Sec. 5.5 and is summarized in Table 5.2. The parameters m_χ and α_l are the only ones which fix the relic density in Eq. 5.5.4. It is thus possible to fix the Dark Matter mass to lie in the TeV range, e.g. $m_\chi = 1.4$ TeV. This implies $\alpha_\ell = 0.06$ or, analogously, $g_i = 0.5$ for $i \in \{e, \mu, \tau\}$. Next, the parameters g_0 and m_{Δ^0} are fixed by requiring the correct cross section for self-interactions as discussed in Sec. 5.5.3. The only free parameter left in the elastic scattering rate between Dark Matter and Δ^0 is the coupling μ_0. Choosing $\mu_0 = 0.02\, m_{\Delta^0}$ yields the correct temperature of kinetic decoupling as in Sec. 5.5.2. This satisfies the constraint $\mu_0/m_{\Delta^0} \lesssim 1$ which allows perturbative expansions. A similar temperature of kinetic decoupling for the elastic scattering between electrons and Dark Matter is obtained if $d = (m_{\Delta^+} - m_\chi)/m_\chi = 1.001$, although the period of contact is not long enough to establish thermal equilibrium. Finally, the parameter μ_+ is only relevant for the decay of Δ^0. The value of μ_+ can thus remain arbitrary as long as it satisfies the constraint $\mu_+/m_{\Delta^+} \lesssim 1$ required by the assumption of perturbativity. Finally, with these parameters, the annihilation channel for Dark Matter into electrons and positrons has a cross section $\langle \sigma_{\overline{\chi}\chi \to \overline{e_R} e_R} v_{\rm rel} \rangle \approx 10^{-27}\mathrm{cm}^3/\mathrm{s}$.

Parameter	Approximate value
m_χ	1.4 TeV
m_{Δ^+}	$1.001 m_e + m_\chi$
m_{Δ^0}	7 keV
g_0	0.06
g_i	0.5
α_l	0.06
μ_0/m_{Δ^0}	0.02
μ_+/m_{Δ^+}	$\lesssim 1$

Table 5.2: The parameters of the leptophilic model.

6 Dark Matter beams of rotating black holes

6.1 Introduction

Astrophysical jets produced by supermassive black holes are usually explained by the magnetic Blandford-Znajek process [81]. In principle, however, gravitational effects can contribute to the resulting jets as well [82, 83]. While a magnetic origin of the jets only works for charged particles, a gravitational one could include neutral particles as well. In particular, Dark Matter particles would be affected too. It is therefore interesting to investigate whether such Dark Matter jets can be formed by rotating supermassive black holes [84]. This is particularly relevant for future prospects of Dark Matter detection.

There have been quite a few experimental signals which are claimed to correspond to indirect Dark Matter detection, e.g. PAMELA [17], ATIC [85], FERMI/LAT [86], H.E.S.S. [87]. However, most possible explanations require the introduction of a *boost factor* in order to produce a signal strong enough to be compatible with the observations [88, 89, 85]. The cause of these boost factors remains uncertain; the proposed possibilities include density inhomogeneities at small scales [90] or Sommerfeld enhanced annihilation cross sections [91].

A further scenario will be discussed in this chapter. Some of the Dark Matter particles within the halo around a supermassive Kerr black hole move along geodesics which lead them into the ergosphere. There, they can collide with other particles (or simply decay) in such a way that one Dark Matter particle is ejected back outside of the ergosphere (see Fig. 6.1). This is the well known Penrose process [92], which allows to extract energy from a black hole. In Ref. [93] it was shown that a set of collimated geodesics along the rotational axis can be produced in this way, by integrating the geodesic equation for Kerr spacetimes numerically.

Here, an upper bound for the density of Dark Matter particles which are present in the jets of supermassive black holes is calculated numerically in order to investigate whether it might enhance the indirect-detection signals. Indeed, the presence of a Dark Matter beam is confirmed and its profile and dependence on the mass of the black hole are analyzed. However, it turns out that this effect must be ruled out as a source of significant Dark Matter overdensities in the proximity of the Earth, due to the faintness of the beam.

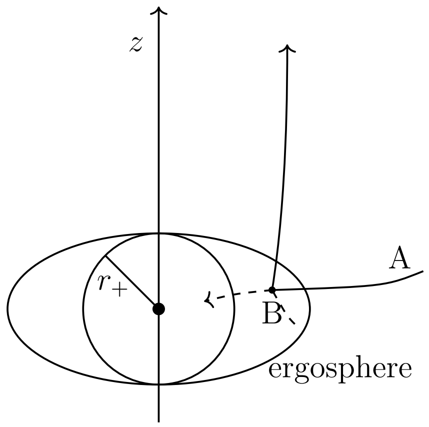

Figure 6.1: A schematic representation of the system under consideration: a particle falls into the ergosphere, interacts with another one and lands into a beam along the rotation axis. r_+ is the outer event horizon of the Kerr spacetime.

6.2 The Carter constant

In this section, the Kerr spacetime and one of its constants of motion along geodesics, the Carter constant, are introduced. The Carter constant will play a crucial role in determining which of the Dark Matter particles falling in from the accretion disk have the potential to end up in the beam.

6.2.1 The Kerr spacetime

The Kerr metric for a rotating black hole in Boyler-Lindquist coordinates is given by

$$\begin{aligned} \mathrm{d}s^2 \;\; = \;\; & -\left(1-\frac{2Mr}{\Sigma^2}\right)\mathrm{d}t^2+\sin^2(\theta)\left(r^2+a^2+\frac{2Mra^2\sin^2(\theta)}{\Sigma^2}\right)\mathrm{d}\phi^2 \\ & -\frac{4Mar\sin^2(\theta)}{\Sigma^2}\mathrm{d}t\mathrm{d}\phi+\frac{\Sigma^2}{\Delta}\mathrm{d}r^2+\Sigma^2\mathrm{d}\theta^2\;, \end{aligned} \tag{6.2.1}$$

where $\Sigma^2 = r^2 + a^2 \cos^2(\theta)$ and $\Delta = r^2 - 2Mr + a^2$ and a is the black hole's angular momentum per unit of mass. This spacetime has two event horizons at $r_+ = M + \sqrt{M^2 - a^2}$ and $r_- = M - \sqrt{M^2 - a^2}$. Furthermore, the region known as the ergosphere between the outer horizon r_+ and the surface described by the equation $(r - M)^2 = r^2 - a^2 \cos^2(\theta)$ is such that all particles within it must move along the direction of rotation of the black hole but can otherwise move towards or away from the center. Within this region, energy can be extracted from the black hole via the Penrose process.

6.2.2 The Carter constant from the geodesic equation

The equation of motion of a particle for a non-rotating neutral black hole is determined by the three constants m, E and L_z, i.e. the particle's mass, energy and angular momentum, respectively. For the case of a Kerr black hole a fourth constant, known as the Carter constant, is needed [94]. Integrating the geodesic equation for the θ-component

$$\Sigma^2 \frac{\mathrm{d}u_\theta}{\mathrm{d}\tau} = -\frac{1}{2}\partial_\theta \left(\Sigma^2 g^{\alpha\beta}\right) u_\alpha u_\beta - \frac{1}{2}\partial_\theta \Sigma^2 \tag{6.2.2}$$

and introducing the conserved quantities $\mathcal{E} = -u_t$ and $\mathcal{L} = u_\phi$ following from the Killing vectors $k^\mu = (1,0,0,0)$ and $\ell^\mu = (0,0,0,1)$ respectively, it follows that the quantity

$$\mathcal{Q} = (u_\theta)^2 + a^2 \cos^2(\theta)\left(1 - \mathcal{E}^2\right) + \frac{\cos^2(\theta)}{\sin^2(\theta)}\mathcal{L}^2 \tag{6.2.3}$$

is conserved. It should be noted that this is the Carter constant for a particle of unit mass. For a particle with arbitrary mass m the Carter constant reads

$$Q = (p_\theta)^2 + \cos^2(\theta)\left(a^2\left(m^2 - E^2\right) + \frac{L^2}{\sin^2(\theta)}\right) . \tag{6.2.4}$$

6.3 The Dark Matter density in the beam

The relevant quantity for determining the existence of a Dark Matter beam is the Dark Matter density of the particles ejected from the ergosphere along the rotation axis $\rho_{\text{out}}(\vec{x})$. In what follows, it will be given in units of the Dark Matter density in the proximity of the Earth, $\rho_{\text{DM},\odot} \approx 0.4~\text{GeV/cm}^3$ [95]. Consequently, the Dark Matter particles can be assumed to have unit mass without loss of generality. An explicit expression for $\rho_{\text{out}}(\vec{x})$ will be derived in this section. The numerical evaluation of this

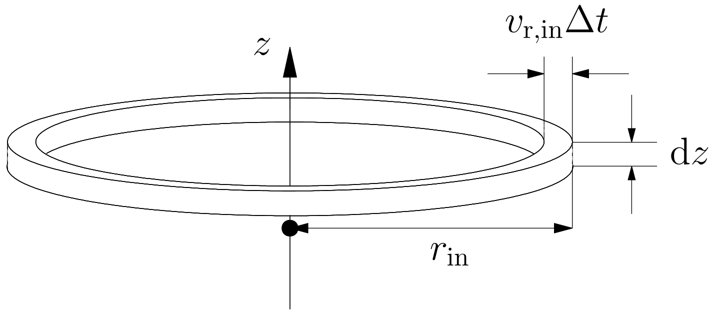

Figure 6.2: The infinitesimal volume of infalling Dark Matter particles. The filled dot denotes the location of the Black Hole.

expression will be discussed in Section 6.5.

It is useful to start by considering the number of particles within an infinitesimal solid ring at some radius r_{in} close to the equatorial plane of the rotating black hole. This is represented in Fig. 6.2. The total number of particles within this ring is given by

$$dN_{\mathrm{in}} = \int_{\vec{v}_{\mathrm{in,\,min}}}^{\vec{v}_{\mathrm{in,\,max}}} d^3\vec{v}_{\mathrm{in}} f\left(\vec{v}_{\mathrm{in}}\right) \rho_{\mathrm{in}} 2\pi r_{\mathrm{in}} v_{r,\,\mathrm{in}} \Delta t \; \mathrm{d}z \; . \tag{6.3.1}$$

In the above expression, ρ_{in} is the Dark Matter density at radius r_{in} and $2\pi r_{\mathrm{in}} v_r \Delta t \mathrm{d}z$ is the volume of the solid ring. $f\left(\vec{v}_{\mathrm{in}}\right)$ is the velocity distribution of the particles for which an explicit expression will be given in Section 6.4.3. dN_{in} thus represents the number (or total mass, since $m = 1$) of particles within this ring with velocities between $\vec{v}_{\mathrm{in,\,min}}$ and $\vec{v}_{\mathrm{in,\,max}}$.

Among the particles falling towards the ergosphere those must be selected which have the potential to emerge from it in a jet along the rotation axis. For a given ingoing velocity $\vec{v}_{\mathrm{in}}$ it is possible to compute the height above the equatorial plane $z\left(\vec{v}_{\mathrm{in}},\, \vec{v}_{\mathrm{out}},\, \theta\right)$ at which particles have to be located in order to end up at the location determined by $\left(r_{\mathrm{out}},\, \theta\right)$ with velocity $\vec{v}_{\mathrm{out}}$. The suitable approximations used to establish the relation $z\left(\vec{v}_{\mathrm{in}},\, \vec{v}_{\mathrm{out}},\, \theta\right)$ are discussed in Sec. 6.4.2.

The infinitesimal interval where particles with initial velocities $\vec{v}_{\mathrm{in}}$ must be in order to end up in the beam within the angle $\mathrm{d}\theta$ and with outgoing velocities in the interval between $\vec{v}_{\mathrm{out}}$ and $\vec{v}_{\mathrm{out}} + \mathrm{d}\vec{v}_{\mathrm{out}}$ is

$$\mathrm{d}z = \frac{\mathrm{d}^4 z}{\mathrm{d}v_{r,\,\mathrm{out}} \mathrm{d}v_{\phi,\,\mathrm{out}} \mathrm{d}v_{\theta,\,\mathrm{out}} \mathrm{d}\theta} \mathrm{d}v_{r,\,\mathrm{out}} \mathrm{d}v_{\phi,\,\mathrm{out}} \mathrm{d}v_{\theta,\,\mathrm{out}} \mathrm{d}\theta \; . \tag{6.3.2}$$

This means that the number of outgoing particles per unit of volume in phase space

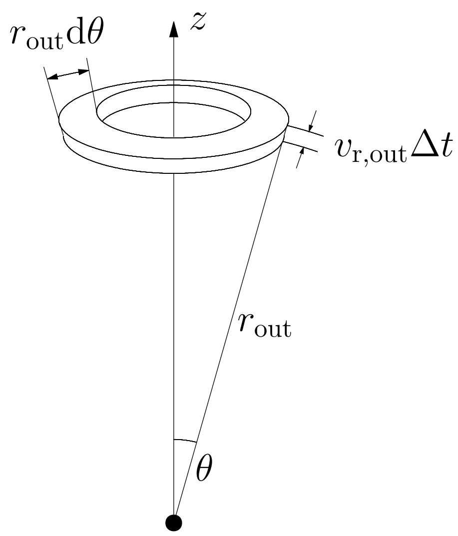

Figure 6.3: The infinitesimal volume occupied by the infalling particles after they have been ejected from the ergosphere. The volume element is given by $\mathrm{d}V = 2\pi r_{\text{out}}^2 \sin(\theta)\,\mathrm{d}\theta$. The filled circle denotes the location of the black hole.

is

$$\begin{aligned} \mathrm{d}N_{\text{out}} &= \eta\frac{2M}{r_{\text{in}}}\int \mathrm{d}^3\vec{v_{\text{in}}} f\left(\vec{v_{\text{in}}}\right)\rho_{\text{in}} 2\pi r_{\text{in}} v_{r,\,\text{in}}\Delta t \\ &\times\frac{\mathrm{d}^4 z}{\mathrm{d}v_{r,\,\text{out}}\mathrm{d}v_{\phi,\,\text{out}}\mathrm{d}v_{\theta,\,\text{out}}\mathrm{d}\theta}\mathrm{d}v_{r,\,\text{out}}\mathrm{d}v_{\phi,\,\text{out}}\mathrm{d}v_{\theta,\,\text{out}}\mathrm{d}\theta\ . \end{aligned} \tag{6.3.3}$$

Here, two additional factors have been added. The first one, η, is the Penrose efficiency. The second one, $2M/r_{\text{in}}$, gives the probability of an interaction happening in the ergosphere.

On the other hand, the number of particles within the phase-space volume $\mathrm{d}^3\vec{v}_{\text{out}}$ can also be written as

$$\begin{aligned} \mathrm{d}N_{\text{out}}\left(\vec{v}_{\text{out}}, r_{\text{out}}, \theta\right) &= \frac{\mathrm{d}^3\rho_{\text{out}}}{\mathrm{d}v_{r,\,\text{out}}\mathrm{d}v_{\phi,\,\text{out}}\mathrm{d}v_{\theta,\,\text{out}}}\left(\vec{v}_{\text{out}}, r_{\text{out}}, \theta\right)\mathrm{d}v_{r,\,\text{out}}\mathrm{d}v_{\phi,\,\text{out}}\mathrm{d}v_{\theta,\,\text{out}} \\ &\times 2\pi r_{\text{out}}^2\sin(\theta)\, v_{r,\,\text{out}}\Delta t\mathrm{d}\theta\ . \end{aligned} \tag{6.3.4}$$

In the above expression $\mathrm{d}V = 2\pi r_{\text{out}}^2 \sin(\theta)\, v_{r,\,\text{out}}\Delta t\mathrm{d}\theta$ was used, i.e. a solid section of a sphere as in Fig. 6.3. The integration around the ϕ direction was possible due to the cylindrical symmetry of the system.

Comparing Eq. (6.3.4) with Eq. (6.3.3) yields the Dark Matter density in the beam,

$$\rho_{\text{out}}\left(\vec{v}_{\text{out}}^{\max}, r_{\text{out}}, \theta\right) - \rho_{\text{out}}\left(\vec{v}_{\text{out}}^{\min}, r_{\text{out}}, \theta\right) = \eta\left(\frac{2M}{r_{\text{in}}}\right)\int \mathrm{d}^3\vec{v}_{\text{out}} \frac{\int \mathrm{d}^3\vec{v_{\text{in}}} f\left(\vec{v}\right) r_{\text{in}} v_r \rho_{\text{in}}}{r_{\text{out}}^2 \sin\left(\theta\right) v_{r,\,\text{out}}} \frac{\mathrm{d}^4 z}{\mathrm{d}v_{r,\,\text{out}}\mathrm{d}v_{\phi,\,\text{out}}\mathrm{d}v_{\theta,\,\text{out}}\mathrm{d}\theta}\,. \tag{6.3.5}$$

This quantity will be computed in Section 6.5.

6.4 Approximations

A number of assumptions and approximations must be made in order to compute the outgoing Dark Matter density in Eq. (6.3.5). They are presented and explained in the following.

6.4.1 Relevant radius for the ingoing particles

The construction described above only takes into consideration infalling particles starting at some fixed radius r_{in} near the equatorial plane. In principle, however, particles landing in the beam could be infalling from any distance from the center of the halo. A more accurate description would thus take into account all of them and trace their geodesics into the ergosphere and in the beam. However, in order to make the numerical calculation easier, only particles starting at r_{in} are considered as an approximation. This is valid for computing an upper bound for ρ_{out}, as long as an appropriate value for r_{in} is chosen. Multiple simultaneous effects lead to a preferred value of r_{in}: on the one hand, further away from the halo's center the Dark Matter density is smaller and thus fewer particles will be falling towards the ergosphere; on the other hand at larger radii a larger volume will be included by the solid ring. It is thus advised to take as a starting radius the one which maximizes the outgoing density ρ_{out}. As an example, for the Andromeda galaxy, a numerical calculation shows that a radius $r_{\text{in}} \approx 0.1$ pc should be taken.

6.4.2 Carter constant

Two assumptions must be made about the Carter constant. First, it is assumed that after the scattering in the ergosphere, each outgoing particle follows a geodesic with the same Carter constant as the infalling one, $Q_{\text{in}} = Q_{\text{out}}$. This is in line with the assumption made in Ref. [93]. Second, it is assumed that all particles whose value of the Carter constant allows it end up in the beam. Since the correct Carter constant is a necessary but not sufficient condition for this to happen, this assumption again leads only to an upper bound for the Dark Matter density.

Keeping all other parameters fixed and solving $Q_{\text{in}} = Q_{\text{out}}$ for $z\,(\vec{v}_{\text{in}}, \vec{v}_{\text{out}})$ gives then the height above the equatorial plane at which particles must find themselves in order to end up in the beam. Differentiation with respect to the outgoing velocities, $\vec{v}_{\text{out}}$, and azimuthal angle at the point of detection, θ, then yields the height of the infalling ring making sure that all particles within that volume have the possibility to produce an overdensity in the beam. This must be done for each velocity $\vec{v}_{\text{in}}$. It should be noted that not all choices of $\vec{v}_{\text{out}}$ and $\vec{v}_{\text{out}}$ yield a real value for z, which reduces the parameter space.

The explicit expression for the Carter constant in Eq. (6.2.3) can be simplified both for the case of ingoing and outgoing particles. For a particle which is located in the accretion disk and is infalling towards the ergosphere of a rotating black hole, the angle θ_{in} satisfies $\cos(\theta_{\text{in}}) \approx z/r_{\text{in}}$, where z is the height above the equatorial plane and r_{in} is the distance to the center of the black hole. Since the particles are assumed to lie close to the equatorial plane [93], the projection of their distance to the center on this plane is approximately equal to r_{in}. Furthermore, in this approximation, $z \ll r_{\text{in}}$ holds. For known black holes which have masses up to $M = 6.6 \times 10^{10}\, M_\odot$, the relation $a^2 \ll r^2$ is valid up to small radii $r_{\text{in}} \approx 0.001\,\text{pc}$. Thus, for the present purpose, the Carter constant for infalling particles is well approximated by

$$Q_{\text{in}} \approx \tilde{\gamma}^2 r^2 v_\theta^2 + \frac{z^2}{r^2}\left[a^2\left(1 - \tilde{\gamma}^2\left(1 - \frac{2M}{r}\right)\right) + \frac{1}{1-\frac{2M}{r}}\tilde{\gamma}^2\left(\frac{2Ma}{r} + r\sqrt{1-\frac{2M}{r}}v_\phi\right)^2\right], \tag{6.4.1}$$

where a modified time-dilation factor, $\tilde{\gamma}$, was introduced as

$$\tilde{\gamma} = \frac{1}{\sqrt{1 - v_\phi^2 + \frac{2Ma}{r^2\sqrt{1-\frac{2M}{r}}}v_\phi - v_r^2 - v_\theta^2}}\,. \tag{6.4.2}$$

For outgoing particles near the rotation axis, i.e. in the jet, the first-order approximation $\sin(\theta) \approx \theta$ and $\cos(\theta) \approx 1$ can be made. This is reasonable as long as the outgoing particles are being detected at a large distance from the black hole. The result will be an approximate angular profile for the Dark Matter density. Of course, for smaller distances or larger angles more terms must be taken into account. The condition $r^2 \gg a^2$ that was used in the case of the infalling particles is even stronger in this case, since the outgoing particles are measured far away from the black hole and close to its axis. With this, the Carter constant for outgoing particles becomes

$$Q_{\text{out}} \approx \gamma^2 r^2 v_\theta^2 + \gamma^2 r^2 v_\phi^2 + a^2 \left(1 - \gamma^2 \left(1 - \frac{2M}{r}\right)\right) + 4\gamma^2 M a v_\phi \theta \, . \tag{6.4.3}$$

Here, γ is the usual Lorentz factor $\gamma^2 = 1/\sqrt{1 - v_\phi^2 - v_r^2 - v_\theta^2}$.

6.4.3 Distribution function

It is assumed that the velocity distribution of the Dark Matter particles in the halo is Gaussian in all three directions,

$$f\left(\vec{v}_{\text{in}}\right) = \frac{1}{(2\pi)^{\frac{3}{2}} \sqrt{|\det\left(\Sigma\right)|}} \exp\left(-\frac{1}{2}\left(\vec{v}_{\text{in}} - \vec{v}_0\right)^T \Sigma^{-1} \left(\vec{v}_{\text{in}} - \vec{v}_0\right)\right) \, . \tag{6.4.4}$$

For simplicity, the covariance matrix Σ is assumed to be diagonal, i.e. $\Sigma = \text{diag}\left(\Sigma_r, \Sigma_\phi, \Sigma_\theta\right)$. $\vec{v}_0$ is the mean velocity of the particles within the halo. Since on average they are orbiting the black hole, the only non-vanishing component is the one in the ϕ direction, i.e. $\vec{v}_0 = (0, v_{\phi,0}, 0)$. At the radius considered here, $r_{\text{in}} \approx 0.1\,\text{pc}$, a mean angular velocity of $v_{\phi,0} \approx 500\,\text{km/s}$ can be estimated from present data on the rotation curve of the Milky Way [96]. However, it should be noted that the final result is not strongly affected by the choice of $v_{\phi,0}$: values of 100 km/s and 1000km/s yield similar outcomes.

In order to estimate the value of Σ_r one can refer to Fig. 2 of Ref. [97] to obtain the mass accretion rate, $\mathrm{d}M/\mathrm{d}t$, of supermassive black holes. Equating this to the infall rate of particles around the black hole a value for the standard deviation $\sigma_r = \sqrt{\Sigma_r}$ can be obtained. Explicitly, the equation to be solved is

$$\frac{\mathrm{d}M}{\mathrm{d}t} = 4\pi r_{\text{in}}^2 \rho\left(r_{\text{in}}\right) \int_0^1 \frac{1}{\sqrt{2\pi\sigma_r^2}} e^{\left(-\frac{v_r^2}{2\sigma_r^2}\right)} v_r \mathrm{d}v_r \, . \tag{6.4.5}$$

The right-hand side is the mass of Dark Matter going through a shell in an infinitesimal time interval. Solving this equation numerically gives an estimate for σ_r. The standard deviation in the other directions is assumed to be the same, i.e. $\sigma_r = \sigma_\phi = \sigma_\theta$.

The velocity distribution must then be multiplied with the density of dark matter at r_{in} in order to obtain the total number of particles with velocity $\vec{v_{\text{in}}}$ per unit of volume. In particular, for $r_{\text{in}} = 0.1$ pc and assuming a cored dark matter profile [41], the dark matter density can be approximated by $\rho_{\text{in}}\,(0.1\,\text{pc}) = 30\rho_{\text{DM},\odot}$, where $\rho_{\text{DM},\odot}$ is the Dark Matter density in the vicinity of the Earth.

6.4.4 Penrose efficiency

The efficiency of the Penrose process is defined as

$$\eta = \frac{E_{\text{extr.}}}{M}\,, \tag{6.4.6}$$

where M is the mass of the black hole and $E_{\text{extr.}}$ is the energy which can be extracted from it via the Penrose process. For neutral extremal black holes a maximal value of 0.52 can be obtained [98]. Here, a much more conservative value of $\eta = 0.01$ corresponding to black holes with angular momentum $a = 0.5M$ will be used. However, as is apparent from Eq. (6.3.5), the exact value of the Penrose efficiency does not affect the final result significantly.

6.5 Numerical results

With the approximations presented in the previous section, Eq. (6.3.5) can be computed numerically. The numerical code takes the parameter set $\{M,\, a,\, r_{\text{in}},\, r_{\text{out}},\, \theta,\, v_{\phi,0},\, \sigma,\, \eta, \rho_{\text{in}}\}$ as an input and yields the Dark Matter density at $(r_{\text{out}},\, \theta)$. Furthermore, the integration limits for the ingoing and outgoing velocities must be set as well. Instead of simply taking the largest possible interval of integration, a more computationally efficient solution is to consider only the region in the velocity space which actually contributes to ρ_{out}. This is the region where the following conditions are satisfied: the impact parameter is real and its fourth derivative appearing in Eq. (6.3.5) is non-vanishing.

6.5.1 Example: Andromeda galaxy

As a first example, the Dark Matter density along the rotation axis of the black hole at the center of the Andromeda galaxy can computed at a distance $r_{\text{out}} = 780\,\text{kpc}$, i.e. the approximate distance to the Solar system. The precise parameters for the numerical calculation are summarized in Table 6.1. For this parameter set the integration bounds for the velocities can be further restricted by logarithmically scanning all possible values and discarding those which contribute by less than a factor of 10^{-3} to the

Andromeda galaxy	
M	$10^8\,M_\odot$
a	$0.5M$
$r_{\rm in}$	$0.1\,$pc
$r_{\rm out}$	$780\,$kpc
$v_{\phi,0}$	$10^{-3}c$
σ	0.006
η	0.01

Table 6.1: The parameters used to compute the Dark Matter density of particles ejected from the ergosphere of the black hole at the center of the Andromeda galaxy.

final result. Specifically, this means that geodesics with very low $|\vec{v}_{\rm in}|$ can safely be neglected and the same holds for outgoing geodesics with large outgoing angular velocities $v_{\theta,\,\rm out}$, $v_{\phi,\,\rm out} > 10^{-8}$. Furthermore, a lower bound on the outgoing radial velocity is given by $v_{r,\,\rm out} > r_{\rm out}/t_{\rm Andromeda}$, where $t_{\rm Andromeda} \approx 10^{10}$ yrs is the age of the Andromeda galaxy. With this, a Dark Matter density of $\rho_{\rm DM} \approx 10^{-12}$ is found at a distance of 780 kpc from the Andromeda galaxy. This result shows that no local Dark Matter overdensities can be produced in this way. However, in the next section it will be shown that a Dark Matter beam is indeed present although a very faint one.

6.5.2 Features of the Dark Matter beam

In order to confirm the presence of a Dark Matter beam along the axis of a rotating black hole, the Dark Matter density has been computed for different distances from the black hole and at various distances from the rotation axis. This is represented in Fig. 6.4 for a black hole of the same mass as the one at the center of the Andromeda galaxy. The distance from the axis of the black hole d is given by $d = r_{\rm out}\theta$. The numerical calculation is not able to go to arbitrarily small values of θ, especially for larger $r_{\rm out}$'s, due to the finite machine precision. In these cases, the central values close to the axis at large distances from the black hole have been approximated by the neighboring values at larger θ (this is the reason for the uniform central behavior for $r_{\rm out} > 10^3$ pc in Fig. 6.4). Indeed, an increase towards the center is expected with higher θ resolution. Furthermore, it should be noted that the results in the lower left and right corners in Fig. 6.4 should be discarded, since the approximation $\theta \ll 1$ is not valid there.

Fig. 6.4 confirms the existence of a faint beam of Dark Matter particles along the rotation axis of a black hole. Indeed, for each value of r_{out} the Dark Matter density is largest near the axis and decreases rapidly away from it. Furthermore, it is noticed that the Dark Matter density increases by many orders of magnitude closer to the black hole.

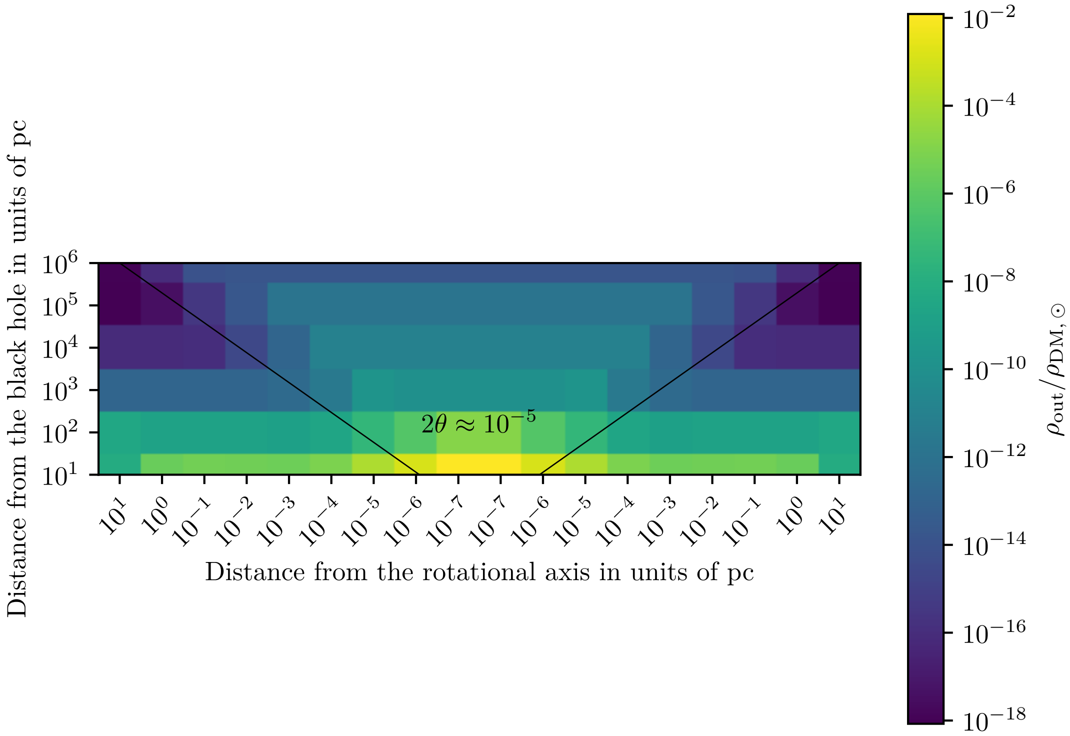

Figure 6.4: The DM density in units of $\rho_{\text{DM},\odot}$, the DM density in the Earth's proximity, at different distances from the rotating black hole, r_{out} and different distances from the rotation axis.

6.5.3 Dependence on mass and distance

Fig. 6.5 shows a 2d scan of the Dark Matter density obtained for different black hole masses and distances from the black hole. The angle from the rotation axis is kept constant at $\theta = 10^{-8}$ for each point. The range of black hole masses maps the range of masses from the observed supermassive (non-stellar) black holes. A minimal distance of 1 pc from the black hole is chosen, corresponding to approximately a thousand Schwarzschild radii for the most massive black holes considered. Fig. 6.5 shows that closer to the black hole the Dark Matter density is larger, as can be seen from the beam profile in Fig. 6.4 as well. Furthermore, black hole masses between $10^8\,M_\odot$ and $10^9 M_\odot$ are found to yield the highest Dark Matter densities. With this information overdensities up to $40\,\rho_{\mathrm{DM},\odot}$ can be found by combining a black hole mass of $10^{8.5}\,M_\odot$ with low r_{out} of 10 pc and small distances to the rotation axis.

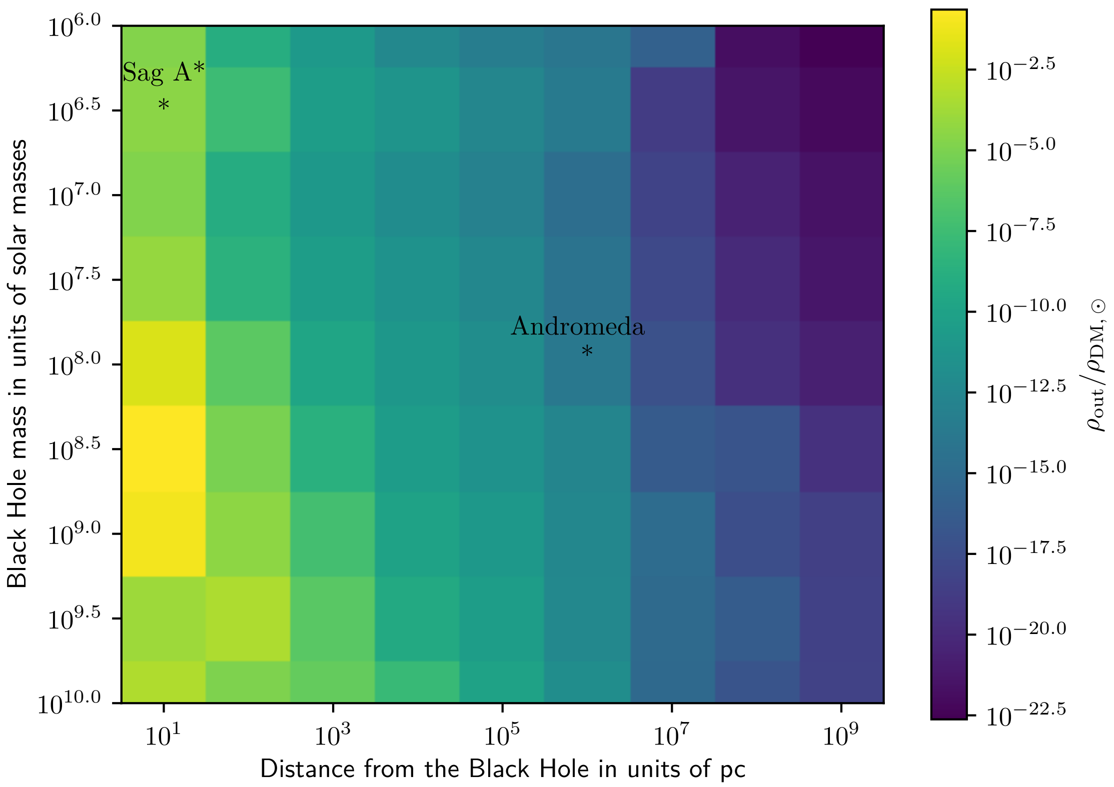

Figure 6.5: The DM density in units of $\rho_{\mathrm{DM},\odot}$, the DM density in the Earth's proximity, at different distances from the rotating black hole and for different values of the black hole's mass.

6.5.4 Dependence on the angular momentum

The dependence of ρ_{out} on the angular momentum a can be analyzed by computing ρ_{out} for different values ranging between $a = 0$ and $a = M$. For $a = 0$, ρ_{out} is eight orders of magnitude smaller than for the case $a = 0.5M$. The reason for a non-vanishing ρ_{out} even in the case $a = 0$ is that this numerical approach based on the Carter constant takes into account all possible geodesics: the result for $a = 0$ is due to those geodesics which go directly from the region considered at a radius r_{in} to the location at which the Dark Matter density is evaluated (r_{out}, θ). The fact that ρ_{out} is significantly lower in the case $a = 0$ shows that the Dark Matter beam is enabled the special properties of the Kerr spacetime.

For different non-vanishing values of a the resulting ρ_{out}'s have similar values, but the following trend is observed: the beam becomes narrower when a approaches the maximal value $a = M$, while it is less collimated for small values of a. A quantitative analysis of this effect would be possible only with higher numerical precision.

6.6 Conclusion

The goal of this chapter was to show the existence of a gravitational mechanism which produces a Dark Matter beam along the axis of a rotating black hole. The main results are summarized by Fig. 6.4 and Fig. 6.5, which show that there is indeed a collimated beam, that the Dark Matter density within the beam is largest close to the black hole and that the largest Dark Matter densities are obtained for black holes with a mass of approximately $10^8 - 10^9\ M_\odot$. Far from the black hole, the density in the beam is found to be many orders of magnitude smaller than the Dark Matter density in the proximity of the Earth. In conclusion, this mechanism can be excluded as a possible source of a boost for the local detection rate of Dark Matter.

7 Conclusion

The first goal of this thesis was to present certain modifications of the ΛCDM model in order to explain the discrepancies between current observations and simulations regarding the small-scale structure of the Universe. The common ground between all three proposed models consists of late kinetic decouplings and self-interactions. If the Dark Matter candidate remains in thermal contact with a relativistic scattering partner until temperatures below approximately 1 keV, the formation of small Dark Matter protohalos with masses below $10^8\,M_\odot$ is suppressed. Interactions between the Dark Matter particles favor an entropy exchange from the center of a halo's core towards outer regions. The result is a flattened Dark Matter density profile. For each model it was explicitly shown that agreement with ΛCDM predictions is guaranteed at large scales. Furthermore, cosmological and astrophysical constraints were also shown to be satisfied. The implications of each new Dark Sector for the small-scale structure of the Universe was discussed in detail and was found to be in agreement with current observations, thus solving the small-scale problems of the ΛCDM model.

The secluded U(1) Dark Sector shows that a simple extension of the usual Cold Dark Matter paradigm is able to successfully address the small-scale problems. Its drawback is that neither direct nor indirect detection of Dark Matter particles is possible. However, tests of this theory are still possible by comparing cosmological predictions and observations with more and more precision. Multiple generations of dark fermions were considered. While the case $N = 1$ is already sufficient for resolving the small-scale problems (albeit only for a strongly restricted parameter space), more generations could still play an important role, for example if observations requiring smaller mediator masses should arise. The fact that the Dark Sector is completely secluded from the Standard Model makes this model particularly flexible, as only few constraints apply.

The neutrinophilic Dark Matter model shows that neutrinos can indeed serve as the relativistic scattering partner of Dark Matter. It was shown that in order to allow for a late kinetic decoupling between Dark Matter and neutrinos, the relic density of

Dark Matter should be generated by a freeze-in mechanism. While this model only serves as a proof of concept, it also suggests possible rare decays into neutrinos which might be detected at neutrino observatories.

Finally, the third model shows the possibity of a coupling between Dark Matter and charged leptons. This can explain some of the tentative Dark Matter signals obtained through cosmic ray detection. The constraints on this model are the strongest ones discussed. In particular, it was shown that in order for the theory to satisfy constraints on the leptonic anomalous magnetic moments, the Dark Matter particles can only couple to right-handed leptons. The charged leptons cannot keep a thermal equilibrium with Dark Matter until late times and thus a further scalar in the Dark Sector had to be introduced for the sake of resolving all small-scale problems of ΛCDM.

In the final part of this work, a new mechanism generating a faint Dark Matter beam along the axis of rotating black holes has been presented. The system considered consists of Dark Matter particles falling into the ergosphere of a Kerr black hole and being ejected close to the rotation axis through the Penrose process. The Dark Matter density was found to drop off sharply further away from the rotation axis, confirming the existence of a collimated beam. The dependence of the Dark Matter density in the beam on the angular momentum and mass of the black hole and on the distance from the ergosphere has been analyzed. The beam is more collimated for larger angular momenta. Furthermore, black hole masses of approximately $10^{8.5}$ solar masses have been shown to yield the largest Dark Matter densities. However, the Dark Matter density is many orders of magnitude smaller than the Dark Matter density near the Earth, which means that detection rates cannot be enhanced through this effect.

Bibliography

[1] N. Aghanim et al. Planck 2018 results. VI. Cosmological parameters. 2018.

[2] F. Zwicky. On the Masses of Nebulae and of Clusters of Nebulae. *Astrophys. J.*, 86:217–246, 1937.

[3] K. G. Begeman, A. H. Broeils, and R. H. Sanders. Extended rotation curves of spiral galaxies: Dark haloes and modified dynamics. *Mon. Not. Roy. Astron. Soc.*, 249:523, 1991.

[4] K.C. Freeman. On the disks of spiral and SO Galaxies. *Astrophys. J.*, 160:811, 1970.

[5] L. V. E. Koopmans and T. Treu. The structure and dynamics of luminous and dark matter in the early-type lens galaxy of 0047-281 at z=0.485. *Astrophys. J.*, 583:606–615, 2003.

[6] Henk Hoekstra, Howard Yee, and Mike Gladders. Current status of weak gravitational lensing. *New Astron. Rev.*, 46:767–781, 2002.

[7] Douglas Clowe, Marusa Bradac, Anthony H. Gonzalez, Maxim Markevitch, Scott W. Randall, Christine Jones, and Dennis Zaritsky. A direct empirical proof of the existence of dark matter. *Astrophys. J. Lett.*, 648:L109–L113, 2006.

[8] Marc Davis, George Efstathiou, Carlos S. Frenk, and Simon D. M. White. The Evolution of Large Scale Structure in a Universe Dominated by Cold Dark Matter. *Astrophys. J.*, 292:371–394, 1985.

[9] Rupert A. C. Croft, David H. Weinberg, Mike Bolte, Scott Burles, Lars Hernquist, Neal Katz, David Kirkman, and David Tytler. Towards a precise measurement of matter clustering: Lyman alpha forest data at redshifts 2-4. *Astrophys. J.*, 581:20–52, 2002.

[10] A. De Rujula, S. L. Glashow, and U. Sarid. CHARGED DARK MATTER. *Nucl. Phys. B*, 333:173–194, 1990.

[11] Savas Dimopoulos, David Eichler, Rahim Esmailzadeh, and Glenn D. Starkman. Getting a Charge Out of Dark Matter. *Phys. Rev. D*, 41:2388, 1990.

[12] Bob Holdom. Two U(1)'s and Epsilon Charge Shifts. *Phys. Lett. B*, 166:196–198, 1986.

[13] Maxim Markevitch, A. H. Gonzalez, D. Clowe, A. Vikhlinin, L. David, W. Forman, C. Jones, S. Murray, and W. Tucker. Direct constraints on the dark matter self-interaction cross-section from the merging galaxy cluster 1E0657-56. *Astrophys. J.*, 606:819–824, 2004.

[14] Marco Taoso, Gianfranco Bertone, and Antonio Masiero. Dark Matter Candidates: A Ten-Point Test. *JCAP*, 03:022, 2008.

[15] E. Aprile et al. Light Dark Matter Search with Ionization Signals in XENON1T. *Phys. Rev. Lett.*, 123(25):251801, 2019.

[16] E. Aprile et al. Excess electronic recoil events in XENON1T. *Phys. Rev. D*, 102(7):072004, 2020.

[17] Oscar Adriani et al. An anomalous positron abundance in cosmic rays with energies 1.5-100 GeV. *Nature*, 458:607–609, 2009.

[18] M. Aguilar et al. First Result from the Alpha Magnetic Spectrometer on the International Space Station: Precision Measurement of the Positron Fraction in Primary Cosmic Rays of 0.5–350 GeV. *Phys. Rev. Lett.*, 110:141102, 2013.

[19] M. G. Aartsen et al. Evidence for High-Energy Extraterrestrial Neutrinos at the IceCube Detector. *Science*, 342:1242856, 2013.

[20] Julio F. Navarro, Carlos S. Frenk, and Simon D.M. White. The Structure of cold dark matter halos. *Astrophys. J.*, 462:563–575, 1996.

[21] W. J. G. de Blok. The core-cusp problem. *Advances in Astronomy*, 2010:1–14, 2010.

[22] B. Moore. Evidence against dissipationless dark matter from observations of galaxy haloes. *Nature*, 370:629, 1994.

[23] Ricardo A. Flores and Joel R. Primack. Observational and theoretical constraints on singular dark matter halos. *Astrophys. J. Lett.*, 427:L1–4, 1994.

[24] A. Burkert. The Structure of dark matter halos in dwarf galaxies. *IAU Symp.*, 171:175, 1996.

[25] B. Moore, S. Ghigna, F. Governato, G. Lake, Thomas R. Quinn, J. Stadel, and P. Tozzi. Dark matter substructure within galactic halos. *Astrophys. J. Lett.*, 524:L19–L22, 1999.

[26] Anne M. Green, Stefan Hofmann, and Dominik J. Schwarz. The power spectrum of SUSY - CDM on sub-galactic scales. *Mon. Not. Roy. Astron. Soc.*, 353:L23, 2004.

[27] Jurg Diemand, Ben Moore, and Joachim Stadel. Earth-mass dark-matter haloes as the first structures in the early Universe. *Nature*, 433:389–391, 2005.

[28] Erik J. Tollerud, James S. Bullock, Louis E. Strigari, and Beth Willman. Hundreds of Milky Way Satellites? Luminosity Bias in the Satellite Luminosity Function. *Astrophys. J.*, 688:277–289, 2008.

[29] K. Bechtol et al. Eight New Milky Way Companions Discovered in First-Year Dark Energy Survey Data. *Astrophys. J.*, 807(1):50, 2015.

[30] Anatoly A. Klypin, Andrey V. Kravtsov, Octavio Valenzuela, and Francisco Prada. Where are the missing Galactic satellites? *Astrophys. J.*, 522:82–92, 1999.

[31] James S. Bullock, Andrey V. Kravtsov, and David H. Weinberg. Reionization and the abundance of galactic satellites. *Astrophys. J.*, 539:517, 2000.

[32] Ottavia Balducci, Stefan Hofmann, and Alexis Kassiteridis. Cosmological Singlet Diagnostics of Neutrinophilic Dark Matter. *Phys. Rev. D*, 98(2):023003, 2018.

[33] Ottavia Balducci, Stefan Hofmann, and Alexis Kassiteridis. Small-scale structure from charged leptophilia. 12 2018.

[34] Ottavia Balducci, Stefan Hofmann, and Alexis Kassiteridis. Cosmic structure formation in a flavoured U(1) dark sector at small scales. 10 2018.

[35] Laura G. van den Aarssen, Torsten Bringmann, and Christoph Pfrommer. Is dark matter with long-range interactions a solution to all small-scale problems of \Lambda CDM cosmology? *Phys. Rev. Lett.*, 109:231301, 2012.

[36] Mark Vogelsberger, Jesus Zavala, Francis-Yan Cyr-Racine, Christoph Pfrommer, Torsten Bringmann, and Kris Sigurdson. ETHOS – an effective theory of structure formation: dark matter physics as a possible explanation of the small-scale CDM problems. *Mon. Not. Roy. Astron. Soc.*, 460(2):1399–1416, 2016.

[37] Stefan Hofmann, Dominik J. Schwarz, and Horst Stoecker. Damping scales of neutralino cold dark matter. *Phys. Rev. D*, 64:083507, 2001.

[38] Kyle A. Oman et al. The unexpected diversity of dwarf galaxy rotation curves. *Mon. Not. Roy. Astron. Soc.*, 452(4):3650–3665, 2015.

[39] Michael Boylan-Kolchin, James S. Bullock, and Manoj Kaplinghat. The Milky Way's bright satellites as an apparent failure of LCDM. *Mon. Not. Roy. Astron. Soc.*, 422:1203–1218, 2012.

[40] Emmanouil Papastergis, Riccardo Giovanelli, Martha P. Haynes, and Francesco Shankar. Is there a "too big to fail" problem in the field? *Astron. Astrophys.*, 574:A113, 2015.

[41] Sean Tulin and Hai-Bo Yu. Dark Matter Self-interactions and Small Scale Structure. *Phys. Rept.*, 730:1–57, 2018.

[42] Sean Tulin, Hai-Bo Yu, and Kathryn M. Zurek. Beyond Collisionless Dark Matter: Particle Physics Dynamics for Dark Matter Halo Structure. *Phys. Rev. D*, 87(11):115007, 2013.

[43] Kim Griest and Marc Kamionkowski. Unitarity Limits on the Mass and Radius of Dark Matter Particles. *Phys. Rev. Lett.*, 64:615, 1990.

[44] Edward W. Kolb and Michael S. Turner. *The Early Universe*, volume 69. 1990.

[45] Jonathan L. Feng, Iftah Galon, Felix Kling, and Sebastian Trojanowski. Dark Higgs bosons at the ForwArd Search ExpeRiment. *Phys. Rev. D*, 97(5):055034, 2018.

[46] P.A. Zyla et al. Review of Particle Physics. *PTEP*, 2020(8):083C01, 2020.

[47] Carlo Giunti and Chung W. Kim. *Fundamentals of Neutrino Physics and Astrophysics*. 2007.

[48] Erik Aver, Keith A. Olive, and Evan D. Skillman. The effects of He I λ10830 on helium abundance determinations. *JCAP*, 07:011, 2015.

[49] Mark Vogelsberger, Jesus Zavala, and Abraham Loeb. Subhaloes in self-interacting galactic dark matter haloes. *Monthly Notices of the Royal Astronomical Society*, 423(4):3740–3752, May 2012.

[50] Jesús Zavala, Mark Vogelsberger, and Matthew G. Walker. Constraining self-interacting dark matter with the milky way's dwarf spheroidals. *Monthly Notices of the Royal Astronomical Society: Letters*, 431(1):L20–L24, Feb 2013.

[51] Manoj Kaplinghat, Sean Tulin, and Hai-Bo Yu. Dark Matter Halos as Particle Colliders: Unified Solution to Small-Scale Structure Puzzles from Dwarfs to Clusters. *Phys. Rev. Lett.*, 116(4):041302, 2016.

[52] David N. Spergel and Paul J. Steinhardt. Observational evidence for selfinteracting cold dark matter. *Phys. Rev. Lett.*, 84:3760–3763, 2000.

[53] Torsten Bringmann and Stefan Hofmann. Thermal decoupling of WIMPs from first principles. *JCAP*, 0704:016, 2007. [Erratum: JCAP1603,no.03,E02(2016)].

[54] Abraham Loeb and Matias Zaldarriaga. The Small-scale power spectrum of cold dark matter. *Phys. Rev. D*, 71:103520, 2005.

[55] Patrick J. Fox and Erich Poppitz. Leptophilic Dark Matter. *Phys. Rev.*, D79:083528, 2009.

[56] Ian M. Shoemaker. Constraints on Dark Matter Protohalos in Effective Theories and Neutrinophilic Dark Matter. *Phys. Dark Univ.*, 2(3):157–162, 2013.

[57] Laura G. van den Aarssen, Torsten Bringmann, and Yasar C Goedecke. Thermal decoupling and the smallest subhalo mass in dark matter models with Sommerfeld-enhanced annihilation rates. *Phys. Rev.*, D85:123512, 2012.

[58] Ranjan Laha, Basudeb Dasgupta, and John F. Beacom. Constraints on New Neutrino Interactions via Light Abelian Vector Bosons. *Phys. Rev.*, D89(9):093025, 2014.

[59] P. S. Pasquini and O. L. G. Peres. Bounds on Neutrino-Scalar Yukawa Coupling. *Phys. Rev.*, D93(5):053007, 2016. [Erratum: Phys. Rev.D93,no.7,079902(2016)].

[60] Lucien Heurtier and Yongchao Zhang. Supernova Constraints on Massive (Pseudo)Scalar Coupling to Neutrinos. *JCAP*, 1702(02):042, 2017.

[61] Torsten Bringmann, Felix Kahlhoefer, Kai Schmidt-Hoberg, and Parampreet Walia. Strong constraints on self-interacting dark matter with light mediators. *Phys. Rev. Lett.*, 118(14):141802, 2017.

[62] R. Foot and S. Vagnozzi. Dissipative hidden sector dark matter. *Phys. Rev. D*, 91:023512, 2015.

[63] P. S. Bhupal Dev, Clara Miralles Vila, and Werner Rodejohann. Naturalness in testable type II seesaw scenarios. *Nucl. Phys. B*, 921:436–453, 2017.

[64] A. V. Artamonov et al. Search for the rare decay $K^+ \to \mu^+\nu\bar{\nu}\nu$. *Phys. Rev. D*, 94(3):032012, 2016.

[65] Lawrence J. Hall, Karsten Jedamzik, John March-Russell, and Stephen M. West. Freeze-In Production of FIMP Dark Matter. *JHEP*, 03:080, 2010.

[66] Julien Baur, Nathalie Palanque-Delabrouille, Christophe Yèche, Christophe Magneville, and Matteo Viel. Lyman-alpha Forests cool Warm Dark Matter. *JCAP*, 08:012, 2016.

[67] Antonella Garzilli, Alexey Boyarsky, and Oleg Ruchayskiy. Cutoff in the Lyman \alpha forest power spectrum: warm IGM or warm dark matter? *Phys. Lett. B*, 773:258–264, 2017.

[68] Torsten Bringmann, Haavard Tveit Ihle, Joern Kersten, and Parampreet Walia. Suppressing structure formation at dwarf galaxy scales and below: late kinetic decoupling as a compelling alternative to warm dark matter. *Phys. Rev. D*, 94(10):103529, 2016.

[69] Paolo Gondolo and Kenji Kadota. Late Kinetic Decoupling of Light Magnetic Dipole Dark Matter. *JCAP*, 06:012, 2016.

[70] Anne M. Green, Stefan Hofmann, and Dominik J. Schwarz. The First wimpy halos. *JCAP*, 08:003, 2005.

[71] Matthew R. Buckley and Patrick J. Fox. Dark Matter Self-Interactions and Light Force Carriers. *Phys. Rev. D*, 81:083522, 2010.

[72] J. Chang et al. An excess of cosmic ray electrons at energies of 300-800 GeV. *Nature*, 456:362–365, 2008.

[73] O. Adriani et al. Extended Measurement of the Cosmic-Ray Electron and Positron Spectrum from 11 GeV to 4.8 TeV with the Calorimetric Electron Telescope on the International Space Station. *Phys. Rev. Lett.*, 120(26):261102, 2018.

[74] O. Adriani et al. Cosmic-Ray Positron Energy Spectrum Measured by PAMELA. *Phys. Rev. Lett.*, 111:081102, 2013.

[75] G. Ambrosi et al. Direct detection of a break in the teraelectronvolt cosmic-ray spectrum of electrons and positrons. *Nature*, 552:63–66, 2017.

[76] S. A. Khrapak, A. V. Ivlev, G. E. Morfill, and S. K. Zhdanov. Scattering in the Attractive Yukawa Potential in the Limit of Strong Interaction. *Phys. Rev. Lett.*, 90(22):225002, 2003.

[77] Stanley J. Brodsky and Jeremiah D. Sullivan. W BOSON CONTRIBUTION TO THE ANOMALOUS MAGNETIC MOMENT OF THE MUON. *Phys. Rev.*, 156:1644–1647, 1967.

[78] Vid Iršič et al. New Constraints on the free-streaming of warm dark matter from intermediate and small scale Lyman-α forest data. *Phys. Rev. D*, 96(2):023522, 2017.

[79] J. A. Schewtschenko, R. J. Wilkinson, C. M. Baugh, C. Bœhm, and S. Pascoli. Dark matter–radiation interactions: the impact on dark matter haloes. *Mon. Not. Roy. Astron. Soc.*, 449(4):3587–3596, 2015.

[80] Annika H. G. Peter, Miguel Rocha, James S. Bullock, and Manoj Kaplinghat. Cosmological Simulations with Self-Interacting Dark Matter II: Halo Shapes vs. Observations. *Mon. Not. Roy. Astron. Soc.*, 430:105, 2013.

[81] R. D. Blandford and R. L. Znajek. Electromagnetic extractions of energy from Kerr black holes. *Mon. Not. Roy. Astron. Soc.*, 179:433–456, 1977.

[82] R. Opher, N. O. Santos, and A. Wang. Geodesic motion and confinement in van Stockum space-time. *Journal of Mathematical Physics*, 37(4):1982–1990, April 1996.

[83] Reva Kay Williams. Collimated escaping vortical polar e- e+ jets intrinsically produced by rotating black holes and Penrose processes. *Astrophys. J.*, 611:952–963, 2004.

[84] Ottavia Balducci, Stefan Hofmann, and Maximilian Kögler. Dark Matter beams of rotating black holes. *In preparation*, 2022.

[85] Adams J. Ahn H. et al. Chang, J. An excess of cosmic ray electrons at energies of 300–800 GeV. *Nature*, 456, 2008.

[86] Aous A. Abdo et al. Measurement of the Cosmic Ray e+ plus e- spectrum from 20 GeV to 1 TeV with the Fermi Large Area Telescope. *Phys. Rev. Lett.*, 102:181101, 2009.

[87] F. Aharonian et al. The energy spectrum of cosmic-ray electrons at TeV energies. *Phys. Rev. Lett.*, 101:261104, 2008.

[88] Lars Bergström, Joakim Edsjö, and Gabrijela Zaharijas. Dark matter interpretation of recent electron and positron data. *Physical Review Letters*, 103(3), Jul 2009.

[89] Lars Bergstrom, Torsten Bringmann, Martin Eriksson, and Michael Gustafsson. Gamma rays from Kaluza-Klein dark matter. *Phys. Rev. Lett.*, 94:131301, 2005.

[90] J. Lavalle, Q. Yuan, D. Maurin, and X. J. Bi. Full Calculation of Clumpiness Boost factors for Antimatter Cosmic Rays in the light of Lambda-CDM N-body simulation results. Abandoning hope in clumpiness enhancement? *Astron. Astrophys.*, 479:427–452, 2008.

[91] Junji Hisano, Shigeki Matsumoto, and Mihoko M. Nojiri. Explosive dark matter annihilation. *Phys. Rev. Lett.*, 92:031303, 2004.

[92] R. Penrose and R. M. Floyd. Extraction of rotational energy from a black hole. *Nature*, 229:177–179, 1971.

[93] Jerome Gariel, Malcolm A. H. MacCallum, G. Marcilhacy, and N. O. Santos. Kerr Geodesics, the Penrose Process and Jet Collimation by a Black Hole. 2 2007.

[94] Brandon Carter. Global structure of the Kerr family of gravitational fields. *Phys. Rev.*, 174:1559–1571, 1968.

[95] Fabrizio Nesti and Paolo Salucci. The Local Dark Matter Density. *PoS*, DSU2012:041, 2012.

[96] Kuantay Boshkayev and Daniele Malafarina. A model for a dark matter core at the Galactic Centre. *Mon. Not. Roy. Astron. Soc.*, 484(3):3325–3333, 2019.

[97] W. N. Brandt and D. M. Alexander. Supermassive black-hole growth over cosmic time: Active galaxy demography, physics, and ecology from chandra surveys. *Proceedings of the National Academy of Sciences*, 107(16):7184–7189, Apr 2010.

[98] Brian P. Dolan. Pressure and volume in the first law of black hole thermodynamics. *Class. Quant. Grav.*, 28:235017, 2011.